AD

RCS OSD-1366

Research and Development Technical Report

ECOM 66-G24-A

STUDIES OF EFFECTS OF BOUNDARY MODIFICATION IN PROBLEMS OF SMALL AREA METEOROLOGY

Annual Reports 1966-1967

By

Heinz H. Lettau, Principal Investigator; Charles R. Stearns, Co-Investigator; Walter F. Dabberdt, and Joseph Zabransky

February 1968

ECOM

UNITED STATES ARMY ELECTRONICS COMMAND
ATMOSPHERIC SCIENCES LABORATORY
FORT HUACHUCA, ARIZONA

Grant No. DA-AMC-28-043-66-G24
Department of Meteorology
University of Wisconsin, Madison, Wisconsin

DISCLAIMER

The citation of trade names and names of manufacturers in this report is not to be construed as official Government endorsement or approval of commercial products or services referenced herein.

The findings in this report are not to be construed as an official Department of the Army position unless so designed by other authorized documents.

DISPOSITION

Destroy this report when it is no longer needed. Do not return it to the originator.

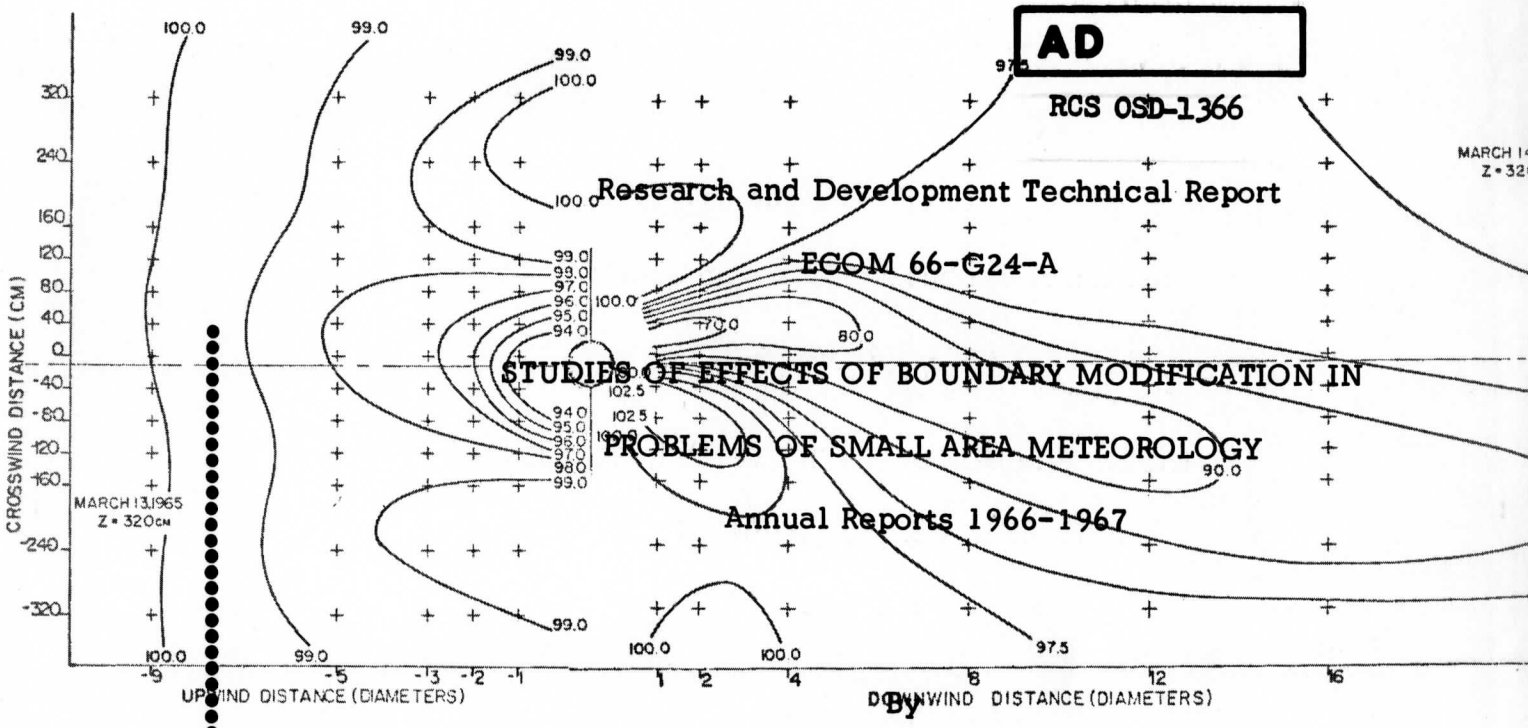

AD

RCS OSD-1366

Research and Development Technical Report

ECOM 66-G24-A

STUDIES OF EFFECTS OF BOUNDARY MODIFICATION IN PROBLEMS OF SMALL AREA METEOROLOGY

Annual Reports 1966-1967

By

Heinz H. Lettau, Principal Investigator; Charles R. Stearns, Co-Investigator; Walter F. Dabberdt, and Joseph Zabransky

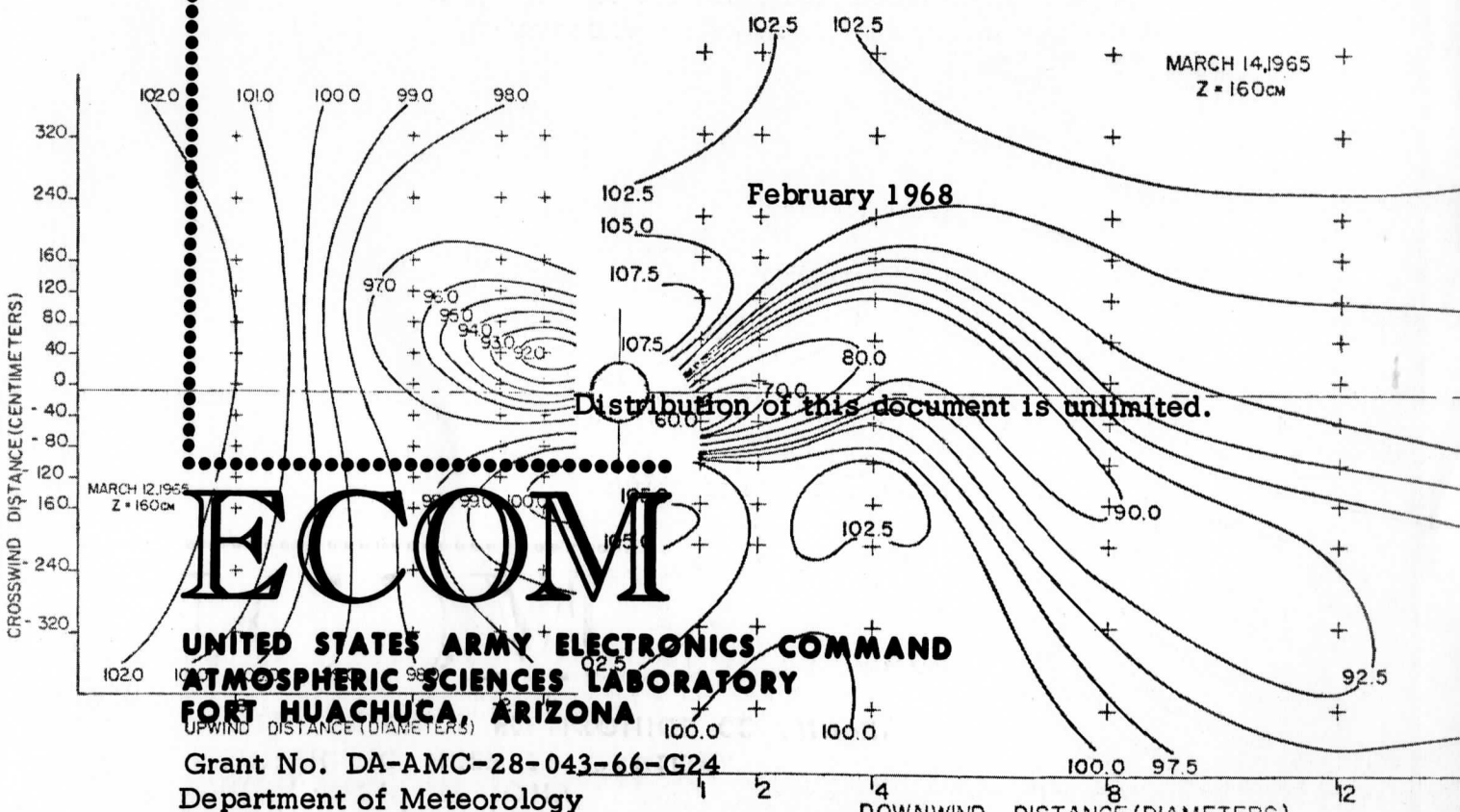

February 1968

Distribution of this document is unlimited.

ECOM

UNITED STATES ARMY ELECTRONICS COMMAND
ATMOSPHERIC SCIENCES LABORATORY
FORT HUACHUCA, ARIZONA

Grant No. DA-AMC-28-043-66-G24
Department of Meteorology
University of Wisconsin, Madison, Wisconsin

Scanner's note:

This page is blank.

Technical Report ECOM 66-G24-A February 1968

STUDIES OF EFFECTS OF BOUNDARY MODIFICATION IN PROBLEMS OF SMALL AREA METEOROLOGY

Annual Reports 1966-67

Grant No. DA-AMC-28-043-66-G24
DA Task No. 1TO-14501-B53A-08

Prepared by

Heinz H. Lettau, Principal Investigator; Charles R. Stearns, Co-Investigator; Walter F. Dabberdt, and Joseph Zabransky
Department of Meteorology, University of Wisconsin
Madison, Wisconsin

For

US Army Electronics Command
Atmospheric Sciences Laboratory
Fort Huachuca, Arizona

Scanner's note:

This page is blank.

TABLE OF CONTENTS

Scanner's note:

This page is blank.

General Introduction

In this report, which covers the work done in 1966 and 1967, scientific results are summarized which concern several phases of the research work specified in the objectives of the grant. In brief, these objectives are the gradual development of a comprehensive theory of how the behavior of the lower atmosphere is related to definable changes in the physical characteristics of the underlying terrain and land cover (such as soil type, thermal and moisture properties of the soil, albedo, aerodynamic roughness, amount and type of vegetation, and topography). This general objective can be characterized as the problem of small-area meteorology. The approach to its solution will include both theoretical models and an experimental program.

It may be added that research potential and talent developed at the University of Wisconsin under direct support by the U. S. Army Electronics Command, Atmospheric Sciences Laboratory, Fort Huachuca, Arizona, appears to have contributed a significant share to our nation's effort in fields of environmental sciences. A few highlights may be mentioned. During recent years the senior principal investigator has been called upon to serve on two panels of the National Research Council of the National Academy of Sciences, on problems which involve small area meteorology (the Panel on Weather and Climate Modification, which issued its report in January 1966 and the Joint Panel on Air-Sea Interaction, which is concerned with the planned international GARP program). Results of work under this grant were presented at several scientific conferences, including two international meetings. At the CSIRO Symposium in Canberra, Australia, September 1966, on the collection and processing of field data, the degree of control in out-of-door experiments was discussed in an invited paper with the title "Problems of Micrometeorol Measurements" (pp. 3-39 of the "Proceedings" of the Symposium, just published in book form by Interscience Publishers, a division of J. Wiley & Sons, New York, 1967). The other international meeting was the conference at Kyoto, Japan, on boundary layer turbulence.

Micrometeorological instrumentation and data evaluation techniques developed at Wisconsin during recent years were called upon in connection with the cooperative field experiment at Davis, California, organized and supported by the U. S. Army Electronics Command, Atmospheric Science Laboratory, at Fort Huachuca, Arizona. The principal investigator of this work at the Meteorology Department of the University of Wisconsin was Professor Stearns, who will report on the specific results separately.

Heinz H. Lettau
Madison, Wisconsin

February, 1968.

Scanner's note:

This page is blank.

Analysis of Diabatic Wind and Temperature Profiles

Charles R. Stearns
University of Wisconsin, Madison

ABSTRACT:

The major problems in the analysis of wind speed and air temperature profiles when used to determine the surface stress and sensible heat flux are the determination of the displacement height of the profiles and of the roughness of the underlying surface. The method discussed here involves two theoretical models of profile structure; one based on the KEYPS model with $K_h/K_m = 1$ and the other a modified KEYPS with $K_h/K_m = 1/\sqrt{\phi}$, where ϕ is the Monin-Obukov nondimensional with shear.

The method of analysis weights equally each measurement of wind and temperature. The selection of the displacement height and the surface roughness is based on the minimum error squares fit between the profile points and the theoretical model in the determination of the surface stress. An estimate of the sensible heat flux to the air results which is then compared to an independent measurement of the sensible heat flux. The results indicate that for forced convection the comparison of the two sensible heat fluxes indicates that $K_h/K_m = 1$ and that for Priestley (free) convection and inversion conditions $K_h/K_m = 1/\sqrt{\phi}$. The possibility is raised for a phase shift between the flux of sensible heat to the air and the mean temperature gradient in the air. Another possibility is that the temperature distribution with respect to time is mono-modal during forced convection and bi-modal during Priestley convection. The above criterion is suggested for defining the two convection regimes over the previously used Richardson number.

1. Scheme for Wind Profile Measurement

Because, in an adiabatic surface layer wind speed varies approximately as the logarithm of the height, the spacing of anemometers (and consequently of levels of air temperature measurement) is usually chosen such that the differences in wind speed between successive levels are nearly the same. The spacing then corresponds to a geometric series, for example, with double heights, i.e., 20 cm, 40 cm,

80 cm, etc. If anemometers and thermometers were perfect sensors, this would be satisfactory. Because of existing instrumental error the number of instruments should be significantly increased so that overlapping double levels would be available. The selected scheme is illustrated in Fig. 1.1, where the same wind profile is presented; once using only adjacent and then using overlapping double levels. Additional values at 30 cm and 100 cm were interpolated from the nearest levels. Actual cup size prohibits mounting the anemometers closer together than about 20 cm in height. It can be seen from Fig. 1.1 that the change of computed curvature characteristics, such as β or DEU[1], with height is more reliable when overlapping rather than adjacent double levels are used.

Figure 1.2 illustrates a few selected wind profiles and the apparent value of $\log z_0$ determined from adjacent levels of measurement. The profiles for lapse and inversion conditions seem to extrapolate to about the same value of $\log z_0$. The extrapolation is based on the assumption that the selected reference level of zero height is correct.

It would seem desirable to find a method that would make equal use of each anemometer and thermometer in the profile. Increasing the number of measurement levels makes the determination of profile characteristics more independent of the accuracy of a single instrument.

2. Surface Layer Model for Wind and Temperature

The profile of wind speed (V, cm/sec) in the neutral atmospheric surface layer is generally assumed to vary with height (z, cm) according to the logarithmic law

$$V_a = (V_a^*)\, k^{-1} \ln(1 + z/z_0) \tag{2.1}$$

where the subscript a refers to neutral or adiabatic conditions, V_a is the wind speed at height z, $V_a^* = (\tau_{oa}/\rho)^{1/2}$, τ_{oa} (dynes/cm^2) the horizontal surface stress, ρ the air density (gm/cm^2) at height z, z_0 (cm) the roughness parameter, and k the Karman constant assumed to be 0.428 (Lettau, 1961). The surface layer is defined as the layer of height h for which $h(\partial\tau/\partial z) < 0.01 \cdot \tau_{oa}$, which means that the existing divergence of stress is less than 1 percent of the surface stress in the surface layer. The one percent level is used because this corresponds to the approximate accuracy which the probable wind speed error places on the τ_{oa} determination.

---

[1] The symbols DEU or β denote the Deacon number of the wind profile, as rigorously defined later by Eq. (2.29).

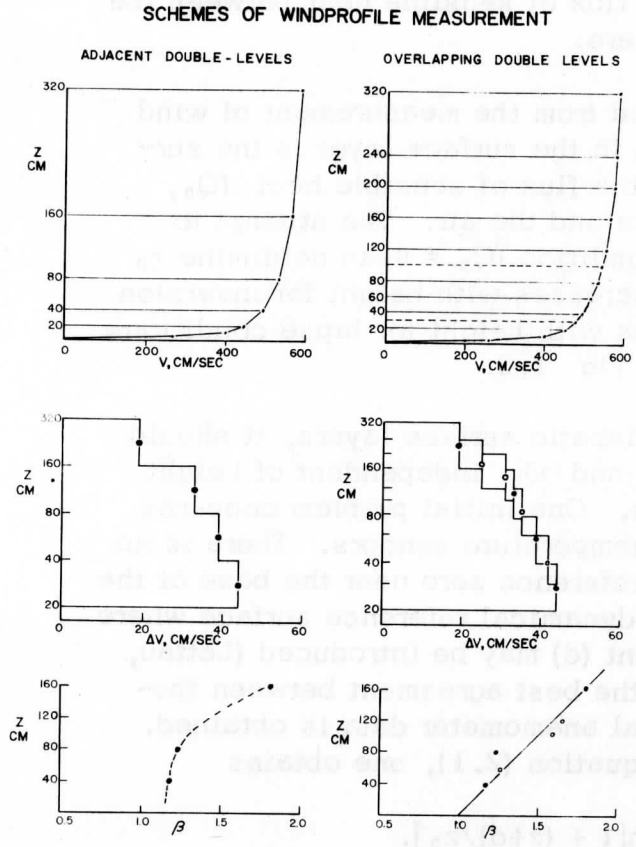

Fig. 1.1. Comparison between adjacent and overlapping double levels for computing β of the wind profile.

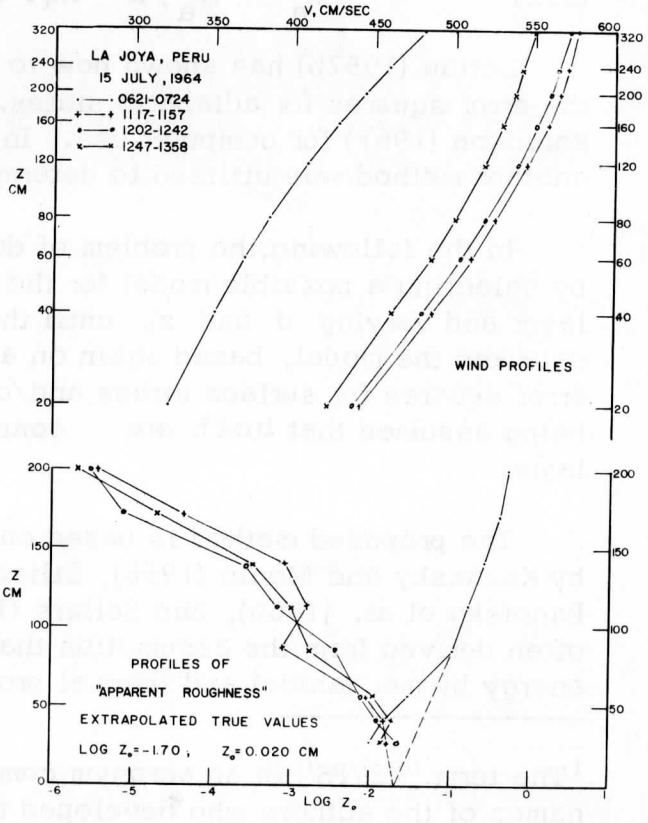

Fig. 1.2. Wind speed profiles and profiles of apparent $\log_{10} z_0$ which upon extrapolation to $z = 0$ yield a value of $z_0 = 0.02$ cm.

Under adiabatic conditions the potential air temperature is assumed constant with height as the flux of sensible heat between the air and the underlying surface is zero.

The information usually desired from the measurement of wind and temperature at several heights in the surface layer is the surface stress (τ_0, dynes/cm^2) and the flux of sensible heat (Q_0, ly/min) between the earth's surface and the air. The attempt to apply equation (2.1) to diabatic condition ($Q_0 \neq 0$) to determine τ_0 will show that the apparent z_0 increases with height for inversion conditions ($Q_0 < 0$) and decreases with height for lapse conditions ($Q_0 > 0$). This is demonstrated in Fig. 1.2.

With an adequate theory for diabatic surface layers, it should be possible to determine z_0, τ_0 and Q_0 independent of height from wind and temperature profiles. One initial problem concerns the actual height of the wind and temperature sensors. There is no reason to suppose that a nominal reference zero near the base of the wind mast coincides with the aerodynamical reference surface where V = 0. Accordingly, a displacement (d) may be introduced (Lettau, 1957a) which may be varied until the best agreement between theoretical profile structure and actual anemometer data is obtained. Introducing the variable d into equation (2.1), one obtains

$$V_a = (V_a^*)\, k^{-1} \ln[1 + (z+d)/z_0]. \qquad (2.2)$$

Lettau (1957b) has shown how to determine d by minimizing the error squares for adiabatic states. This method was adapted by Robinson (1961) for computer use. In Dalrymple, et al. (1963), another method was utilized to determine d for inversional profiles.

In the following,the problem of determining d will be approached by selecting a possible model for the diabatic atmospheric surface layer and varying d and z_0 until the best fit is found between the data and the model, based again on a minimum condition of sums of error squares for surface stress and/or sensible heat flux as it is being assumed that b o t h are constant with height in the surface layer.

The proposed method is based on the KEYPS model, developed by Kazansky and Monin (1956), Ellison (1957), Yamamoto (1959), Panofsky et al. (1960), and Sellers (1962).[1] The model is most often derived from the assumption that the production of turbulent energy by mechanical and thermal processes is equal to the dissi-

[1] The term "KEYPS" is an acronym composed of the first letters of the names of the authors who developed the concept.

pation of kinetic energy by the eddy viscosity. This involves the following:

A length-scale of turbulence ℓ is defined as

$$\ell = k(z + z_0) \tag{2.3}$$

and the dissipation of kinetic energy per unit mass ϵ_I is assumed to be

$$\epsilon_I = K_m^3 \ell^{-4} \tag{2.4}$$

where K_m is the eddy diffusivity for momentum which is defined as

$$K_m = (\tau/\rho)/V', \tag{2.5}$$

where V' denotes the wind shear at the height z.

The production of turbulent energy by mechanical friction ϵ_{II} is assumed to be given by

$$\epsilon_{II} = \tau V'/\rho, \tag{2.6}$$

and the production of turbulent energy by buoyant forces ϵ_{III} by

$$\epsilon_{III} = B g Q/c_p \rho T \tag{2.7}$$

where B is a numerical constant to be determined empirically, g is the acceleration of gravity (cm/sec^2), T the temperature (deg K), Q the vertical sensible heat flux (ly min^{-1}), and c_p the heat capacity per unit mass of air (cal/gm °K).

The essential model assumption is that

$$\epsilon_I = \epsilon_{II} + \epsilon_{III} \tag{2.8}$$

whereupon we obtain from equations (2.4, 5, 6, 7) that

$$K_m^3 \ell^{-4} = \tau V'/\rho + B\, gQ/c_p \rho T. \tag{2.9}$$

The flux Richardson number $\underline{RI}$ is defined as

$$\underline{RI} = - g Q/(c_p T \tau V'). \tag{2.10}$$

Solving for Q in equation (2.10) and substituting in equation (2.9), one obtains

$$K_m^3 \ell^{-4} = \tau V'/\rho (1 - B\, \underline{RI}). \tag{2.11}$$

The defining equation for K_m can be substituted in equation (2.11) obtaining

$$\tau^3 \rho^{-3} \ell^{-4} = (1 - B\underline{RI}). \tag{2.12}$$

It is convenient to introduce a function ϕ which is the diabatic influence function (Lettau, 1962), or the dimensionless wind shear (Monin and Obukhov, 1954) defined as

$$\phi = k(z + z_0)V'(\tau/\rho)^{-1/2}. \tag{2.13}$$

Substitution of equation (2.13) into equation (2.12) yields

$$\phi^{-4} = 1 - B\,\underline{RI}. \tag{2.14}$$

Equation (2.14) is the basic KEYPS equation utilizing the flux Richardson number. If it were possible to determine $\underline{RI}$ in equation (2.10), the heat flux Q and the surface stress τ_0 would already be known. What can be directly determined from profiles of wind and temperature is $\underline{Ri} = g\theta'/T V'^2$ from the gradients of wind and temperature.

The eddy diffusivity for momentum K_m was previously defined in equation (2.5). A similar eddy diffusivity for heat K_h may be defined as

$$K_h = -Q_0/(\rho c_p \theta'). \tag{2.15}$$

Thus the relationship between the flux and gradient Richardson number becomes

$$RI = -g Q/(c_p T \tau V') = (K_h/K_m)\underline{Ri}. \tag{2.16}$$

Following Lettau (1957b), it is convenient to introduce the abbreviation

$$N_Q = K_h/K_m, \tag{2.17}$$

with the possibly simplifying assumption that $N_Q = 1$. A second important possibility is that N_Q be some specified function of $\underline{Ri}$.

It would be desirable to find a function of N_Q which varies in a known way with height and Richardson number. Substitution of the diabatic influence function ϕ into the equation for the flux Richardson number yields

$$\begin{aligned} \underline{RI} &= -g Q/(T c_p \tau V') \\ &= -g k c_p^{-1} Q \phi^{-1} \tau^{-3/2} \rho^{1/2} T^{-1}(z + z_0). \end{aligned} \tag{2.18}$$

Using the equation of state for a perfect gas in the form $\rho = P/R_dT$, ρ may be substituted in equation (2.18) obtaining

$$\phi \underline{RI} = -gkQc_p^{-1}\tau^{-3/2}(P/R_d)^{1/2}T^{-3/2}(z+z_0). \qquad (2.19)$$

Gravity (g), the Karman constant (k), the gas constant (R_d) and the specific heat of air at constant pressure (c_p) are absolute constants in the surface layer. The pressure P will vary slightly; according to the hydrostatic equation ($dP = -\rho g\, dz$), we have $dP_{(0-10m)} = 10^3$ dynes/cm^2 or approximately 0.1 percent of the surface pressure of 10^6 dynes/cm^2. Thus, pressure can safely be assumed constant in the surface layer at the 1 percent level. On the basis of the definition of the surface layer, the height variation of both Q and τ can be neglected so that $Q \approx Q_0$ and $\tau \approx \tau_0$. From equation (2.19), the relationship which may be considered linear in height is

$$\tau^{3/2}\phi \underline{RI} = -gkc_p^{-1}Q(P/R_d)^{1/2}\tau^{-3/2}(z+z_0). \qquad (2.20)$$

It would simplify matters considerably if air temperature (T) could be assumed constant with height. However, a temperature gradient of $\pm 3°C$/meter will produce an error of the order of one percent and will cause bias in a certain direction. Temperature gradients in the surface layer do often exceed the above order of magnitude, and the temperature dependency with height should be taken into account if possible. The equation is simplified if the substitution $V^* = \sqrt{\tau_0/\rho}^{1/2}$ is made and the mean temperature of the profile is used to determine τ. Then V^* will be assumed constant with height in the surface layer.

Since $\underline{Ri}$ rather than $\underline{RI}$ will be directly determined in the surface layer, equation (2.17) is substituted in equation (2.20) allowing $(\tau_0/\rho)^{1/2} = V^*$ obtaining

$$\phi N_Q \underline{Ri}\,(z+z_0)^{-1} = -gkc_p^{-1}R_d P^{-1} Q V^{*-3} \qquad (2.21)$$

Equation (2.21) will also be assumed constant with height in the surface layer. Equation (2.21) may be written as:

$$\phi N_Q \underline{Ri} = -(z+z_0)L^{-1} \qquad (2.22)$$

where the characteristic length L is defined by

$$L = g^{-1}k^{-1}c_p R_d^{-1} P Q^{-1} V^{*3} \qquad (2.23)$$

In the literature L is usually referred to as Monin-Obukhov length scale. However, the essential form of this scale already appears in a paper by Lettau (1949) a few years prior to the most often quoted publi-

cation by Monin and Obukhov (1954). J. Neumann (1964), after pointing out these historical facts, refers to L as the Lettau-Obukhov-Monin length scale of stratified shear flows. In analogy to the previously mentioned acronym (the "KEYPS" formula), it could be suggested to speak of the "LOM" scale of turbulence.

If, in determining the gradient Richardson number at any level in the surface layer, the mean temperature over the profile is used, the effect of a temperature gradient of $\pm$ 3°C/meter will be reduced from about 1 percent to 0.3 percent. $\underline{Ri}$ then is defined as

$$\underline{Ri} = (g/T_m)(\theta'/V'^2). \tag{2.24}$$

Utilizing the KEYPS model assumption embodied in equation (2.14) and from equation (2.17) we have that

$$B\, N_Q \underline{Ri} = 1 - \phi^{-4} \tag{2.25}$$

which may be substituted in equation (2.22) yielding

$$\phi\, N_Q \underline{Ri} = \phi(1 - \phi^{-4})B^{-1} = -(z + z_0)L^{-1} \tag{2.26}$$

neglecting the variation of temperature with height.

The above model may be tested by the use of relations between a scaling factor such as $\underline{Ri}$ and a shape factor such as the Deacon numbers. The Deacon numbers defined in formal analogy to the exponent β introduced by Deacon (1953) in the following equation

$$V' \equiv \partial V/\partial z = k^{-1} V^* (z + z_0)^{-\beta} \tag{2.27}$$

Logarithmic differentiation of equation (2.27) yields

$$\beta = -d \ln V'/d \ln (z + z_0) \tag{2.28}$$

assuming that both β, and V^* are constant with height. Basically, β is a convenient shape factor since it is nondimensional and does express the relative curvature of the wind profile, and, likewise, with an obvious extension, the temperature profile. However, the symbol β will not be used because this was assumed to be constant with height by Deacon. Instead, two new symbols will be used which denote, in general, two functions of height defined as

$$\underline{DEU} = -d \ln V'/d \ln(z + z_0) \tag{2.29}$$

which will be a nondimensional shape factor for the wind profile, and

$$\underline{DET} = -d \ln \theta'/d \ln(z + z_0) \tag{2.30}$$

which will be a nondimensional shape factor for the potential temperature profile. Lettau (1962) defined the Deacon numbers of the wind profile and potential temperature profile for the testing of model assumptions.

Two identities are obtained by logarithmic differentiation of both $\underline{Ri}$ and N_Q with respect to height:

$$d \ln \underline{Ri}/d \ln(z+z_0) \equiv 2\ DEU - \underline{DET} \tag{2.31}$$

with $\underline{Ri}$ determined from equation (2.24) using the mean temperature of the surface layer, and

$$d \ln (N_Q)/d \ln(z+z_0) \equiv \underline{DET} - \underline{DEU}. \tag{2.32}$$

The function ϕ in equation (2.13) will now be referred to as the diabatic influence function. Logarithmic differentiation of equation (2.13) with respect to height yields

$$d \ln \phi/d \ln(z+z_0) = 1 - \underline{DEU} - 1/2\ d \ln T/d \ln(z+z_0). \tag{2.33}$$

For conciseness, the following abbreviations will be used:

$$\alpha_T = d \ln T/d \ln(z+z_0) \tag{2.34}$$

where α_T is the profile contour number for temperature after Lettau's definition of the profile contour number for wind (Lettau, 1957c). α_T was evaluated for strong lapse and inversion temperature profiles and found to be less than 0.01 in absolute value and will be neglected as small compared to 1 and well within the uncertainty in determining $\underline{DEU}$ as will be discussed in section 5. The simplification that the air temperature is constant with height is in keeping with the magnitude of α_T.

Logarithmic differentiation of equation (2.26) with respect to height assuming $\alpha_T = 0$ yields

$$d \ln \phi/d \ln(z+z_0) = (1 - \phi^{-4})/(1 + 3\phi^{-4}). \tag{2.35}$$

Substitution of equation (2.35) into (2.33) neglecting α_T results in

$$DEU = 4\phi^{-4}/(1 + 3\phi^{-4}). \tag{2.36}$$

If $N_Q = 1$, then it follows that $\underline{DEU} = \underline{DET}$ and $d \ln \underline{Ri}/d \ln(z+z_0) = \underline{DEU}$. This assumption has been made by many investigators and serves as a starting point when the actual relationship for N_Q is not known. If $\underline{DEU}$ is plotted as a function of $\underline{Ri}$ for lapse conditions, the limiting

value for large negative $\underline{Ri}$ for quasi-free convection is 1.33 according to Priestley (1959). As $\underline{Ri} \to -\infty$, ϕ goes to zero from equation (2.25). From equation (2.35),

$$\lim_{\phi \to 0} \underline{DEU} = \lim_{\phi \to 0} 4/(3 + \phi^4) = 4/3 \tag{2.37}$$

If $N_Q = 1$, then $\underline{DET}$ will have the same limiting value as $\underline{DEU}$.

From observations analyzed by Dalrymple et al. (1963), the value of $\underline{DEU}$ as $\underline{Ri}$ increases positively and $\phi \to \infty$ is never less than 0. From equation (2.36)

$$\lim_{\phi \to \infty} \underline{DEU} = \lim_{\phi \to \infty} [4\phi^{-4}/(1 + 3\phi^{-4})] \approx 0. \tag{2.38}$$

If the assumption is made that $N_Q = 1$, then $\phi^{-4} = 1 - B\underline{Ri}$ and $\underline{DEU} = (4 - 4B\,\underline{Ri})/(4 - 3B\,\underline{Ri})$ which has a pole at the point where $\underline{Ri} = 4/3B$, and $\underline{DEU}$ goes from $-\infty$ to $+\infty$ as $\underline{Ri}$ increases above $4/3B$.

Lettau (oral communication, 1965) suggested the assumption that $N_Q = N\phi^{-n}$ where the constants N and n are to be determined from the limiting values of $\underline{DEU}$ and $\underline{DET}$. In this procedure, it is possible to eliminate the pole for the expression of $\underline{DEU}$ versus $\underline{Ri}$. Equation (2.38) remains unchanged by the introduction of $N_Q = N\phi^{-n}$, but the expression relating ϕ and Ri is altered. From equation (2.27), we obtain

$$\underline{Ri} = \phi^n(1 - \phi^{-4})/NB. \tag{2.39}$$

If N and n are positive and $0 < n < 4$, then $\underline{Ri} \to -\infty$ as $\phi \to 0$ and $\underline{Ri} \to +\infty$ as $\phi \to \infty$. The pole associated with the assumption that $N_Q = 1$ will be eliminated.

From equation (2.32) and using the assumption that $N_Q = N\phi^{-n}$, we obtain

$$\underline{DET} - \underline{DEU} = -n\, d \ln \phi / d \ln(z + z_0) = -n(1 - \underline{DEU}). \tag{2.40}$$

The limiting value as $\phi \to \infty$ for $\underline{DEU}$ remains unchanged at 0 but $\underline{DET}$ becomes

$$\underline{DET} = (n+1)\underline{DEU} - n \tag{2.41}$$

Taking the limit as $\phi \to \infty$ on equation (2.41) we have

$$\lim_{\phi \to \infty} \underline{DET} = \lim_{\phi \to \infty} [(n+1)\,\underline{DEU} - n] = -n, \qquad (2.42)$$

using the previously determined limits for $\underline{DEU}$.

Similarly for $N_Q = N\,\phi^{-n}$

$$\lim_{\phi \to 0} \underline{DET} = \lim_{\phi \to 0} 1.5\,\underline{DEU} - 0.5 = 2.0 - n \qquad (2.43)$$

An examination of the data on $\underline{DET}$ (β_θ) versus Ri presented by Dalrymple et al. (1963) shows that the minimum observed value of $\underline{DET}$ as $\underline{Ri} \to \infty$ is about -0.5. If this is true, then $N_Q = N\,\phi^{-1/2}$ where N still remains to be determined and the limiting value of $\underline{DET}$ as $\underline{Ri} \to +\infty$ is then 1.5.

An estimate of the value of $B \cdot N$ may be obtained from the value of $\partial(\underline{DEU})/\partial\underline{Ri}$ at $\underline{Ri} = 0$ according to Lettau (1962). Since $\underline{DEU}$ and $\underline{Ri}$ are both functions of ϕ we can write that

$$\partial(\underline{DEU})/\partial\underline{Ri} = (\partial\,\underline{DEU}/\partial\phi)/(\partial\,Ri/\partial\phi). \qquad (2.44)$$

Since

$$\partial(\underline{DEU})/\partial\phi = -16\,\phi^3/(1 + 3\phi^{-4})^2$$

then

$$\partial\,\underline{DEU}/\partial\phi = -1 \text{ at } \phi = 1.$$

$$\partial\underline{Ri}/\partial\phi = [1/2\,\phi^{-1/2}(1 - \phi^{-4}) + \phi^{1/2}\,4\phi^{-5}](BN)^{-1}.$$

At $\underline{Ri} = 0$ and $\phi = 1$

$$\partial\underline{Ri}/\partial\phi = 4\,(BN)^{-1}.$$

From Lettau (1962)

$$\partial\underline{DEU}/\partial\underline{Ri} = -BN/4 = -4.5, \text{ or } BN = 18.$$

Panofsky et al. (1961) also conclude that $\gamma = BN = 18$.

The defining equation of the diabatic influence function, equation (2.13), may be rewritten as

$$V' = \phi\,V^*\,k^{-1}(z + z_0)^{-1} \qquad (2.45)$$

Integration of equation (2.45) from $V = 0$ at height zero to V at height z yields

$$V = V^* k^{-1} \int_0^z \phi(z+z_0)^{-1} dz \tag{2.46}$$

With the aid of the substitution of $\phi = 1 + \phi - 1$, equation (2.46) becomes

$$V = V^* k^{-1} [\ln(1 + z/z_0) + \int_0^z (\phi - 1)(z+z_0)^{-1} dz]. \tag{2.47}$$

The remaining integral has been designated the integral diabatic influence function Φ_V for the wind profile by Lettau (1962).

The temperature variation with height may be obtained from equations (2.13), (2.22), (2.23) and (2.24) as

$$\theta' = -T_m k^{-2} g^{-1} L^{-1} V^{*2} N_Q \phi(z+z_0)^{-1} \tag{2.48}$$

$$= -T^* N_Q^{-1} \phi(z+z_0)^{-1}$$

where $T^* = T_m k^{-1} c_p^{-1} R_d P^{-1} Q V^{*-1}$ and is assumed constant with height in the surface layer.

The variation of potential temperature with height may be found by integrating equation (2.48) with respect to height obtaining

$$\theta - \theta_0 = \int_{\theta_0}^{\theta} d\theta = -T^* \int_0^z N_Q^{-1} \phi(z+z_0)^{-1} dz \tag{2.49}$$

where θ_0 is the potential temperature at the height z_0 and may be different from the actual surface temperature. θ is the temperature at the height $z + z_0$.

The two assumptions about N_Q will result in different forms of the integral with respect to height of $\phi N_Q^{-1}(z+z_0)^{-1} dz$. If $N_Q = 1$ then equation (2.49) becomes

$$\theta - \theta_0 = -T^* \int_0^z \phi(z+z_0)^{-1} dz \tag{2.50}$$

With the substitution of $\phi = 1 + (\phi - 1)$ equation (2.50) becomes

$$\theta - \theta_0 = -T^*[\ln(1 + z/z_0) + \Phi_T] \tag{2.51}$$

where Φ_T is the integral diabatic influence function for the temperature profile defined as

$$\Phi_T = \int_0^z (\phi - 1)(z + z_0)^{-1} dz. \tag{2.52}$$

For the case where $N_Q = 1$ we have $\Phi_T = \Phi_V$ and the wind and temperature profiles are similar.

From equation (2.49) for the case where $N_Q = 1/\sqrt{\phi}$ we have that

$$\theta - \theta_0 = -T^* \int_0^z \phi^{3/2}(z + z_0)^{-1} dz. \tag{2.53}$$

Letting $\phi^{3/2} = 1 + \phi^{3/2} - 1$, equation (2.54) becomes

$$\theta - \theta_0 = -T^* [\ln(1 + z/z_0) + \int_0^z (\phi^{3/2} - 1)(z + z_0)^{-1} dz] \tag{2.54}$$

where

$$\Phi_T = \int_0^z (\phi^{3/2} - 1)(z + z_0)^{-1} dz \tag{2.55}$$

and $\Phi_V \neq \Phi_T$. For this case the wind and temperature profiles are not similar to each other.

Because θ_0 the temperature at the height z_0 will not be known, equations (2.55) and (2.53) may be integrated between two heights z_1 and z_2 at which the potential temperatures θ_1 and θ_2 are known.

It is being assumed that at the boundary $\phi = 1$, $\underline{Ri} = 0$, $\Phi_V = 0$ and $\Phi_T = 0$ regardless of the two assumptions about the possible values of N_Q. The two choices of N_Q may be tested with data which includes independent measurements of the flux of sensible heat to the air from the surface provided the relationship between $\underline{Ri}$ and ϕ is correct.

The values of N and B in equation (2.39) are still open to question although the product NB has been established as approximately 18 (Lettau, 1962; Panofsky, et al. 1961). It has usually been assumed that $N_Q = 1$ at the boundary. If the flow is smooth rather than rough, it is possible for the limiting value of N at height zero to be the inverse of the Prandtl number (Pr), which is the ratio of the viscosity to the thermal diffusivity for air. 1/Pr is approximately 1.43 for air near the earth's surface (Sutton, 1953).

If the limit of N is 1.43 as $z \to 0$, then B should have a value of about 12.6 because, as has previously been established, $NB = 18$.

Nikuradse provides criteria for deciding if the flow is smooth or rough based on the idea that for rough flow the motion becomes virtually independent of viscosity. According to Nikuradse (Sutton, 1953), one should expect for

$z_0 V^*/\nu > 2.5$ rough flow, and for

$z_0 V^*/\nu < 0.13$ smooth flow.

For $z_0 \approx 0.03$ cm and with $\nu = 0.15$ cm^2/sec at an air temperature of 20 deg C, and $V^* = \sqrt{\tau_0/\rho} = 15$ cm/sec we have a value of $z_0 V^*/\nu = 3.0$ and the flow should be rough and the air motion independent of viscosity and the Prandtl number. Wind profiles are seldom measured below $V^* \approx 15$ cm/sec because the conditions are usually erratic in time. If the flow is rough, the limiting value of N as $z \to 0$ is open to question but, according to Sutton (1953), and Lumley and Panofsky (1964), the limiting value of N is 1 as $z \to 0$ or at the height z_0 above the surface.

3. Calculation and Application of Synthetic Wind and Temperature Profiles

It is possible to construct synthetic wind and temperature profiles in the surface layer by assuming an initial set of values for τ, Q, T_m, P, g, k, and z_0 for any displacement height including $d = 0$. The assumed initial values determine $1/L$ from equation (2.23). Additionally, an assumption is necessary about $K_h/K_m \equiv N_Q$. Then, the value of $\phi N_Q \underline{Ri}$ is determined at any $z + z_0$ from equation (2.26) assuming a constant mean temperature for the entire profile. Thus, it is possible to calculate ϕ at any z based on $\phi(1 - \phi^{-4})/B = -(z + z_0)/L$. In addition, $\Phi_V(z)$ and $\Phi_T(z)$ are determined from equation (2.47) and (2.52) or (2.55), respectively, with equations (2.49) and (2.51) used to obtain v and $\theta - \theta_0$ at any z. τ, Q, T_m, P, g and z_0 may be varied to construct profiles for different conditions.

Once the synthetic wind and temperature profiles have been determined, it is possible to calculate the height derivatives θ' and V' at any height in the surface layer in addition to difference quotients of θ and V over double levels. It is interesting to compare the difference quotients of θ and V to the height derivatives, θ' and V', at the same reference height given by equations (2.45) and (2.48). If the wind and temperature profiles are strictly logarithmic with height,

then the difference quotients calculated from double levels may be assigned to the geometric mean height with an error which depends only on the displacement height and z_0. From equation (2.1), we have that

$$V(z_2) - V(z_1) = (V^*)\, k^{-1} [\ln(z_2 - z_0) - \ln(z_1 - z_0)] \qquad (3.1)$$

so that $V' = [v(z_2) - v(z_1)/[z_2 - z_1])$ would be the wind shear determined from the profile measurements. The height at which this difference quotient would be valid, z_{12} would be

$$\ln(z_{12} + z_0) = [\ln(z_2 + z_0) + \ln(z_1 + z_0)]/2$$
$$= \ln[(z_2 + z_0)(z_1 + z_0)]^{1/2}. \qquad (3.2)$$

Therefore

$$z_{12} + z_0 = [(z_2 + z_0)(z_1 + z_0)]^{1/2} \qquad (3.3)$$

which is the geometric mean height of the two levels z_1 and z_2. If double levels are used for measurements such that $z_2 = 2z_1$ then

$$z_{12} + z_0 = (2z_1^2 + 3z_1 z_0 + z_0^2)^{1/2}. \qquad (3.4)$$

If z_0 is much smaller than z_1, equation (3.4) may be written as

$$z_{12} = (2z_1^2 + 3z_1 z_0)^{1/2} \approx 1.414 z_1 (1 + 0.75\, z_0/z_1). \qquad (3.5)$$

Thus, when a series expansion is considered, z_0 will alter the geometric mean height between two levels of measurement at which the difference quotient (which is taken as a substitute for the height derivative) would be valid if the logarithmic law holds true.

Given a z_0 value of 0.03 cm, equation (3.4) results in a geometric mean height of $z_{12} = 28.33$ cm for $z_1 = 20$ cm as compared to 28.28 for the geometric mean height calculated on the basis of $z_{12} = (z_1 \cdot z_2)^{1/2} = 28.28$. The height error is about 0.20 percent.

When a comparison is made between the actual gradient or height derivative at the geometric mean height, $z_{12} = (z_1 \cdot z_2)^{1/2}$, and the gradient or difference quotient calculated over double levels, $2z_1 = z_2$, the gradient determined from values of V or θ at z_1 and z_2 is about 2 percent smaller than the true gradient at the height $(z_1 \cdot z_2)^{1/2}$ for the above value of z_0.

If the parameter, for example wind or temperature, does not vary logarithmically with height, the error between the actual gradient at a height z_{12} and the determined gradient from the values at z_1 and

z_2 will vary with the departure from a logarithmic profile. If the curvature is less than logarithmic, then the determined gradient will be smaller. In addition, if there is a difference in curvature between the wind and temperature profile, then the measured gradients would be at different heights and there will be an error in the calculated values of Ri at the height z_{12}.

Calculations were made on synthetic profiles and the results are presented in Fig. 3.1 for $z_0 = 0.03$ cm. The ratio of the actual gradient at the geometric mean height to the gradient as determined from the double levels are graphed against the measured value of Ri for $N_Q = (\phi)^{-1/2}$. The value of Ri determined from differences in V and θ over double levels is used for comparison because it is nearly constant over the entire range of Ri and could be used to correct the difference quotient to the height derivative. If $z_2 = 4z_1$ rather than $z_2 = 2z_1$, the slope of V' (actual/measured) remains the same but the intercept at Ri = 0 will be different. This is shown in (3.4) where we would now have

$$z_{14} + z_0 = (4z_1^2 + 5z_1 z_0 + z_0^2)^{1/2} \tag{3.6}$$

which may be rewritten as

$$z_{14} = z_1(4 + 5z_0/z_1)^{1/2} \approx 2.0(1 + 0.62\ z_0/z_1) \tag{3.7}$$

assuming $z_0 \ll z_1$. Thus, it is apparent that the larger the height z_1, the smaller the influence of z_0 on the geometric mean height and also the greater the ratio of the height of the upper level to the height of the lower level the smaller the difference between equation (3.7) and $z_{14} = (z_1 z_4)^{1/2}$. One could use equation (2.45) and (2.48) to determine the actual height at which the measured gradient would apply as

$$z_{12} = \phi(z_2 - z_1)\{\ln[(z_2 + z_0)/\ln(z_1 + z_0)] + \int_{z_1}^{z_2} (\phi - 1) z^{-1} dz\} \tag{3.8}$$

However, this method has the disadvantage that the temperature profile and wind profile might have different heights for the value of the measured gradient. Therefore, the procedure selected was to correct the measured gradient to the actual gradient at the geometric mean height by the relationship between Ri measured and the ratio of actual to measured gradients shown in Fig. 3.1.

The possible effect of averaging wind speed and air temperature profiles over periods of time when the stress τ and the sensible heat flux Q are varying with respect to time must be considered and may

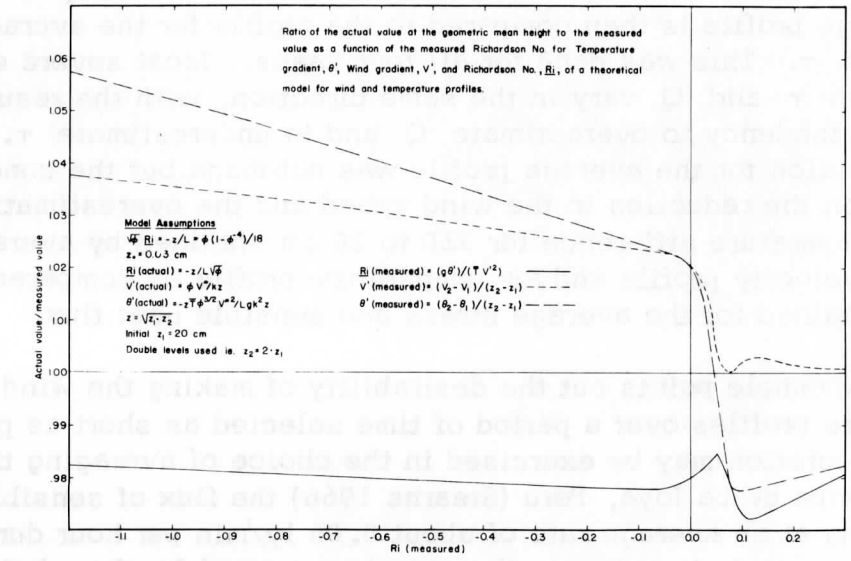

Fig. 3.1. The ratio of the actual gradient (θ', V') at the geometric mean height to the value determined from differences over double levels varies as $\underline{Ri}$ calculated over the double levels. This relationship may be used to correct the difference quotients of θ', V' as determined by differences over double levels to the height derivative at the geometric mean height.

be checked by the use of synthetic profiles. The results of such a comparison are given in Table 3.1 for four examples: Q varying, τ varying, and both τ and Q varying in the same and in opposite directions. The method used was to generate synthetic wind speed and air temperature profiles based on the model assumption that $N_Q = 1/\sqrt{\phi}$ and B = 18 for several values of Q and τ. The wind speed and air temperature obtained at each level are averaged for the two profiles which then represent the mean of wind and temperature. The average profile is then compared to the profile for the average of the Q and τ. This was done for all four cases. Most severe effects occur when τ and Q vary in the same direction, with the result that there is a tendency to overestimate Q and to underestimate τ. The actual solution for the average profile was not made but the conclusion is based on the reduction in the wind speed and the overestimation of the air temperature difference for 320 to 20 cm obtained by averaging the wind velocity profile and air temperature profile as compared to the profile obtained for the average stress and sensible heat flux.

This example points out the desirability of making the wind and temperature profiles over a period of time selected as short as possible so that discretion may be exercised in the choice of averaging times. On the Pampa de La Joya, Peru (Stearns 1966) the flux of sensible heat is changing at an average rate of about 0.06 ly/min per hour during the afternoon and, in general, the averaging period for the wind and temperature profiles was one half-hour. The variation of τ with time would not be as predictable but the tendency to decrease in the afternoon would be expected and was observed. Since both τ and Q are decreasing with time Q would be overestimated from the wind and temperature profile, but the overestimation of Q would have been reduced if averaging periods of about 10 instead of 30 min would have been used.

4. Determination of the Displacement Height and $\ln z_0$

It should be kept in mind that the practical information ultimately desired from the measurement of wind and temperature profiles is the surface stress τ_0 and the sensible heat flux Q_0. The first problem encountered after installation of the instruments at a micrometeorological site is to determine the exact height of the instruments relative to the aerodynamic reference level $z = 0$ at which the boundary condition $V = 0$ is satisfied. The importance of the height of the aerodynamic reference level may be seen in Figs. 4.1 and 4.2 which show the variation of τ and Q with displacement height. The height of the instruments above the local terrain can be directly measured with a precision of $\pm$ 0.5 cm. However, there is no reason to believe that the physical

TABLE 3.1. The effect of averaging the wind speed ($\bar{V}$, cm/sec) and air temperature (T, deg C) profiles over periods of time when the stress (τ, dynes/cm^2) is constant and the sensible heat flux (Q, ly/min) varies, Q constant and τ varies and with both varying is demonstrated by the use of synthetic wind and air temperature profiles. If both v^* and Q_0 vary over the averaging period an overestimate of τ and Q will be made.

τ constant (1.58 dynes/cm^2)

z cm	Q_0=0.36 V	Q_0=0.12 V	Average $\bar{V}$	Q_0=0.24 V	Difference ΔV
320	484	512	498	496	2
160	464	484	474	473	1
80	439	451	445	444	1
40	409	416	413	412	1
20	375	378	376	376	0
		$V_{320} - V_{20}$	122	120	
	T	T	$\bar{T}$		ΔT
320	18.48	15.87	17.18	17.12	0.06
160	19.06	16.18	17.62	17.58	0.04
80	19.81	16.54	18.17	18.17	0.00
40	20.78	16.95	18.86	18.89	-0.03
20	21.94	17.39	19.67	19.71	-0.04
		$T_{320} - T_{20}$ -	-2.49	-2.59	

Effect on τ and Q small

τ and Q varied in same direction

	τ=1.73 Q_0=0.36 V	τ=1.41 Q_0=0.12 V	Average $\bar{V}$	τ=1.58 Q_0=0.24 V	Difference ΔV
320	600	372	486	496	-10
160	570	359	464	473	- 9
80	535	342	438	444	- 8
40	495	321	408	412	- 4
20	452	297	374	376	- 2
		$V_{320} - V_{20}$	112	120	
	T	T	$\bar{T}$	T	ΔT
320	20.77	15.35	18.06	17.12	0.94
160	21.38	15.88	18.63	17.58	1.05
80	22.19	16.59	19.37	18.17	1.20
40	23.09	17.53	20.31	18.89	1.42
20	24.16	18.73	21.45	19.71	1.74
		$T_{320} - T_{20}$	-3.39	-2.59	

τ underestimated, Q_0 overestimated by 50%.

Q_0 Constant (0.24 ly/min)

τ=1.73 V	τ=1.41 V	Average $\bar{V}$	τ=1.58 V	Difference ΔV
611	382	496	496	0
578	367	472	473	-1
540	348	444	444	0
498	325	411	412	-1
453	299	376	376	0
$V_{320}-V_{20}$		120	120	
T	T	$\bar{T}$	T	ΔT
18.73	14.93	16.83	17.12	-0.29
19.21	15.30	17.25	17.58	-0.33
19.79	15.92	17.85	18.17	-0.32
20.47	16.65	18.56	18.89	-0.33
21.21	17.54	19.37	19.71	-0.34
$T_{320} - T_{20}$		-2.54	-2.59	

Effect on τ and Q small

τ and Q varied in opposite direction

τ=1.75 Q=0.12 V	τ=1.41 Q=0.36 V	Average $\bar{V}$	τ=1.58 Q=0.24 V	Difference ΔV
626	373	500	496	4
588	359	473	473	0
546	342	444	444	0
501	321	411	412	-1
454	297	375	376	-1
$V_{320} - V_{20}$	125	120		
T	T	$\bar{T}$	T	ΔT
16.75	15.35	16.05	17.12	-1.07
17.05	15.88	16.47	17.58	-1.11
17.39	16.59	16.99	18.17	-1.18
17.77	17.53	17.65	18.89	-1.24
18.15	18.73	18.44	19.71	-1.27
$T_{320} - T_{20}$	-2.39	-2.59		

Effect on τ small, Q_0 slightly underestimated.

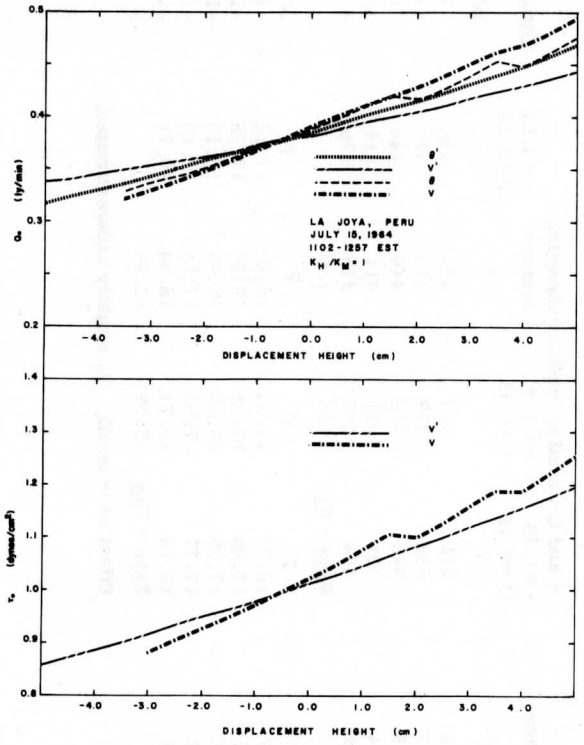

Fig. 4.1. τ's and Q's as a function of displacement height for $N_Q \equiv K_h/K_m = 1$. The importance of the correct displacement in the determination of τ and Q is obvious.

Fig. 4.2. τ's and Q's as a function of displacement height for $N_Q = 1/\sqrt{\phi}$.

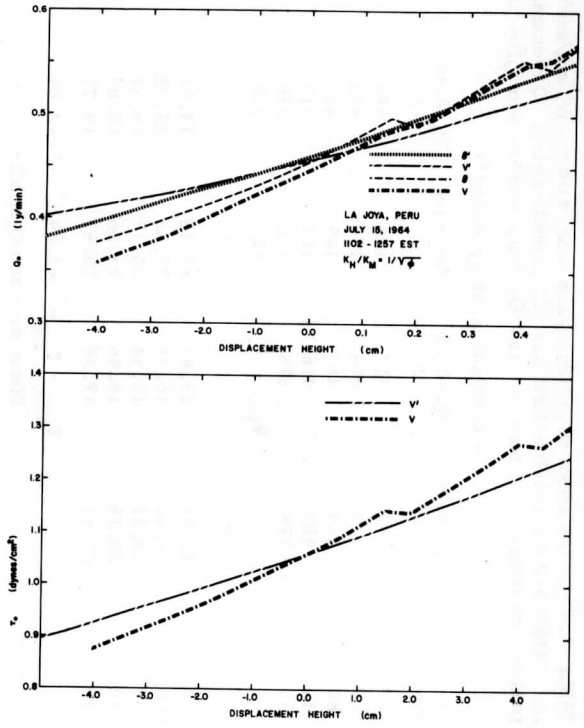

interface between the soil and the air coincides with the aerodynamic reference level. Furthermore, it is generally assumed that for any given mean time the approach to $V = 0$ as $z \to 0$ follows simplified mathematical laws of representative profile structure, such as the logarithmic law for the adiabatic surface layer and reality may not be as simple as the mathematical law. Therefore, a displacement height d must be introduced into the equations to allow for a correctional height adjustment of the wind and temperature profile. Equation (2.1) would now be written as

$$V_a = k^{-1} (V^*) \ln[1 + (z+d)/z_0] \tag{4.1}$$

or letting $D = d + z_0$

$$V_a = k^{-1} (V^*) \ln[(z+D)/z_0]. \tag{4.2}$$

The change of variable, $z+D$ for $z+z_0$, will be carried out for all equations involving height.

The diabatic surface layer theory and consequent reconstruction of the wind and temperature profile will provide a method of determining the most appropriate values of the parameters D, z_0, Q and τ within the limitations of the theory and the data. The method is based on an error squares fit between the theoretical profile and the actual profile of wind and temperature. Those parameter values may be selected for which the sum of the error squares is a minimum. The application of this method was introduced by Lettau (1957b) using the logarithmic wind profile to determine D and z_0 and was refined for electronic computer operation by Robinson (1961).

The first step is to decide if all the measurement levels on the profiles are in the surface layer. Assuming that $T^{1/2} \approx T_m^{1/2}$ and replacing $z + z_0$ with $z + D$, equation (2.26) is used to determine $-1/L$. Ri is calculated from the wind and temperature profile at the available levels and corrected for an estimate of the departure from the actual value at the geometric mean height of the two levels used to determine Ri. The necessity for this correction was presented in the previous section. Based on the previously proposed models we are left with a choice of $N_Q \equiv K_h/K_m = N$ or $N_Q = N/\sqrt{\phi}$ where $N = 1$, $B = 18$ or $N = 1.47$ and $B = 12.6$ or other possible relationships. The above relationships would also affect the correction of Ri determined from differences of wind and temperature to the value of Ri determined from the height derivatives of wind and temperature at the geometric mean height. Due to uncertainties in the available measurements, and consequently, the determination of Ri, a clear-cut decision cannot be made at the present time about the constancy of $1/L$ with

height, on the choice of models or of the height of the surface layer. The errors in the determination of $\underline{Ri}$ will be discussed in the next section.

From equation (2.25) a value of ϕ may be approximated and $-1/L$ determined from equation (2.26) for each measurement of $\underline{Ri}$. If, as the height at which Ri is measured increases, the value of $\phi N_Q Ri/(z+D) = -1/L$ departs by more than a desired amount in keeping with the possible errors in $\underline{Ri}$, that level and higher levels should be rejected as not fitting the proposed model and only possibly being outside the surface layer. The departure of $-1/L$ from being constant with height could also be due to other reasons such as poor instrument exposure rather than not being in the surface layer or where the model is valid. Often the top anemometer on a profile mast will read high because its exposure may differ from that of the other anemometers, especially if it does not have the supporting mast behind the cups.

We will now assume that $-1/L$ has been determined as the average value of several determinations from the available and usable data. Then, with a chosen value of D it is possible to calculate $\underline{Ri}$ and ϕ at any level where wind and temperature have been measured or where a height derivative of wind and temperature has been determined.

Employing equation (2.26) in the form $\phi(1-\phi^{-4})/B = -(z+D)/L$, it is possible to obtain ϕ at the desired height $z+D$ if B is known. Introducing ϕ into equation (2.45), $\tau = (V^*)^2/\rho$ can be calculated from wind data at each level where an estimate of V' is available. The several estimates of τ at a given time may be averaged and the average error squares determined. Since the mean value of τ is changing with D a minimum error squares will not necessarily correspond to the best fit between the data and the model. Therefore, the average error square is divided by the mean value times 100 percent to obtain a relative error square, or more simply a relative error, on which to judge the fit between the data and the model.

In a corresponding manner, equation (2.48) is solved for Q using the value of τ obtained above. The several values of Q obtained by the above method from τ and the θ's may be averaged and the relative error $\sigma(\theta')$ calculated to again provide an estimate of the fit between theory and the actual temperature gradient data.

It should be noted that having determined $-1/L$ it is possible to use the above value of τ to determine another value of Q from the defining equation for L. It would be pointless to calculate another value of τ by using Q determined from equation (2.48) as agreement between the two values of Q is sufficient to determine the differences between the two methods. Figures 4.1 and 4.2 give

a comparison between the two Q's for one profile. If the theoretical model, the choice of D, and the data are correct, then the two values of Q should be in agreement.

The corresponding procedure can be followed using the integrated forms of equations (2.45) and (2.48). The integral diabatic influence function $\Phi_V(z+D)$ cannot be calculated explicitly so the value of $\Phi_V(z+D)$ at a height $z + D$ was obtained by summing $(\phi-1)/(z+D)$ from z_0 to $z + D$ by the equation

$$\Phi_V(z+D) = \Phi_V(z+D-\Delta z) + \{[\phi(z+D)-1]/(z+D) + [\phi(z+D-\Delta z)-1]/(z+D-\Delta z)\}\Delta z/2. \quad (4.3)$$

Δz is chosen small enough so that errors in $\Phi_V(z+D)$ are below one percent with $\Phi_V = 0$ at $z = 0$.

Having obtained a value of Φ_V at height $z + D$, it is possible to solve for τ using equation (2.47) and a selected value of z_0 for the profile.

The average τ determined at several levels is obtained and the relative error $\sigma(V)$ calculated. Notice that $\ln z_0$ now enters into the determination of τ which in this case is a function of both D and z_0.

Once a mean value of τ is obtained, an estimate of Q may be determined from the integrated equation (2.51) for the temperature profile. $\Phi_T(z+D)$ is calculated in a manner similar to $\Phi_V(z+D)$ in equation (4.3).

Q is determined from the available level of air temperature measurement using the average value of τ determined from the integrated form for the wind profile. θ_0 is the potential temperature at the boundary where $V = 0$ and is not directly measurable. Therefore, the equation must be altered by consideration of a reference level where the air temperature is known. This could be chosen as the lowest level at which the air temperature is actually measured, which will be referred to as z_1, and then successively higher levels as z_n. Solving for Q, equation(2.52) now becomes

$$Q = k c_p R_d^{-1} P T_m^{-1} V^*[\theta(z_1+D) - \theta(z_n+D)]/\{\ln[(z_n+D)/(z_1+D)] + \Phi_T(z_n+D) - \Phi_T(z_1+D)\} \quad (4.4)$$

The values of Q, corresponding to one less than the number of levels of valid temperature measurement, may be averaged and the relative error $\sigma(\theta)$ computed. Using the same value of τ it is possible to use the defining equation for L to again obtain a fourth estimate of Q. A comparison between the Q's estimated by the above method is seen in Fig. 4.1 and 4.2.

In summary, we now have two values of τ, one derived by a method which depends only on D, the other on D and z_0. Using these values of τ we obtained four values of Q, two of which depended only on D, and the other two on D and z_0. It should be remarked that z_0 is a site parameter, which should not depend on the equipment used or the displacement height. The zero point displacement D however relates exclusively to the arbitrary installation of the mast equipment and may be influenced by the upwind terrain. The problem is to determine both D and z_0 from actual profile measurements.

The relative error is not necessarily a minimum at the same value of D for the temperature gradient, wind gradient, the wind speed and air temperature. The method of determining the best fit simultaneously for all values was to select initial values of D and z_0. The computations involving only D are performed, and then $\ln z_0$ is changed in preselected increments from an initial value large enough so that the relative error decreases with each successively decreasing value of $\ln z_0$. The intervals were chosen small enough so that the values of τ did not change more than 2 percent with each step in $\ln z_0$. When the relative error of the mean τ calculated from V starts to increase as $\ln z_0$ is decreased, the value of D was decreased by one step and the calculation process started over again until a sufficiently wide range of D values was covered. In practice, D was stepped in increments of 0.5 cm while the increment in $\ln z_0$ was 0.1 neither of which greatly changed the values of τ and Q from one step to the next.

Finally, that particular D value was selected for which the relative error of τ calculated from equation (2.45) and (2.47) was an absolute minimum. A similar procedure was followed for Q from equation (2.48) and (2.51). In general, the relative error $\sigma(V)$ calculated from the wind velocity, showed a minimum for a D value within ± 1 cm of that calculated from V'. If the theory and the data were correct, then all methods for calculating τ and Q from absolute and gradient values of V and θ would have a minimum relative error at the same D value. The value of τ, selected on the basis of $\sigma(V)$ a minimum, would provide an estimate of both D, $\ln z_0$ and Q. In addition, the two values of τ should be in agreement as likewise would the four values of Q. Naturally, this ideal

situation is not realized in practice. There are certain limitations on this expectation, some of which shall be discussed in the next section.

In Figs. 4.1 and 4.2, it may be seen that where the values of Q and τ are in agreement, at a D of about -0.75 cm, the magnitudes of $\sigma(V)$, $\sigma(\theta)$, $\sigma(V')$ and $\sigma(\theta')$ given in Fig. 4.3 and 4.4 are also near their minimum value. A second criterion which might be used to determine the fit between theory and data is to select those values of D and $\ln z_0$ for which the differences between the τ's and the Q's is the least. This does not provide a direct measure of the fit between the theoretical model and the actual data but perhaps in the future the above method could be used as an additional check on the agreement between the theoretical model and the actual data. In Figs. 4.1 and 4.2, it appears that near the displacement height for which the σ's are a minimum, the τ's and Q's are also most nearly in agreement.

A computer program was written which uses as input the measured air temperature and wind speed data at the nominal heights above the surface and produces a measure of the fit between the data and a selected theoretical model of profile structure, such as the KEYPS model. Corrections were applied to the measurements of the gradients of wind and temperature on the basis of Fig. 3.1. For each of a variety of assumed displacement heights the computer output consisted of the following:

a. The original data

b. The values of Ri, DEU and DET computed from difference quotients using observed data at the available levels.

c. The theoretical values of Ri, DEU and DET from the selected theoretical model at the same heights as b.

d. The stress τ and the sensible heat flux Q calculated from the gradients of potential temperature and wind speed, including the relative error for each.

e. The stress τ and the sensible heat flux Q calculated from the absolute value of the wind speed and the potential temperature for the selected values of $\ln z_0$ together with the relative error for each.

An initial displacement height of 5 cm is chosen which then is decreased by small increments of height, such as 0.5 cm, until a final value of -5.0 cm is reached. For each displacement height, the value of $\ln z_0$ is systematically varied starting at -2.0 and changing by increments of 0.1 until a value of -4.0 is reached. The process may

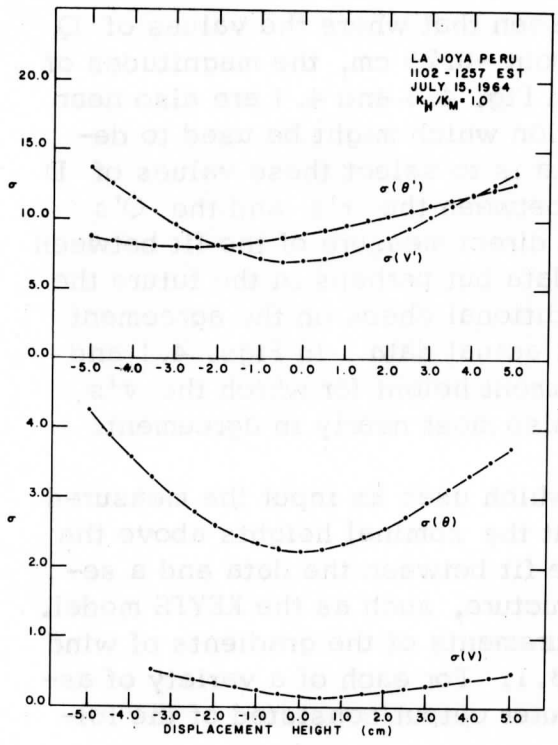

Fig. 4.3. Relative error (σ, %) for τ determined from V and V' and for Q determined from θ and θ' as a function of displacement height illustrating the minimizing of $\sigma(V)$, $\sigma(V')$, $\sigma(\theta)$ and $\sigma(\theta')$ for $N_Q \equiv K_h/K_m = 1$.

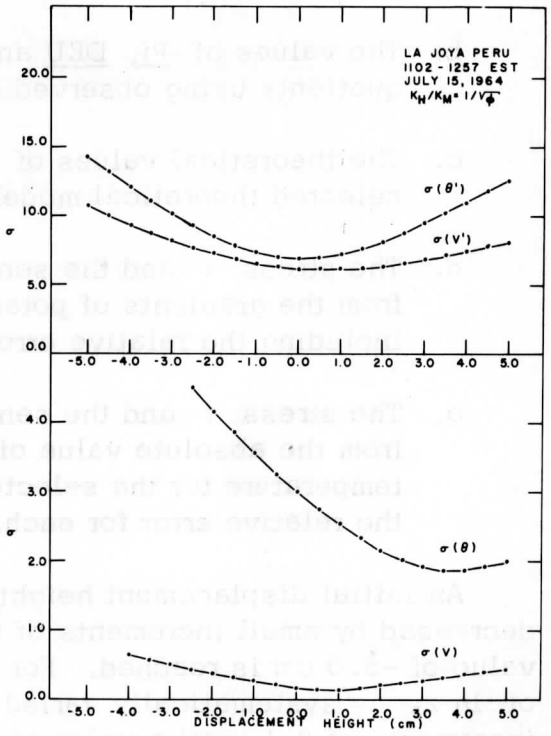

Fig. 4.4. The relative error (σ, %) for τ and Q determined as in Fig. 4.3 with $N_Q \equiv K_h/K_m = 1/\sqrt{\phi}$.

be terminated if the relative error $\sigma(V)$ of τ has reached a minimum value and starts to increase. Then the displacement height is decreased by another step and the process starts over. The initial, incremental change, and final values of both displacement height and $\ln z_0$, including the value of the constant B for the theoretical model, are indicated on the first card read into the computer. The output is quite voluminous, but this extensive method was chosen so that the manner in which the profiles behaved could be inspected in detail. Once the method of minimizing relative errors is understood, it is always possible to restrict the output to those values which represent an actual minimum.

The minimizing of $\sigma(V)$, $\sigma(\theta)$, $\sigma(V')$ and $\sigma(\theta')$ as the displacement height is varied is shown in Fig. 4.3 and 4.4. The value of $\ln z_0$ selected is for the minimum value of $\sigma(V)$ in the sequence of $\ln z_0$, at a given value of D.

The range of $\ln z_0$ may be unknown before the analysis of the data and since the output is extensive it may be desirable to have a better estimate of $\ln z_0$. An apparent "$\ln z_0$" may be obtained by assuming that adiabatic conditions exist and the displacement height is 0. Then

$$\text{"}\ln z_0\text{"} = \ln z_0 - 1/\alpha \qquad (4.5)$$

where α is the profile contour number for wind (Lettau, 1957c). The values thus obtained may be graphed against $\underline{Ri}$ as was done in Fig. 4.5. Extrapolation of the data to $\underline{Ri} = 0$ results in a range of $\ln z_0$ between -2.0 and -4.0 for the Pampa de La Joya, Peru data.

The importance of knowing the proper displacement height is illustrated in Fig. 4.1 and 4.2 where the values of τ and Q are graphed against the variety of chosen D-values. Figure 4.1 is for the theoretical model where $N_Q = 1$ and seems to provide better agreement between the τ's for this set of data than Fig. 4.2 where $N_Q = 1/\sqrt{\phi}$ and ϕ is the diabatic influence function. Since the relative error is calculated from six values of V, five values of V', and four values for θ and θ', a single error in measurement could change drastically the point at which a minimum is obtained. The data above the 160 cm level on the profile was not used as it often failed the test of a constant L as has previously been mentioned. The data presented in Figs. 4.1 and 4.2 is for a wind and temperature profile on the Pampa de La Joya, Peru, for July 15, 1964, from 1102 to 1257 EST and is the average of 8 ten-minute profiles spaced five minutes apart in time.

Figure 4.5 illustrates the variation of $\sigma(V)$ versus $\ln z_0$ for three displacement heights, 5.0, 1.0, and -3.0 cm. $\sigma(V)$ is a minimum for D = 1.0 cm and $\ln z_0 = -2.9$. Values are not available after $\sigma(V)$ started to increase because another value of D was selected to

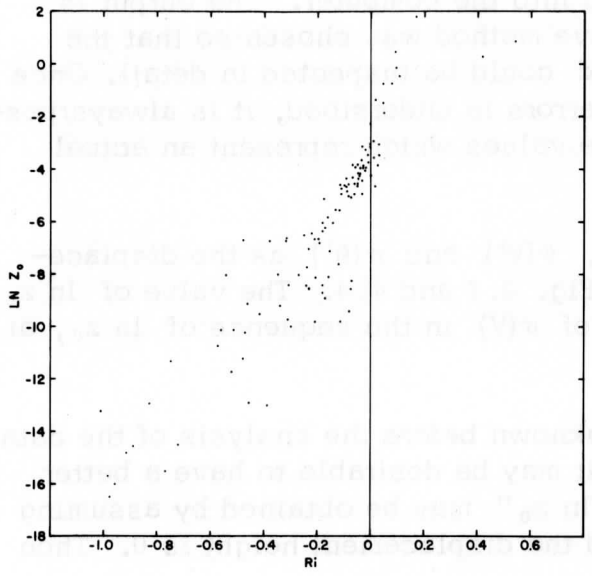

Fig. 4.5. The apparent "ln z_0" as a function Ri for wind and temperature profile data collected in July 1964, on the Pampa de La Joya, Peru. The apparent "ln z_0" is calculated on the assumption that the wind profile is adiabatic. The range of ln z_0 at Ri = 0 is between -2.0 and -4.0 which corresponds to a possible z_0 range of 0.019 to 0.14 cm.

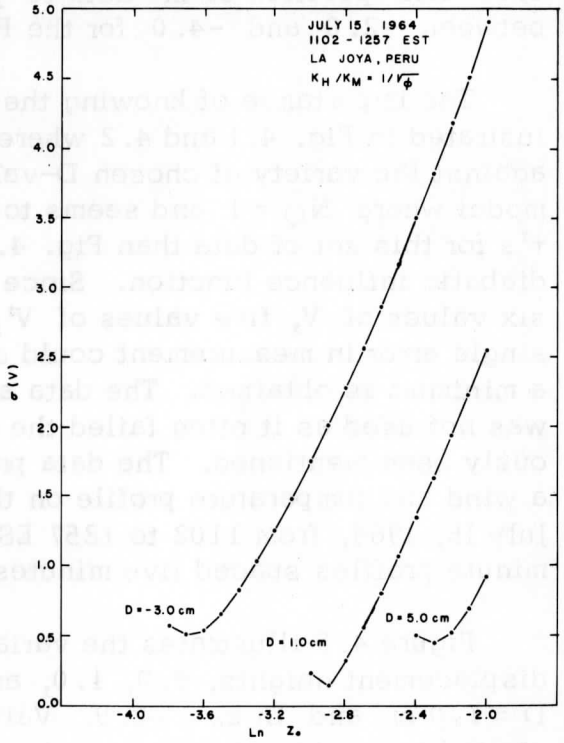

Fig. 4.6. Comparison between the relative error, σ(V), for τ and ln z_0 for three displacement heights. σ(V) was a minimum for ln z_0 = -2.9 which would then be considered the most nearly correct value. The resulting value of z_0 is 0.055 ± 0.005 cm.

prevent the accumulation of unnecessary information.

The particular wind and temperature profile used as an example was judged to be one of the best taken on the Pampa de La Joya, Peru, in view of the agreement between the D values for the minimum relative error, while the absolute values of the relative error were among the lowest. The conditions for the flux of sensible heat to the air and the variation of the wind and temperature during the period of measurement were as nearly uniform as could possibly be obtained during the daytime.

The criterion for selecting a particular displacement height and subsequently, the value of $\ln z_0$, for the other profiles was a minimum relative error of τ calculated from the wind speed. The other errors minimize in the same vicinity for apparently good profiles and often $\sigma(V)$ and $\sigma(V')$ are minimum at displacement heights within 1 cm of each other. This procedure provides an estimate of both $\ln z_0$ and D. The value of τ used is the average of the τ's determined from V and V' and the Q is the average of the four Q's determined from θ, θ', $-1/L$ and τ.

5. Errors in the Determination of Ri, DEU and DET

The accurate determination of Ri is necessary for the calculation of $-1/L$ by means of equation (2.22) and ϕ by equation (2.26). Ri is dependent only on the difference in height between the sensors from which the gradients are determined and not on the absolute height. However, it should be remembered that $-1/L$ is dependent on height and thus will vary with the displacement height.

The differences in level for measurement of wind speed can be determined to better than 2 percent for height differences of 20 cm or more. The assumed error in wind speed at any one level will be $\pm$ 1 cm/sec which is the best that can be obtained by the type of anemometer used in Peru. This gives an error in speed differences between double levels of 2 percent or more for the level used and the maximum measured speed differences of about 50 cm/sec for double levels.

The height differences of the temperature sensors can again be determined to 2 percent or better but this does not guarantee that the temperature element is on the isotherm which is actually at the measured level of the sensor in the atmosphere. Since $\Delta T'$s are measured, the assumed resolution of air temperature difference measurement will be that of the recording system or $\pm$ 0.015 deg C. The

actual temperature data used for the wind profiles are means of several values taken at discreet intervals and it would be more proper to use the standard deviation of the sample as an indication of the error. This would have the advantage of determining the error in temperature in terms of the sensed fluctuations which are larger than the resolution of the temperature sensing system. The use of the resolution of the temperature system does put a lower limit on the error of any parameter calculated by the use of temperature data. As an example a sample of 20 values one minute apart in time of air temperature differences for the 40 to 20 cm levels during the period of 1200 - 1200 EST July 15, 1964, on the Pampa de La Joya, Peru, resulted in a standard deviation of 0.10 deg C which is about six times as large as the resolution of the recording system. It now appears advisable to calculate the standard deviation for any mean value of an atmospheric variable such as air temperature, which is the mean of several discreet measurements, so that an estimate of the error of the mean value of the sample is available. The wind recording system which totals the anemometer cup revolutions rules out the calculation of a standard deviation for a wind speed.

The resolution in the absolute value of T_m, the mean temperature of the profile, will be taken as ± 0.1 deg C. This is the resolution of the diode thermometer used to determine the absolute temperature.

Logarithmic differentiation of equation (2.25) yields

$$d \ln \underline{Ri} = - d \ln T_m + d \ln \theta' - 2 \, d \ln V' . \tag{5.1}$$

Using, as an example, the mean profile of wind speed and air temperature for the period 1102 to 1257 EST, July 15, 1964, La Joya, Peru, the errors in Ri at 40 and 80 cm nominal height are calculated assuming the maximum possible error. That is, the wind speed is 1 cm/sec high at one level and 1 cm/sec low at the other level. The same is true for the error in temperature. Since the sign of the error is arbitrary, the direction chosen will be such that the error is maximum in d ln Ri.

The error in DEU and DET due to an error in the absolute value of the height may be seen in Fig. 5.1 and 5.2. The error in Ri, DEU and DET due to errors in measurements are presented in Table 5.1. The largest contribution to the error in Ri is the possible error in the wind speed difference and the total error is more than 5 percent of the value of Ri. These errors are on the conservative side so it should be apparent that a single value of Ri is not to be trusted. The error in DEU is more than 10 percent of the determined value based on the error in the wind speed.

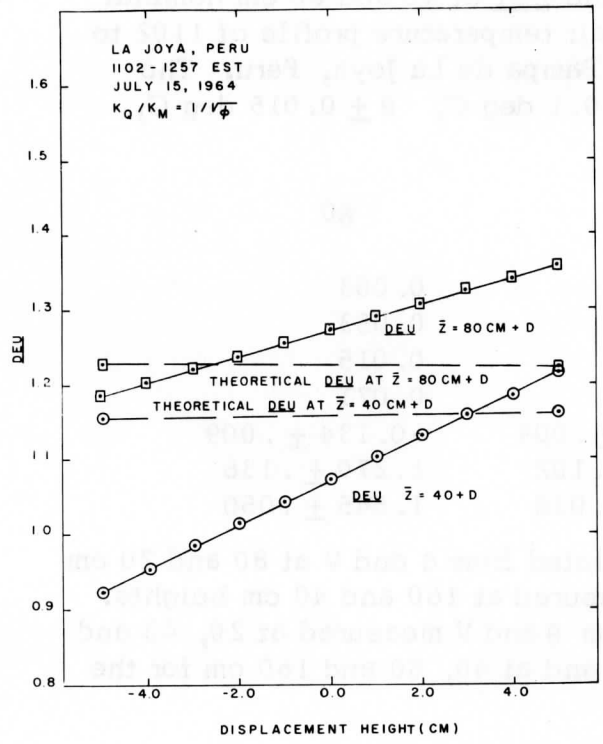

Fig. 5.1. DEU as a function of displacement height. The theoretical value of DEU is obtained from a theoretical model which assumes $N_Q \equiv K_h/K_m = 1/\sqrt{\phi}$, at the height z + D.

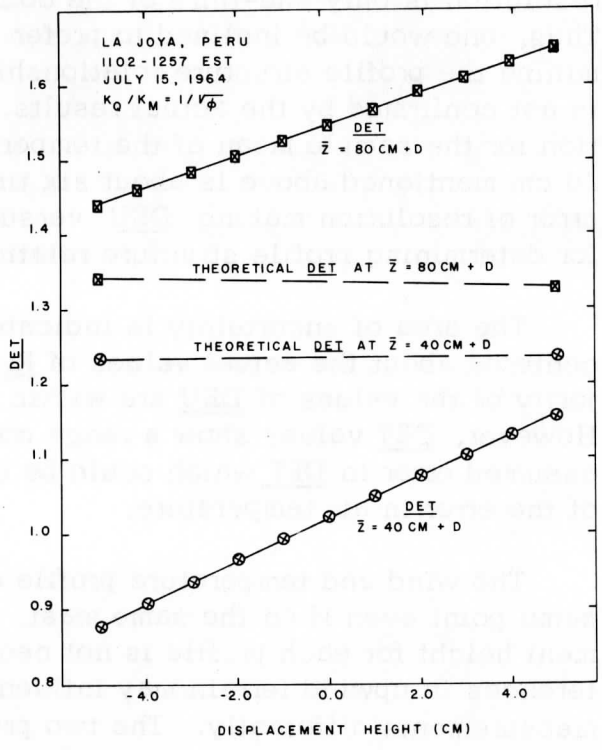

Fig. 5.2. DET as a function of displacement height. The theoretical value at the height z + D is based on the assumption that $N_Q = 1/\sqrt{\phi}$. If $N_Q = 1$ had been assumed then DET = DEU at z + D.

TABLE 5.1. Errors in Ri, DEU and DET at 40 and 80 cm nominal heights for the wind speed and air temperature profile of 1102 to 1257 EST July 15, 1964, on the Pampa de La Joya, Peru. The errors in measurement are $T_m \pm 0.1$ deg C, $\theta \pm 0.015$ deg C, and $V \pm 1$ cm/sec.

z(cm)	40	80
$d(\ln T_m)$	0.003	0.003
$2d(\ln V')$	0.047	0.053
$d(\ln \theta')$	0.013	0.015
$d(\ln Ri)$	0.063	0.071
Ri	$-0.064 \pm .004$	$-0.134 \pm .009$
DEU	$1.069 \pm .102$	$1.270 \pm .136$
DET	$1.018 \pm .038$	$1.545 \pm .050$

Ri for the 40 cm height is calculated from θ and V at 80 and 20 cm while for 80 cm θ and V are measured at 160 and 40 cm heights. DEU and DET are calculated from θ and V measured at 20, 40 and 80 cm for 40 cm nominal height and at 40, 80 and 160 cm for the 80 cm nominal height.

The error in DET due to the limitation in temperature difference resolution is only one-third of the corresponding error in DEU. Thus, one would be inclined to prefer DET versus Ri for determining the profile structure relationship. However, this reliability is not confirmed by the actual results. In fact, the standard deviation for the sample mean of the temperature difference from 40 to 20 cm mentioned above is about six times greater than the assumed error of resolution making DEU versus Ri a slightly better choice for determining profile structure relationships.

The area of uncertainty is indicated on Fig. 6.1 as a rectangle centered about the actual values of Ri and DET or DEU. The majority of the values of DEU are within the range of error assumed. However, DET values show a range considerably larger than the assumed error in DET which could be due to the underestimation of the error in air temperature.

The wind and temperature profile equipment cannot be at the same point even if on the same mast. Therefore, the displacement height for each profile is not necessarily the same, as differences in upwind terrain may influence the separate profile measurements differently. The two profiles are combined in determining Ri from the several levels of measurement, and are

assumed to be at the same relative levels. It is not easy to change the heights of the profiles of wind and temperature relative to each other and this was not attempted although the calculation of Ri will be strongly affected particularly at the lower profile levels where DET and DEU are rapidly changing with height.

The minimum relative error for V, θ, V' and θ' can be used to determine an appropriate displacement height for each profile separately. This was done for the data taken from 1102 - 1257 EST, July 15, 1964, on the Pampa de La Joya, Peru, for each of the eight profiles and for the mean of the profiles. The wind mast was approximately 10m from the temperature mast during the above measurements. The results are summarized in Table 5.2. The displacement height for the wind profile as determined from the minimum of $\sigma(V)$ does not significantly differ from the displacement height for the temperature profile based on $\sigma(\theta)$, a minimum, nor does the average displacement height determined as the mean for the several profiles differ significantly from the displacement height of the mean profile.

TABLE 5.2. Displacement height (D, cm) for minimum relative error for τ determined from wind speed (V, cm/sec) and wind shear (V', 1/sec) and for Q determined from the potential temperature (θ, deg C) and the potential temperature gradient (θ', deg C/cm) for several wind and temperature profiles recorded on July 15, 1964, on the Pampa de La Joya, Peru.

EST	V	V'	θ	θ'
1102-1112	6.5	5.5	4.0	1.5
1117-1127	1.0	3.0	-1.0	-3.5
1132-1142	-1.0	-0.5	0.5	-2.0
1147-1157	-0.5	0.5	1.5	-1.0
1202-1212	-2.5	-3.0	0.0	-3.0
1217-1227	-3.0	-3.5	-2.0	-5.0
1223-1242	-1.0	-0.5	1.0	-2.0
1247-1257	1.5	1.0	-4.0	-
Average	0.1	0.4	0.0	-2.1
1102-1257	0.5	-0.5	0.0	-3.0
Difference	-0.4	-0.8	0.0	0.9

A significant error in displacement height may be considered one which would cause an error of more than 2 percent in the values of Q and τ. This corresponds to a range of about $\pm$ 0.5 cm in the displacement height. No attempt was made to displace the wind and temperature masts relative to each other because of the absence of an apparent

systematic error in height between the two masts.

6. Results of Wind and Temperature Profile Analysis

Let us require that $\sigma(V)$ be a minimum for determining the displacement height D of both the wind and temperature profile, and of $\ln z_0$ for the wind profile. Subsequent values of τ and Q are obtained as the mean of the two τ's and four Q's determined at the selected D and $\ln z_0$. The results are given in Table 5.3.

Ri, DEU and DET for the 40 and 80 cm nominal heights are presented in Fig. 6.1 in comparison with the theoretical relationships between Ri and DEU or DET for the two theoretical model assumptions of $N_Q = 1$ and $1/\sqrt{\phi}$, with B = 18. Figure 6.2 reveals only a slight difference, averaging about 0.5 cm, in D determined by the two theoretical models with $N_Q = 1$ yielding the lower value. This difference in D due to the two model assumptions will cause only a negligible error (of approximately 1%) in DEU or DET as may be seen in Fig. 5.1 and 5.6. There seems to be a systematic difference between the 40 and 80 cm values for DET in Fig. 5.2 and 6.1 as the 40 cm values appear low and the 80 cm values high in comparison with the theoretical relationship. This could possibly be caused by an error in height differences. An attempt to correct for such an error was made but was not successful since lapse and inversion conditions produced inconsistent results. This problem will be discussed in greater detail later in this section.

The scatter of points on Fig. 6.1, even after the careful selection of the displacement height, does not permit us to decide which of the two theoretical models provides the better fit. Averages would have to be obtained over much longer periods of time during which Ri tended to remain constant. Actually, Ri is seldom at one particular value for more than a few minutes. This means that the averages would have to be of several runs at selected class interval for Ri or possible $-1/L$, which is related to the slope of Ri with respect to height, and a theoretical model assumption. Lettau (1962) maintains that the empirical relationship between the scaling factor Ri and the shape factors such as DEU or DET is by far the best and most unbiased basis for testing theoretical model assumptions about the wind and temperature structure in the diabatic surface layer. The practical difficulties in the testing of a theoretical model are evident in the measurement error in Ri and DEU or DET for the data collected on the Pampa de La Joya, Peru.

TABLE 5.3. Displacement height (D, cm), $\ln z_0$, stress (τ, dynes/cm^2), sensible heat flux (Q, ly/min) determined from the wind and temperature profile, sensible heat flux (Q_0 ly/min) determined from the heat budget, relative error ($\sigma(v)$, %), of τ determined from the wind speed ($\sigma(v)$, %), and relative error ($\sigma(\theta)$, %) of Q determined from the temperature profile for those wind and temperature profiles which could be solved assuming $N_Q \equiv K_h/K_m = 1$ and $1/\sqrt{\phi}$ using B = 18. The data was obtained on the Pampa de La Joya, Peru, during July, 1964.

			D		$\ln z_0$		τ		Q		Q_0	$\sigma(v)$	$\sigma(v)$	$\sigma(\theta)$	$\sigma(\theta)$
Date	Time Period EST	N_Q	1	$1/\sqrt{\phi}$	1	$1/\sqrt{\phi}$	1	$1/\sqrt{\phi}$	1	$1/\sqrt{\phi}$	Heat Budget	1	$1/\sqrt{\phi}$	1	$1/\sqrt{\phi}$
July 11	1534-1554		4.0	3.5	-2.8	-2.8	1.168	1.176	0.242	0.263	0.149	0.844	0.851	2.52	2.51
	1600-1625		-0.5	-0.5	-3.5	-3.5	0.926	0.934	0.149	0.156	0.091	0.163	0.189	4.81	6.02
	1630-1700		1.5	1.0	-3.0	-3.0	0.985	0.982	0.086	0.089	0.032	0.192	0.207	3.77	4.92
	1709-1800		-5.0	-5.0	-3.6	-3.6	0.480	0.480	0.003	0.003	-0.018	0.458	0.458	14.44	14.55
	2004-2103		-	-0.5	-	-3.9	-	0.140	-	-0.019	-0.024	-	1.134	-	6.14
July 12	1430-1455		10.5	13.0	-3.4	-2.9	0.787	0.901	0.343	0.473	0.248	0.086	0.087	4.88	3.40
	1504-1529		6.0	8.0	-4.0	-3.7	0.526	0.601	0.224	0.308	0.169	0.511	0.134	2.64	1.78
	1531-1550		17.5	18.0	-2.9	-2.6	0.569	0.637	0.237	0.316	0.113	0.237	0.240	7.38	4.92
	1601-1630		15.5	17.0	-2.9	-2.6	0.543	0.595	0.160	0.204	0.044	0.123	0.124	4.93	3.25
	1631-1700		13.0	11.5	-3.1	-3.2	0.632	0.602	0.076	0.080	0.007	0.257	0.244	1.25	0.99
July 14	1230-1240		8.0	8.5	-3.0	-2.6	0.340	0.391	0.203	0.306	0.350*	0.524	0.524	4.95	1.89
	1246-1256		1.0	1.5	-3.0	-2.5	0.243	0.292	0.190	0.321	0.350*	1.285	1.285	2.17	3.24
	1315-1328		-4.0	-3.5	-3.5	-3.3	1.024	1.086	0.366	0.436	0.350*	0.314	0.309	3.94	5.71
	1329-1359		-1.5	-1.5	-3.2	-3.1	1.537	1.582	0.350	0.505	0.336	0.267	0.251	2.57	4.13
	1400-1425		1.5	2.0	-2.9	-2.7	0.888	0.949	0.358	0.441	0.277	0.338	0.331	1.81	1.69
	1431-1459		-0.5	0.0	-3.5	-3.0	0.235	0.275	0.146	0.227	0.182	0.510	0.513	3.47	1.23
July 15	0621-0724		-	13.5	-	-2.2	-	0.606	-	-0.050	-0.042	-	0.302	-	4.63
	0621-0641		-	6.5	-	-3.5	-	0.442	-	-0.043	-0.044	-	0.295	-	2.75
	0642-0702		-	14.0	-	-2.0	-	0.763	-	-0.061	-0.053	-	0.319	-	2.00
	0704-0724		-	9.0	-	-3.2	-	0.414	-	-0.028	-0.030	-	0.250	-	5.92
	0725-0735		-	5.0	-	-4.0	-	0.207	-	-0.008	-0.007	-	0.647	-	8.86
	1102-1257		0.5	1.0	-3.1	-2.9	1.040	1.105	0.396	0.476	0.344*	0.161	0.159	2.28	2.53
	1102-1112		6.5	6.5	-2.3	-2.2	1.567	1.650	0.537	0.619	0.371*	0.432	0.433	2.14	1.53
	1117-1128		1.0	1.0	-3.1	-3.0	1.156	1.199	0.390	0.462	0.360*	0.287	0.288	2.65	2.39
	1132-1142		-1.5	-0.5	-3.5	-3.2	0.896	0.974	0.346	0.429	0.347*	0.189	0.168	2.33	3.67
	1147-1157		-0.5	0.0	-3.2	-3.0	1.096	1.161	0.381	0.453	0.356*	0.197	0.202	2.07	3.41
	1202-1212		-3.0	-2.0	-3.8	-3.4	0.792	0.877	0.343	0.441	0.350*	0.284	0.298	2.82	4.46
	1217-1227		-3.0	-3.0	-3.7	-3.6	0.933	0.982	0.355	0.407	0.358*	0.184	0.187	3.26	4.21
	1232-1242		-1.0	0.0	-3.3	-3.0	0.927	1.011	0.380	0.475	0.377*	0.129	0.128	2.59	3.74
	1247-1257		1.5	2.0	-2.8	-2.6	0.923	0.980	0.390	0.477	0.354*	0.350	0.346	4.57	2.75
	1312-1332		-0.5	-0.5	-3.3	-3.1	0.847	0.899	0.354	0.432	0.364	0.531	0.525	2.39	2.16
	1333-1358		1.5	2.0	-2.9	-2.7	1.096	1.164	0.405	0.483	0.333	0.219	0.209	2.06	2.13

*Estimated Q_0 from July 12, 1964, because thermal response experiment distorted the flux of sensible heat in the area of the soil sensors.

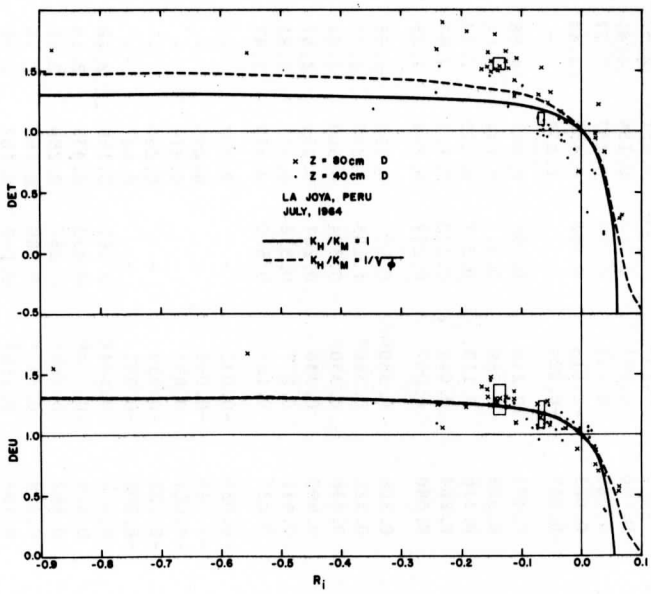

Fig. 6.1. Theoretical relationship between DEU, DET and Ri for two theoretical model assumptions $N_Q \equiv K_h/K_m = 1$ and $N_Q = 1/\sqrt{\phi}$. The data is based on a displacement height determined for $\sigma(V)$ a minimum and the rectangles indicate the area of uncertainty to be expected on the basis of the measuring system used.

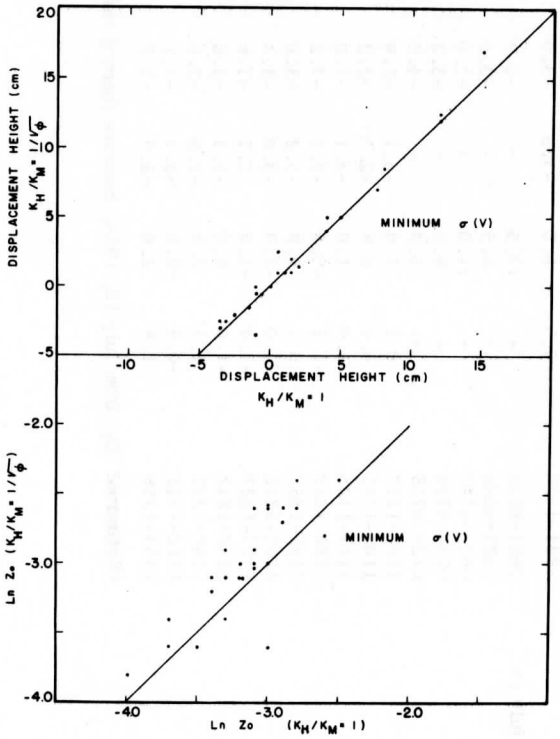

Fig. 6.2. Comparison between displacement heights and ln z_0 determined for $\sigma(V)$ a minimum for two theoretical models using $N_Q \equiv K_h K_m = 1$ and $N_Q = 1/\sqrt{\phi}$ where ϕ is the diabatic influence function.

The stress obtained from the wind and temperature profiles at the selected values of D and $\ln z_0$ are assumed to be equal to the surface stress. Assuming $N_Q = 1/\sqrt{\phi}$ produces τ values which are generally not more than 10% higher than for $N_Q = 1$. A comparison between the two values of τ is shown in Fig. 6.3 for lapse conditions only. Differences in τ are largely dependent on the selected D and $\ln z_0$. Either model could be used for estimating the surface stress in view of the possible uncertainties present in the estimate of D $\ln z_0$ and the value of k, the Karman constant. An independent measure of τ_0 was not available for comparison.

The remaining possibility for an independent testing of the theoretical models is to compare the sensible heat flux Q calculated from the profile of wind and temperature to the sensible heat flux Q_0 as determined from the heat budget (Stearns, 1967). The comparisons are presented in Fig. 6.4 for $N_Q = 1$ and Fig. 6.5 for $N_Q = 1/\sqrt{\phi}$. Figure 6.6 shows that, for lapse conditions only, Q based on $N_Q = 1/\sqrt{\phi}$ is approximately 25% higher than for $N_Q = 1$. This relative difference is larger than for the similar comparison of the τ's. It can be concluded that Q is more sensitive to the theoretical model assumptions and may be related to Q_0, an independent quantity, for testing theoretical assumptions about profile structure.

The graph of Q versus Q_0 for $N_Q = 1$ in Fig. 6.4 shows satisfactory agreement at higher values of positive heat flux. Those values above 0.300 ly/min for Q_0 were obtained during lapse conditions when the rate of change of Q_0 with respect to time was the least and τ was greater than 0.50 dynes/cm^2.

The theoretical dependence between $\underline{Ri}$ and N_Q is given in Table 6.1 together with z/L, ϕ and Φ_v for $N_Q = 1$ and $1/\sqrt{\phi}$. When $N_Q = 1/\sqrt{\phi}$ the value is unity at $\underline{Ri} = 0$ and increases as $\underline{Ri}$ decreases. The varying degrees of agreement between Q and Q_0 as presented in Fig. 6.4 and 6.5 suggests that $N_Q = 1$ is still the best assumption over the 160 cm height of the wind and temperature profile but for lapse conditions only. Under inversion conditions the assumption that $N_Q = 1/\sqrt{\phi}$ provides excellent agreement between Q and Q_0 as is shown in Fig. 6.5.

The Karman constant k enters into the determination of Q. The usually chosen value is k = 0.40 (Priestley, 1959) or 0.39 (Lettau and Davidson, 1957). A summary of possible values reported in the literature was presented by Slotta (1962). A value for k of 0.428 was used for the present calculations based on Lettau (1961). Using k = 0.40 instead of 0.428 would reduce Q by a factor of 0.87. The number of points on which to make a really trustworthy estimate of k is not satisfactory, but, if $N_Q = 1$, the value of k = 0.428 appears to be a good choice for the higher values of Q and τ.

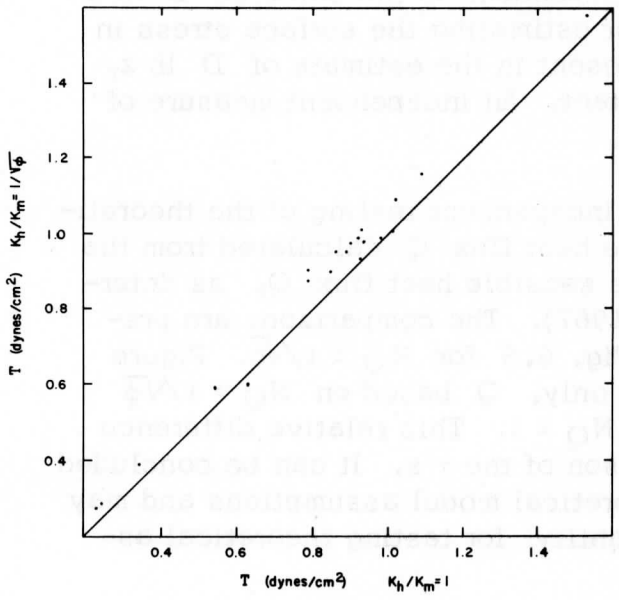

Fig. 6.3. A comparison between the wind stress, τ, determined from wind and temperature profiles assuming $N_Q \equiv K_h/K_m = 1$ and $1/\sqrt{\phi}$. The differences are due to the relative error being a minimum at a slightly larger value of D and $\ln z_0$ for $N_Q = 1/\sqrt{\phi}$.

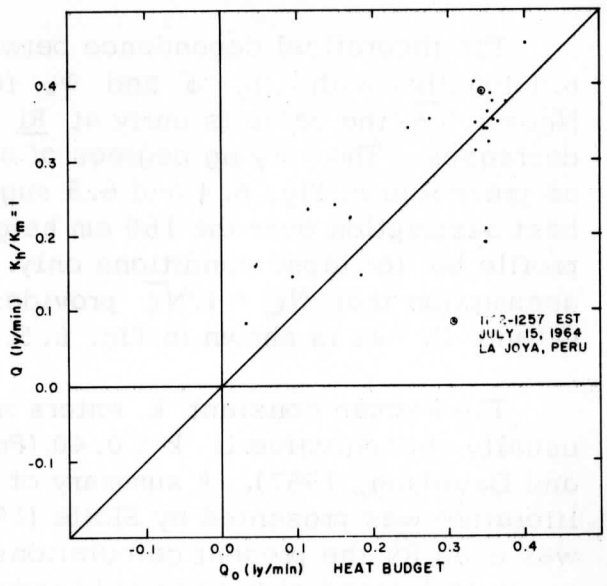

Fig. 6.4. The sensible heat flux, Q_0, determined from the heat budget versus Q determined from the wind and temperature profile assuming $N_Q = 1$. The data is for lapse conditions only.

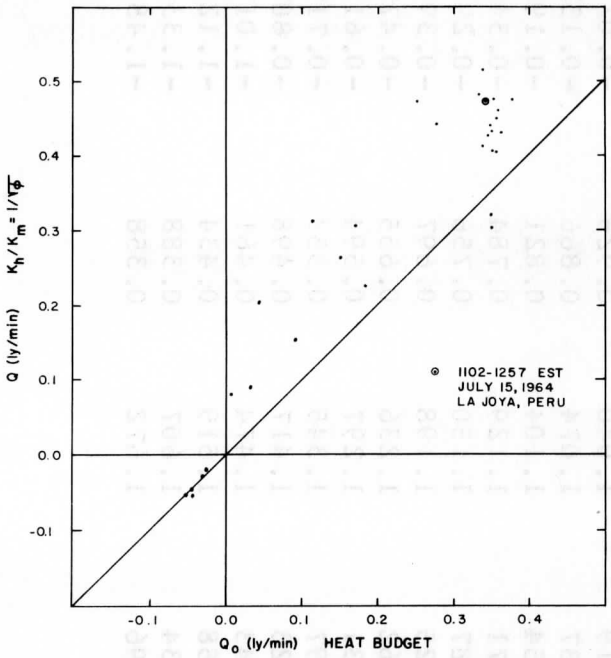

Fig. 6.5. The sensible heat flux Q_0 determined from the heat budget versus Q determined from the wind and temperature profile assuming $N_Q = 1/\sqrt{\phi}$ for lapse and inversion conditions.

Fig. 6.6. A comparison between the sensible heat flux determined from the wind and temperature profile assuming $N_Q \equiv K_h/K_m = 1$ to $N_Q = 1/\sqrt{\phi}$ results in a larger value of the sensible heat flux for the latter assumption.

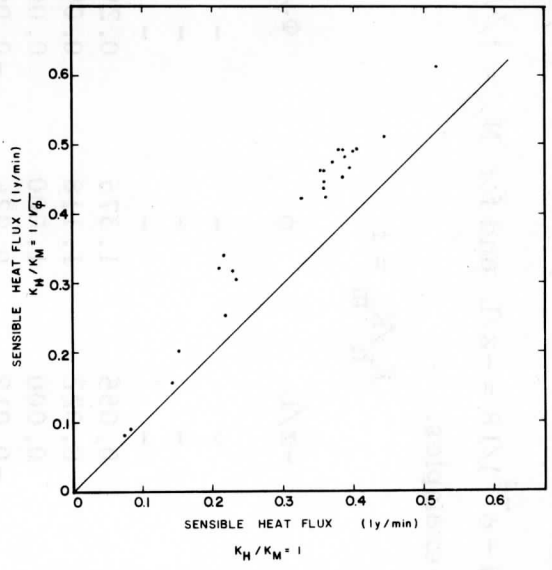

TABLE 6.2. Theoretical dependence of z/L, ϕ, Φ_v based on Richardson number $\underline{Ri}$ for $N_Q = 1$ where $\phi\underline{Ri} = \phi(1-\phi^{-4})/18 = -z/L$ and for $N_Q = 1/\sqrt{\phi}$ where $\sqrt{\phi}\,Ri = \phi(1-\phi^{-4})/18 = -z/L$. $\Phi_v = \int_{z_0}^{z+z_0} (\phi-1)\,d\ln z$ for both examples.

	$K_h/K_m = 1$			$K_h/K_m = 1/\sqrt{\phi}$			
Ri	$-z/L$	ϕ	Φ_v	$-z/L$	K_h/K_m	ϕ	Φ_v
0.10	-	-	-	0.180	0.550	3.235	1.540
0.08	-	-	-	0.119	0.671	2.210	0.845
0.06	-	-	-	0.076	0.792	1.596	0.451
0.04	0.055	1.375	0.294	0.045	0.880	1.291	0.235
0.02	0.022	1.118	0.097	0.021	0.047	1.115	0.093
0.00	0.000	1.000	0.000	0.000	1.000	1.000	0.000
-0.02	-0.019	0.926	-0.068	-0.019	1.040	0.925	-0.070
-0.04	-0.035	0.873	-0.130	-0.037	1.074	0.866	-0.137
-0.06	-0.050	0.833	-0.182	-0.054	1.104	0.821	-0.195
-0.08	-0.064	0.800	-0.228	-0.071	1.129	0.784	-0.348
-0.10	-0.077	0.773	-0.268	-0.087	1.150	0.756	-0.295
-0.15	-0.108	0.721	-0.353	-0.125	1.198	0.697	-0.394
-0.20	-0.137	0.683	-0.422	-0.162	1.236	0.655	-0.477
-0.30	-0.189	0.629	-0.534	-0.231	1.297	0.594	-0.612
-0.40	-0.236	0.591	-0.622	-0.297	1.345	0.553	-0.719
-0.60	-0.324	0.540	-0.759	-0.423	1.417	0.498	-0.887
-0.80	-0.404	0.505	-0.864	-0.543	1.474	0.461	-1.017
-1.0	-0.479	0.479	-0.951	-0.658	1.519	0.434	-1.123
-1.5	-0.652	0.435	-1.119	-0.934	1.607	0.388	-1.330
-2.0	-0.811	0.405	-1.245	-1.196	1.672	0.358	-1.485

The assumption that N from equation (2.39) is unity rather than 1.47 seems to be the best as the latter value will result in Q being approximately 47% higher at the larger fluxes of sensible heat.

The theoretical model with $N_Q = 1$ was tried for inversion conditions, but because of the presence of the pole in the determination of ϕ from equation (2.39), answers could not be obtained for the complete range of D and $\ln z_0$. Therefore, only the results using $N_Q = 1/\sqrt{\phi}$ were calculated and presented in Fig. 6.5. A few of the wind and temperature profiles during inversion conditions did not produce a $\sigma(V)$ minimum within reasonable values of D and $\ln z_0$.

In summary, it is concluded that $N_Q = 1$ for lapse conditions and $N_Q = 1/\sqrt{\phi}$ for inversion conditions, with $k = 0.428$. A possible variation in the value of B has not been considered since the overall effect of choosing B equal to 16 or 20, rather than 18, is small.

The value of τ and Q obtained from measurements can be used to construct synthetic profiles which could then be compared with the original data to discover any systematic differences. The method of calculating synthetic profiles was discussed in Section 4. Table 6.3 gives a comparison between two measured and synthetic wind and temperature profiles.

It was hoped that a comparison between the synthetic and actual temperature profile would allow for temperature corrections to remove the apparent systematic discrepancy between the 40 and 80 cm nominal height values of DET in Fig. 6.1. Example I in Table 6.3 shows a nearly uniform difference between the synthetic and actual profile except at the 320 cm level indicating a negligible discrepancy at the levels used to determine DET. Example II does suggest a discrepancy at 80 cm between the synthetic and actual temperature profile which would tend to make DET at 80 cm large and at 40 cm small. This agrees with what is shown in Fig. 6.1. The difference in the appearance of the discrepancy at 80 cm in Example II and not in I is as yet unexplained by possible errors in the data processing. Other comparisons were made between synthetic and actual temperature profiles with the discrepancy at the 80 cm nominal height present in varying degrees but not no iceably at the other sampling levels. The random magnitude of the variation indicates that the 80 cm temperature has an error which is not related to the actual height of the temperature sensors or the location of the sensors in the shield. At this level a wet bulb thermometer was located in the same tube. This could have reduced the ventilation velocity along the sampling tube and conceivably affect the level of air temperature measurement.

TABLE 6.3. Synthetic wind (V, cm/sec), temperature (T, deg C) calculated from τ, Q and ln z_0 compared to the actual profile for which the values were obtained assuming $N_Q = 1$, B = 18 and D = 0. Example I is for 1246-1256 EST, July 14 and II for 1102-1157 EST, July 15, 1964, on the Pampa de La Joya, Peru. The differences (ΔV, cm/sec; ΔT, deg C) are given at common levels, from 160 to 20 and 320 to 20 cm for comparison.

	z cm	V profile	V model	ΔV diff	T profile	T model	ΔT diff
I	z_0	0	0	0	-	35.00	-
	20	205	206	-1	25.60	25.36	0.24
	40	220	222	-2	24.79	24.58	0.21
	80	233	235	-2	24.07	23.87	0.20
	160	243	245	-2	23.47	23.41	0.06
	320	253	254	-1	22.99	23.05	-0.06
	160-20	48	48	0	-2.61	-2.41	0.21
	320-20	38	39	-1	-2.13	-1.95	0.18
II	z_0	0	0	0	-	35.00	-
	20	449	448	1	22.87	23.08	-0.21
	40	492	492	0	21.73	21.92	-0.18
	80	533	531	2	20.61	20.88	-0.27
	160	567	564	3	19.83	19.98	-0.15
	320	589	592	-3	19.23	19.23	0.00
	160-20	118	118	0	-3.04	-3.10	-0.06
	320-20	140	144	-4	-3.64	-3.85	-0.21

Only wind and temperature data up to 160 cm height was used for determining τ and Q. Consequently, the wind and temperature at 320 cm could be considered as independent predictions by the synthetic profile. However, the conditions at 320 cm are hardly consistent with those at 160 cm and below. This is the empirically established reason why only the data between 20 and 160 cm was actually used to compute the final values of τ, Q, Ri, DEU and DET.

Looking into the other direction, that is, the downward direction, the synthetic wind and temperature profile allow a prediction of the air temperature at the height z_0 above the surface. In computing the synthetic profile the established temperature at z_0 was adjusted until the 20 cm synthetic temperature agreed within a few tenths of a deg C with the measured profile temperature at 20 cm. This resulted in a temperature of 35 deg C at z_0 for both profiles presented in Table 6.3. The estimated surface temperature for 1102-

1257 EST on July 15, 1964, was approximately 45 deg C. Assume that the transfer of sensible heat from the surface to the height z_0 takes place by the molecular conductivity of still air with a temperature gradient of 10 deg C/0.05 cm. The thermal diffusivity of air at 30 deg C is 0.23 cm^2 sec^{-1} (Johnson, 1954), and ρc_p = 0.24 mcal cm^{-3} deg^{-1} resulting in an estimate of the sensible heat flux to the air of 0.64 ly/min. This is larger than the value of 0.396 ly/min from the wind and temperature profile or 0.350 ly/min estimated from the heat budget. The above estimate is intended only to show that the z_0 temperature, the surface temperature and molecular conductivity are of the correct order of magnitude to support the estimate of the sensible heat flux. In the process of minimizing $\sigma(v)$, it is possible to predict the temperature at the height z_0 which is determined only from the wind profile and represents an extrapolation of a mathematical relationship for the wind profile to a height above the surface where the boundary condition V = 0 is satisfied. Thus, the length z_0 is related to the sinks of momentum, but the momentum sinks are not necessarily the heat sources or sinks. For example, the wind may lose its momentum at the tops of the larger sand grains but the transformation of insolation, or the source of sensible heat could mainly occur between the larger sand grains. About 50% of the sand grains on the pampa are less than 0.025 cm in diameter. The results of bushel basket experiments reported by Kutzbach (1961) have shown that z_0 was not altered drastically by increasing the area covered by baskets relative to the total area above 25%. Thus, on the desert floor part of the sensible heat could be transferred over a vertical distance considerably larger than z_0, assuming that the large sand grains projected above the small sand grains. This would reduce the air temperature gradient which would in turn reduce the flux of sensible heat to the air as determined above.

It was observed on the Pampa de La Joya that during the morning with lapse conditions the wind was erratic; therefore, wind profile data was not collected. In contrast, the wind direction and speed during the afternoon were usually steady. With the daily regularity in the flux of sensible heat with respect to time and the absence of morning profiles, a given value of $Q_0 > 0$ is closely related to time in the afternoon. The Q determined from the profiles of temperature and wind depart from the 45° line in Fig. 6.4 and seem to intercept the axis, $Q_0 = 0$, at a value of $Q \approx 0.08$ ly/min. This is of the order of magnitude of the possible error in the results of the heat budget. There is a tendency to overestimate Q when the profiles are averaged over a period when Q and τ are changing in the same manner with respect to time. This was the case every afternoon and could account for part of the apparent lag between Q and Q_0 at this time of the day. When Q_0 goes through zero from positive to negative heat flux, the temperature profile is still lapse and does not change sign until about 40 minutes later, which is the observed five-day average for this lag. In the morning the change in Q_0 and the change from inversion to lapse temperature

profiles occurs within a few minutes of each other. The afternoon lag suggests that either the heat budget may be incorrect due to a possible tilt in the radiometer plate, irregularities in the surface seen by the plate, an error in the flux of heat into the soil, or the possibility of a phase shift between the temperature gradient and the sensible heat flux. It is normally assumed that the flux of sensible heat in the air directly related to the temperature gradient in the air without any time lag. Suomi and Kuhn (1957) made measurements of the flux of sensible and latent heat to the air using air temperature and moisture gradients to determine the ratio of sensible to latent heat (Lettau, 1957a). The time when heat available as sensible and latent heat in the afternoon changes sign preceded by one-half hour the change from lapse to inversion in the air temperature gradient. The above is a 27-day average, but the data was presented as hourly means, consequently, a really meaningful average time lag cannot be determined. This does tend to confirm the observations on the Pampa de La Joya, Peru, but the possibility of errors in the heat budget should not be forgotten.

If Q_0 is decreasing at the rate of about 0.06 ly/min per hour during the afternoon, a lag of 40 min would amount to 0.04 ly/min. This would reduce the discrepancy between Q_0 and Q at $Q_0 = 0$ to within an error of 0.04 ly/min which would correspond to a more realistic error in the heat budget values of Q_0 together with the possible effect of averaging the wind and temperature profile over a time period where τ and Q are both decreasing which would result in a larger estimate of Q_0.

The data collected from 1200 to 1430 EST on July 14, 1964, on the Pampa de La Joya, Peru, is of interest because there was a marked change in the structure of the surface layer from 1310 to 1315 EST, followed by a less sharp one about 1400 EST. A few dust devils were observed on the pampa between 1227 and 1242 EST. Between 1310 and 1315 EST the wind speed increased rapidly and sand started streaming over the pampa. Figure 6.7 shows the changes which took place in the ten minute averages of the 320 cm wind speed and direction before and after the increase in wind speed. It was necessary to substitute the sensible heat flux determined at the same times for July 12, 1964, because a thermal response experiment was being conducted between 1200 and 1310 EST resulting in distorted estimates of the soil heat flux, soil temperature and net radiation. The change in the -0.1 cm soil temperature as a result of the thermal response experiment can be seen in Fig. 6.8. It is unfortunate that during the transition from light to strong winds the thermal response experiment was disguising the true response of the soil temperature and sensible heat flux to the overall change in the wind and temperature structure.

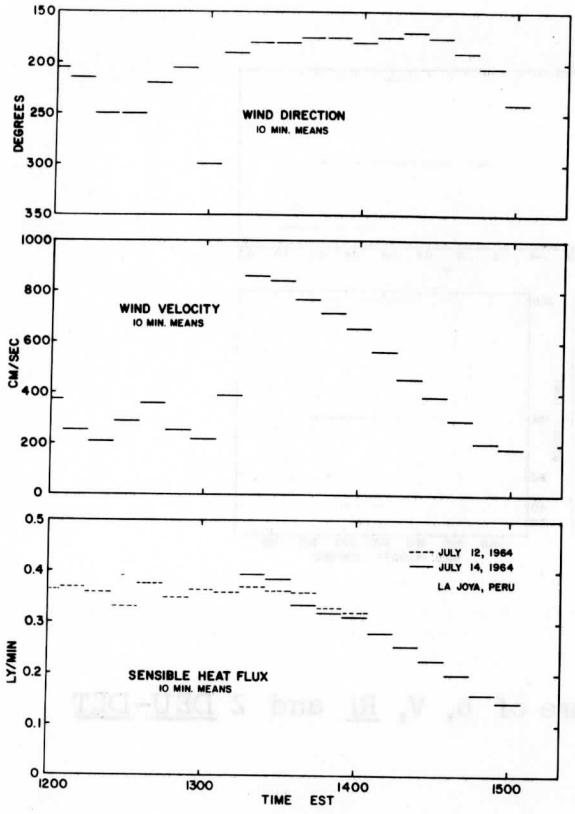

Fig. 6.7. 10-min means of wind direction and wind speed at 320 cm height and the sensible heat flux to the air as determined from the heat budget from 1200 to 1500 EST July 14, 1964, on the Pampa de La Joya, Peru.

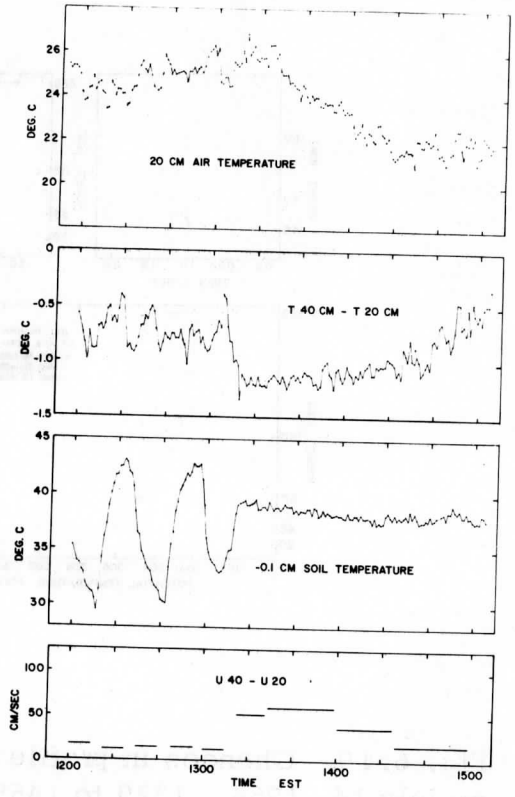

Fig. 6.8. 1-min values of 20 cm air temperature, 40-20 cm air temperature difference, and -0.1 cm soil temperature from 1200 to 1500 EST July 14, 1964, on the Pampa de La Joya, Peru. The 40 to 20 cm wind speed difference are averages over the time intervals indicated by the length of the horizontal line.

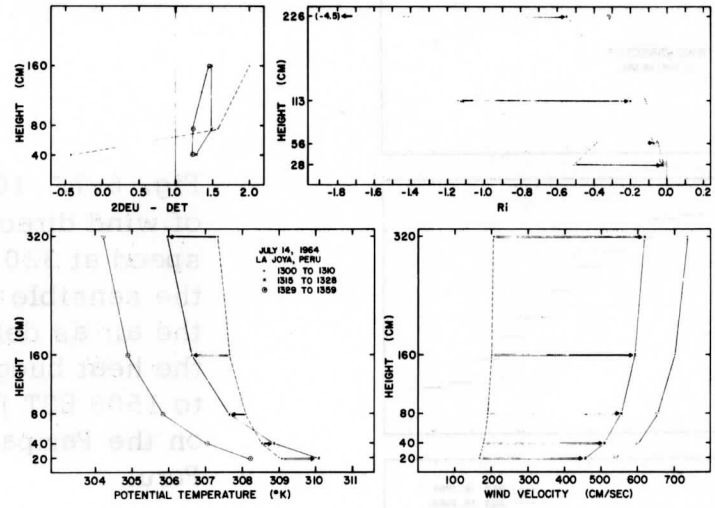

Fig. 6.9. Changes in profile structure of θ, V, Ri and 2 DEU-DET on July 14, 1964, 1310 to 1359 EST.

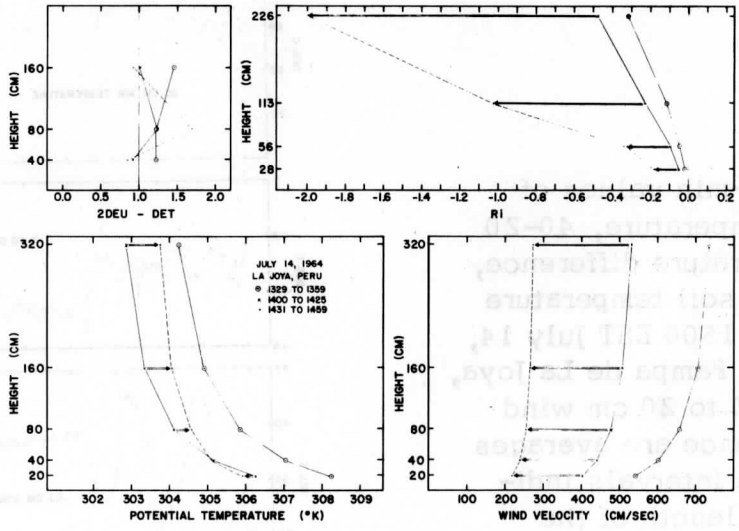

Fig. 6.10. Changes in profile structure of θ, V, Ri and 2 DEU-DET on July 14, 1964, 1329 to 1459 EST.

The two changes in the surface layer present that afternoon are similar. The transition from a phase with dust devils to one with blowing sand may be seen in Fig. 6.9 with the late afternoon change in Fig. 6.10. In each case the air temperature gradient decreases with the light wind speed. Similar observations are reported by Priestley (1959) who states that the strongest temperature gradients are associated with moderate wind speeds and not with the lightest winds. The wind and temperature profiles between 1200 and 1310 EST for which it was possible to determine D and $\ln z_0$ provide estimates of the sensible heat flux which are directly related to the temperature gradient through the theoretical model and the surface stress. The theoretical model with $N_Q = 1$ was used to obtain Q from the wind and temperature profile for 1230-1240 and 1246-1256 EST. The estimates obtained were about 0.200 ly/min for Q as compared to Q_0 of 0.350 ly/min from the July 12, 1964 heat budget results. Using $N_Q = 1/\sqrt{\phi}$ the Q values are 0.306 and 0.321 ly/min which are more in keeping with the estimated Q_0. The 1315 to 1328 and 1329 to 1358 EST profiles yielded an estimate of Q which was in reasonable agreement with Q_0 assuming that $N_Q = 1$. In these two cases of strong winds, the wind and temperature profile apparently explained the entire flux of sensible heat in the air while the profiles under the very light wind speeds underestimate by nearly 50% the sensible heat flux in the air using $N_Q = 1$ and only about 20% using $N_Q = 1/\sqrt{\phi}$. The results for all of the profiles of wind and temperature are summarized in Table 6.1. Table 7.1 gives all of the wind temperature and heat budget data collected on the Pampa de La Joya, Peru, during July 1964 (Stearns, 1967).

In Fig. 6.8, the most noticeable change in the 20 cm temperature and 40-20 cm temperature difference which occurred at 1315 EST was merely a reduction in the amplitude of the short term fluctuations. In addition, the increase in the magnitude of the temperature difference with an increase in wind speed is apparent. The profiles from 1431 to 1459 EST are visually similar to those between 1200 to 1310 EST but dust devils were not observed during this time period. Again the estimated Q of 0.146 ly/min assuming $N_Q = 1$ is less than the measured Q_0 of 0.182 ly/min while the assumption that $N_Q = 1/\sqrt{\phi}$ results in a Q_0 of 0.227 ly/min which is higher than the heat budget results. All other values of Q for $N_Q = 1$ at the times that Q_0 is decreasing are greater than Q_0. From Fig. 6.8, it can be seen that the amplitude of the 20 cm temperature and the 40-20 cm temperature fluctuations are greater again when the magnitude of the temperature gradient and the wind speed decreases.

Conditions such as were observed on July 14, 1964, between 1200 to 1310 and 1431 to 1459 EST are considered as a "free" convection regime in the surface layer by a number of investigators. However, this must be considered a misnomer. True free convection can only

occur when the Richardson number is infinite. Because of the role which Priestley (1959) has had in the discussion of the "free" convection regime it would be appropriate to follow a suggestion by Lettau (personal communication) and call the "free" convection regime Priestley convection and prevent the misnomer. Priestley defines the two regimes as follows: forced convection if the motion of the medium is set up by a force other than buoyancy, Priestley (free) convection if that part of the motion which carries sensible heat is primarily due to buoyancy.

The criterion for selecting one of the two regimes is usually the Richardson number, but this will be questioned because it does not relate directly to Priestley's definition of the two regimes. Table 6.4 presents a summary of the results of several investigators who are relating the gradient of potential temperature with height to the convection regime present. It is assumed that the gradient of potential temperature varies with height according to a power law of the form

$$\theta' = \text{constant} \cdot z^{-\beta_\theta} \tag{6.1}$$

where β_θ is the Deacon number for the temperature profile and assumed constant with height. β_θ is defined the same as $\underline{DET}$ in equation (2.33). The difference is that $\underline{DET}$ is allowed to vary with height. Equation (2.52) expresses θ' as a function of height with ϕ and possibly N_Q as a function of height depending on the model assumptions.

TABLE 6.4. β_θ for forced and Priestley convection together with the value of $\underline{Ri}$, where known, which separates forced convection (0 to $\underline{Ri}$) from Priestley convection ($\underline{Ri}$ to $-\infty$) as determined by several investigators from theory or measurement.

Investigator	β_θ Forced	β_θ Priestley	$\underline{Ri}$
Sutton (1953)		1.8	
Bryson(1955)		1.5	
Priestley (1959)	1	1.33	$\underline{Ri} = -0.02$
Lumley and Panofsky (1964)	1	1.33	$\underline{RI} = -1.0$

Table 6.4 could include more data which would illustrate beyond any doubt the lack of agreement on the shape of the temperature profile for the two regimes. This is probably due to the uncertainties associated with the measurement of the temperature profile and the lack of adequate theory. Reference to Fig. 6.1 will show that at $0 > \underline{Ri} > -0.02$ the value of $\underline{DET}$ is approximately 1 and could fit the definition of forced convection supporting the data given in Table 6.4. For $\underline{Ri}$ less than -0.2 $\underline{DET}$ is nearly constant at 1.33 for $N_Q = 1$ or 1.5 for $N_Q = 1/\sqrt{\phi}$. Since L is assumed constant over the profile

height it would be more appropriate to determine the value of z/L at which DET becomes nearly constant with increasing height. For $Ri \leq -0.2$, z/L is -0.14 for $N_Q \equiv 1$ and -0.16 for $N_Q = 1/\sqrt{\phi}$ as given in Table 6.2.

Bryson (1955) observed convective cells in light wind delineated by fog and developed a theory which related the temperature gradient to the -1.5 power of the height. On the basis of data supplied by Bryson and assuming that $\sqrt{\tau_0/\rho} = 15$ cm/sec as an upper limit for the conditions which he observed, the value of L obtained is approximately 225 cm. This was about the height where Bryson observed that the convective cells became indistinct due to mixing. Using the above value of L, DET becomes essentially constant with height at approximately 34 cm for either model assumption.

When dust devils were present on the Pampa de La Joya, Peru, on July 14, 1964 between 1230 and 1256 EST, the best prediction of the sensible heat flux was obtained with the theoretical model assumption that $N_Q = 1/\sqrt{\phi}$ which agrees with Bryson's theoretical value of 1.5 for β_θ in equation (6.1). Bryson noted a bimodal distribution in the temperature during the observed convective conditions which reflects the temperature fluctuations present in Fig. 6.8 but smoothed out due to the slow response of the sensors.

It is suggested that, in line with Priestley's definition of forced convection, the effect of buoyant forces does not influence the profile structure in the surface layer even though Ri may decrease with height beyond -0.2 or more and $K_h/K_m = 1$. Following the definition of Priestley convection, buoyant forces are important in the regime for the transfer of sensible heat throughout the surface layer. This is reflected in K_h/K_m increasing with the distance from the boundary and included in the theoretical model assumption that $K_h/K_m = 1/\sqrt{\phi}$. Priestley convection may be distinguished from forced convection by the greater amplitude of the fluctuations in the air temperature with respect to time. This could indicate a bimodal temperature distribution as was reported by Bryson (1955). In forced convection the frequency distribution of temperature with respect to time would more likely be monomodal. The observations are not available for confirming the above speculation about the frequency distribution temperature serving as the criterion for deciding if the convection is forced or Priestley.

7. Conclusion

The analysis of the wind and temperature profiles has shown that the displacement height for the wind and temperature profile and $\ln z_0$ for the wind profile cannot be left to an arbitrary decision because of the strong dependence of the surface stress and the sensible

heat flux on the displacement height as illustrated in Figs. 4.1 and 4.2. The criterion used here for making that decision is that the relative error squares of τ calculated from the measurements of wind speed at the several levels should be a minimum. Theoretical model assumptions can be used to decide how the profile structure of wind and temperature should vary with height resulting in an estimate of the sensible heat flux. This estimate can then be compared to a completely independent measurement of the sensible heat flux based on the heat budget. The result is that the theoretical model assumptions are tested for every wind and temperature measurement on the profile reducing the dependence of the result on the individual measurements of the gradients of wind or temperature which could so easily be in error.

The theoretical model assumption that $N_Q = 1$ applies best to the forced convection regime where the temperature fluctuations are small. The assumption that $N_Q = 1/\sqrt{\phi}$ allows for a variation of $N_Q \equiv K_h/K_m$ with height such that N_Q increases with height under lapse conditions and decreases with height for inversion conditions. The estimates of the sensible heat flux to the air are in good agreement with the heat budget data for inversion conditions and for lapse conditions in the Priestley convection regime using the theoretical model assumption that $N_Q = 1/\sqrt{\phi}$.

REFERENCES

Bryson, Reid A. (1955). "Convective Heat Transfer with Light Winds," Transactions of the American Geophysical Union, Vol. 36, No. 2, pp. 209-212.

Dalrymple, P., H. Lettau, and S. Wollaston (1963). South Pole Micrometeorology Program, Part II: Data Analysis, Technical Report ES-7, Quartermaster R & E Center, Natick, Mass., 1963.

Ellison, T. H. (1957). Turbulent Transfer of Heat and Momentum from an Infinite Rough Plate, J. Fluid Mech., Vol. 2, pp. 456.

Hastenrath, S. (1965). Personal communication, Dept. of Meteorology, Univ. of Wisconsin, Madison, Wisconsin.

Johnson, J. C. (1954). Physical Meteorology, John Wiley & Sons, Inc., New York.

Kazansky, A. B., and A. S. Monin (1956). Turbulence in the Inversion Layer near the Surface, Acad. Nauk, SSSR, Ser. Geophys. No. 1.

Kutzbach, J. E. (1961). Investigations of the Modification of Wind Profiles by Artificially Controlled Surface Roughness, Annual Report, Contract DA-36-039-SC-80282, USAEPG, Fort Huachuca, Arizona, Univ. of Wisconsin, pp. 71-114.

Lettau, H. H. (1949). Isotropic and Non-Isotropic Turbulence in the Atmospheric Surface Layer, Geophys. Research Paper No. 1, AFCRC, Cambridge, Mass.

Lettau, H. H. (1957a). Computation of Richardson Numbers, Classification of Wind Profiles, and Determination of Roughness Parameters, Exploring the Atmosphere's First Mile, Vol. I (Lettau and Davidson, Eds.), Pergamon Press, Inc., New York and London, Sec. 7.4, pp. 328-366.

Lettau, H. H. (1957b). Summary of Non-Dimensional Characteristics of Boundary Layer Theory, Exploring the Atmosphere's First Mile, Vol. I (Lettau and Davidson, Eds.), Pergamon Press, Inc., New York and London, Sec. 7.5, pp. 337-372.

Lettau, H. H. (1959). Research Problems in Micrometeorology, Final Report, Contract DA-36-039-SC-80282 (USAEPG, Fort Huachuca, Arizona), Univ. of Wisconsin.

Lettau, H. H. (1961). A Generalized Mathematical Model of the Mean-Velocity Distribution in Fully Turbulent Duct Flow, Annual Report, Contract DA-36-039-SC-80282 (USAEPG, Fort Huachuca, Arizona), Univ. of Wisconsin, pp. 115-140.

Lettau, H. H. (1962). Notes on Theoretical Models of Profile Structure in the Diabatic Surface Layer, Final Report, Contract DA-36-039-SC-80282 (USAEPG, Fort Huachuca, Arizona), Univ. of Wisconsin, pp. 195-226.

Lettau, H. H. (1964). Proposal for Microclimatological Field Studies in the Barchan Region of Southern Peru, Dept. of Meteor., Univ. of Wisconsin.

Lettau, H. H. (1965). Longitudinal Versus Lateral Eddy Length-Scale, Jour. Atmos. Sci., Vol. 23, No. 2, pp. 151-158.

Lumley, J. L., and H. A. Panofsky (1964). The Structure of Atmospheric Turbulence, John Wiley & Sons, New York, London, Sydney.

Monin, A. S., and A. M. Obukov (1954). Dimensionless Characteristics of Turbulence in the Surface Layer, Akad. Nauk. SSSR, Geofis. Trudy, No. 24, pp. 151-163.

Neumann, J. (1964). Turbulent Convection of Turbulent Kinetic Energy in Stratified Shear Flows, Sixth Annual Conference on Aviation and Astronautics, Feb. 1964, pp. 47-49, Tel Aviv and Haifa, Israel.

Panofsky, H., A. K. Blackadar, and G. E. McVehil (1960). The diabatic Wind Profile, Quart. J. Roy. Meteor. Soc. (London), 86, 390.

Priestley, C. H. B. (1959). Turbulent Transfer in the Lower Atmosphere, Univ. of Chicago.

Robinson, S. M. (1961). A Method for Machine Computation of Wind Profile Parameters, Annual Report, Contract DA-36-039-SC-80282 (USAEPG, Fort Huachuca, Arizona), Univ. of Wisconsin, pp. 63-70.

Slotta, L. S. (1963). A Critical Investigation of the Universality of Karman's Constant in Turbulent Flow, Annual Report, Contract DA-36-039-AMC-00878 (USAERDA, Fort Huachuca, Arizona), Univ. of Wisconsin, pp. 1-36.

Sellers, W. D. (1962). Simplified Derivation of the Diabatic Wind Profile, J. of the Atmos. Sci., Vol. 19, No. 2, pp. 180-181.

Stearns, C. R. (1967). Micrometeorological studies in the coastal desert of southern Peru, Ph. D. Thesis, Department of Meteorology, University of Wisconsin, Madison, Wisconsin.

Suomi, V. E. and P. M. Kuhn (1957). Energy Budget Data, Project Prairie Grass, Dept. of Meteorology, Univ. of Wisconsin.

Sutton, C. B. E. (1953). Micrometeorology, McGraw-Hill, New York.

Yamamoto, G. (1959). Theory of Turbulent Transfer in Non-Neutral Conditions, J. Meteor. Soc. Japan, Vol. 37, No. 2.

APPENDIX TABLE 7.1. Wind speed (cm/sec), and temperature (deg C) at the nominal heights (cm) above the surface, net radiation (R_0, ly/min), soil heat flux (S_0, ly/min) and the sensible heat flux (Q_0, ly/min) for the indicated date and time interval (EST) on the Pampa de La Joya, Peru.

Height (cm)	July 11, 1964 1512-1532	1534-1554	1600-1625	1630-1700	1709-1800	1802-1901	1904-2002	2004-2103	2104-2204	July 12, 1964 1430-1455	1504-1529	1531-1550	1601-1630
Wind Velocity (cm/sec)													
320	556.	593	597	591	464	405	291	340	329	540	477	430	421
240	548	583	590	582	449	384	275	310	323	529	468	422	412
200	547	570	570	563	435	369	264	294	310	520	464	417	409
160	539	571	575	563	432	362	254	280	296	518	454	412	402
120	503	550	554	541	412	343	236	256	277	504	449	400	390
80	495	521	523	507	384	314	207	225	250	487	430	387	375
60	486	510	519	501	378	309	203	221	244	479	423	381	365
40	468	490	493	476	359	292	190	205	230	460	413	370	359
20	427	446	447	430	317	264	170	184	209	434	389	351	340
Air Temperature (deg C)													
320	19.90	18.70	17.58	17.25	16.30	14.67	14.50	14.13	12.99	23.22	23.05	22.77	22.12
160	20.35	19.13	17.95	17.51	16.31	14.41	13.47	13.04	10.52	23.72	23.49	23.13	22.42
80	20.88	19.62	18.37	17.78	16.34	14.30	12.93	12.45	9.97	24.32	24.01	23.54	22.77
40	21.61	20.28	18.88	18.07	16.36	14.20	12.59	12.08	9.67	25.19	24.73	24.13	23.21
20	22.29	20.88	19.32	18.31	16.37	14.12	12.41	11.87	9.51	26.05	25.45	24.72	23.64
Heat Budget (ly/min)													
R_0	0.155	0.084	-0.005	-0.086	-0.157	-0.136	-0.123	-0.116	-0.108	0.261	0.158	0.081	-0.021
S_0	-0.033	-0.064	-0.097	-0.119	-0.138	-0.117	-0.106	-0.091	-0.085	0.012	-0.010	-0.031	-0.066
Q_0	0.188	0.149	0.091	0.032	-0.018	-0.019	-0.016	-0.024	-0.022	0.248	0.169	0.113	0.044

*Estimated values

Wind Speed (cm/sec)

Height (cm)	July 12, 1964 1631-1700	1701-1730	July 14, 1964 1200-1210	1215-1225	1230-1240	1246-1256	1300-1310	1315-1328	1329-1359	1400-1425	1431-1459	July 15, 1964 0621-0641	0642-0702
320	476	373	319	212	314	253	208	620	734	526	273	484	519
240	464	358	315	203	310	247	199	610	725	521	268	461	493
200	458	353	313	204	308	245	203	602	711	511	265	446	478
160	450	345	312	206	309	242	202	588	704	508	264	427	459
120	437	332	310	201	306	243	200	580	678	498	261	408	439
80	417	315	300	193	296	233	192	558	658	479	252	383	411
60	406	307	291	186	288	228	189	536	632	464	247	367	393
40	394	297	281	181	280	220	180	511	602	442	238	349	374
20	370	283	263	169	264	205	171	459	542	405	221	320	343

Air Temperature (deg C)

320	21.47	20.83	21.95	23.31	22.84	23.05	24.98	23.83	20.18	18.87	19.74	8.12	9.87
160	21.68	20.87	22.25	23.59	23.15	23.41	24.86	24.40	20.85	19.36	20.05	7.58	9.45
80	21.91	20.92	22.71	23.95	23.64	23.87	24.95	25.43	21.78	20.10	20.45	7.27	9.19
40	22.15	20.96	23.40	24.49	24.25	24.58	25.06	26.39	22.94	21.10	21.08	7.00	8.96
20	22.36	21.00	24.17	25.19	24.06	25.36	25.21	27.56	24.07	22.16	21.84	6.80	8.79

Heat Budget (ly/min)

R_0	-0.107	-0.156	0.572	0.540	0.570	0.517	0.537	0.465	0.451	0.364	0.262	-0.084	-0.056
S_0	-0.099	-0.117	-0.100	-0.049	-0.100	-0.074	-0.103	0.153	0.114	0.087	0.080	-0.039	-0.002
Q_0	-0.007	-0.037	0.673	0.590	0.350*	0.350*	0.350*	0.312	0.336	0.277	0.182	-0.044	-0.053

*Estimated values because of shading experiment

Wind Speed (cm/sec)

Height (cm)	July 15, 1964 0704-0724	0725-0735	1102-1112	1117-1128	1132-1142	1147-1157	1202-1212	1217-1227	1232-1242	1247-1257	1312-1332	1333-1358
320	441	340	672	616	568	614	547	605	560	527	535	587
240	420	323	660	608	560	605	541	594	553	519	529	578
200	409	312	653	604	556	600	537	590	550	515	526	574
160	394	304	637	596	549	589	530	581	542	509	518	567
120	378	295	626	579	536	574	519	569	529	497	507	553
80	357	279	601	557	517	553	502	548	510	478	490	531
60	343	268	578	540	502	535	427	531	494	465	476	517
40	327	257	551	516	478	509	464	506	472	441	451	490
20	301	236	507	469	436	463	423	458	429	404	413	447

Air Temperature (deg C)

320	11.28	13.23	19.69	19.58	19.39	19.31	19.17	19.12	18.89	18.65	19.06	18.83
160	10.99	13.04	20.32	20.17	20.02	20.01	19.71	19.70	19.51	19.21	19.60	19.39
80	10.83	12.97	21.19	20.92	20.80	20.82	20.51	20.43	20.32	19.88	20.32	20.18
40	10.68	12.90	22.30	22.02	21.89	21.90	21.67	21.62	21.49	20.98	21.39	21.28
20	10.55	12.85	23.35	23.13	22.98	22.98	22.86	22.83	22.65	22.19	22.55	22.39

Heat Budget (ly/min)

R_0	0.000	0.054	0.314	0.560	0.583	0.572	0.596	0.561	0.370	0.543	0.491	0.438
S_0	0.030	0.061	-0.070	0.294	-0.052	0.216	-0.054	0.201	-0.053	0.188	0.126	0.108
Q_0	-0.030	-0.007	0.371*	0.360*	0.347*	0.356*	0.350*	0.358*	0.377*	0.354*	0.364	0.330

*Estimated values because of shading experiment

Scanner's note:

This page is blank.

2

Interrelated Changes of Wind Profile Structure and Richardson Number in Air Flow from Land to Inland Lakes

H. Lettau and J. Zabransky
University of Wisconsin, Madison

ABSTRACT:

A semi-empirical model for wind profile modification in airflow from land to water on the 2 km scale, is discussed using 1950 Lake Hefner data. Initial (rough-surface) and final (smooth-surface) profiles are derived and an interpolation model is developed and used to calculate intermediate profiles. A distribution of vertical velocity with height is determined with the aid of the assumption that the divergence in the x-direction near the surface is compensated by convergence in the y-direction aloft. The rate of growth of the internal boundary layer follows as a direct consequence of the model. Theoretical computation is compared to Super's (1964) observations of wind profile variations with fetch on Lake Mendota. A diurnal variation of subsidence, found over Lake Hefner, is related to the variation in thermal stratification and its effect on the wind profile structure. Momentum budgets between land and lake are constructed and give evidence of a diurnal variation in surface stress over Lake Hefner.

1. Introduction

If air has been flowing over a surface of uniform roughness for a certain length of time, a steady-state or equilibrium state of a wind profile is developed. For adiabatic surface-layer conditions this equilibrium profile can be satisfactorily described by Prandtl's "log-law," relating windspeed to the logarithm of height. Upon encountering a surface of a new aerodynamic character, be it rougher or smoother than the original, the wind profile gradually begins to adjust to the new roughness, and another equilibrium tends to be established after a sufficiently long fetch downwind. One can also say that at the leading

edge of the new surface an internal boundary layer begins to develop. If the new surface is rougher, mechanical turbulence is increased and the internal boundary layer is likely to grow faster than if the new surface were smoother than the original. The thickness of this layer is also in direct proportion to the amount of momentum extracted from the moving air. Along the downwind fetch one finds that within the internal boundary layer the air undergoes readjustment to the new surface, while outside this layer, the airflow remains undisturbed. There have been many significant contributions to the study of wind profile modification; for references see Section 12 of Munn (1966). Special consideration will be given here to theoretical work by Elliott (1958) and Panofsky and Townsend (1964).

In addition to a change in roughness as air flows from one surface type to another, there may be a change in temperature or moisture profiles due to changes in the energy budget of the surfaces. Horizontal advection of sensible and latent heat will occur. Surface heating or cooling must affect the curvature of the wind profile, since there will be a change in the stability of the air. Diabatic effects are always involved when air moves from land out across a lake. Super (1964) showed that the wind across Lake Mendota behaved differently under lapse as opposed to inversion conditions. During inversion conditions the wind would accelerate for a horizontal fetch up to about 2 km, then decrease in speed at greater travel distances. If lapse conditions existed the speed was observed to increase across the entire available length (about 5 km).

Super's experimental work had been carried out for relatively large fetches in comparison with wind profile modification experiments in other studies of the order of centimeters to meters in wind tunnels, and hardly more than a few meters in natural field experiments. In this study, wind profile modification over Lake Hefner will be discussed, for a fetch of approximately 2 km.

Previously, as in Elliott's, or Panofsky and Townsend's models, an initial steady-state profile was assumed, and the subsequent modified profiles are extrapolated. In this analysis both the initial and final equilibrium profiles are assumed, and a semi-empirical interpolation model is proposed to calculate intermediate profiles in various stages of development. The growth rate of the internal boundary layer then follows as a direct consequence of the model, and the diurnal variation in Richardson number effects can and will be considered.

2. Lake Hefner Project and Analysis Preparation

The Lake Hefner Project was initiated in April, 1950, as a cooperative effort among the Department of Navy, Geological Survey, Bureau of Reclamation, and the United States Weather Bureau; it was concluded in August, 1951. Its main objective was the problem of evaporation. Hopefully, the results of the analysis would not only be useful for estimating or predicting evaporation from reservoirs but could also be applied to different types of inland lakes.

Voluminous hydrological and micrometeorological data were accumulated during the sixteen months of the Project. For a complete account of the instrumentation, reference is made to Anderson (1954). The evaporative flux was to be derived by three independent methods via (1) the hydrological water budget, (2) the interface heat budget, and (3) the mass transfer or vertical diffusion of water vapor into the lower atmosphere. Dry and wet bulb temperatures as well as wind speed and direction at heights of two, four, eight, and sixteen meters were recorded at four micrometeorological stations about the lake; surface water temperature and rainfall were measured at these sites as well.

Most important for profile modification studies appeared to be the data from the south shore, barge, and north intake-tower stations. Since our analysis was to be limited to two-dimensional but horizontally unidirectional flow in the lower sixteen meters, all data were reviewed to isolate those days when there was persistent wind direction from the south. Out of the many days with persistent southerly flow, only fifteen had complete instrument records at the three stations. From these fifteen it was decided to choose a day with strong winds to insure that all anemometer levels of the upwind station were within the surface layer. September 28, 1950, met this requirement and in addition exhibited a significant variation in temperature gradient throughout the diurnal period.

Upon plotting the wind profiles (u versus the log of height z) for several 24-hour periods, it was found that the points for the north (intake-tower) station were erratic. An apparent profile discontinuity between the four meter and the eight meter level suggested a disturbing influence of the dam around the north shore of the lake, especially in strong wind cases. Hence, the wind data from the intake-tower station was considered unusuable for the intended detailed analysis, and the study was limited to the profile changes from the south shore to the center of the lake only. In the following discussion, the south shore site will be referred to as the upwind station, and the barge as the downwind station.

3. Data Analysis

The presentation of the 3-hourly wind and temperature data in the Lake Hefner report make Richardson and Deacon numbers readily computable. First, both the temperature and wind data at the upwind and downwind stations were smoothed for the entire diurnal period using an equally-weighted 3-value running time mean. Then Deacon and Richardson numbers were computed at both stations, using equations of definition, $\beta = -\partial \log(\partial u/\partial z)/\partial \log z$, and $\underline{Ri} = (g/\theta_M)(\partial\theta/\partial z)/(\partial u/\partial z)^2$ respectively, where $\partial u/\partial z$ is the vertical shear, g the acceleration of gravity, θ is the potential temperature, and θ_M its layer-mean value. It is conventionally assumed that the Deacon number (or the nondimensional profile curvature β) represents a "shape factor," while the Richardson number serves as a "scaling factor." This distinction suggests that a shape factor can be compared with the role of a dependent variable, the scaling factor with that of an independent variable.

A plot of β versus Ri is shown in Figure 1. The upwind station shows some scatter, but points tend to follow the requirement that $\beta = 1$ for $\underline{Ri} = 0$, with $\beta(\underline{Ri})$ corresponding tolerably well to the "KEYPS" relation,

$$\beta = (1 - 18\,\underline{Ri})/(1 - 13.5\,\underline{Ri}).$$

Throughout the diurnal period the wind profile at the downwind station, however, shows persistent curvature which obviously does not conform to any direct extension of the logarithmic law. Namely, computed values of the shape factor β of the wind profile range between 1.2 and 1.6 for the entire diurnal period during which the thermal stratification changes back and forth between lapse and inversion conditions. This can be verified in Figure 1 where it is immediately apparent that the points for the downwind station disagree significantly with the semi-empirical "KEYPS" relation, because β remains larger than unity even for strongly positive $\underline{Ri}$.

Such "anomalous" values of β could be attributed to three causes: (1) prevailing lapse conditions, (2) anemometer levels being outside the surface layer, or (3) a wind profile not fully developed. Persistent lapse conditions are ruled out because $\underline{Ri}$ changes its sign during the diurnal period. Since wind speeds for the period of this analysis were sufficiently high (8 to 11 m/sec), most of the anemometer levels can be assumed within the surface layer. This suggests that the anomalous curvature evidenced in Figure 1 for the lake-station is probably due to incomplete profile adjustment. However, even though the Richardson-number dependency can be too weak to alter the overriding influence of incomplete adjustment on the profiles, thermal structure does affect

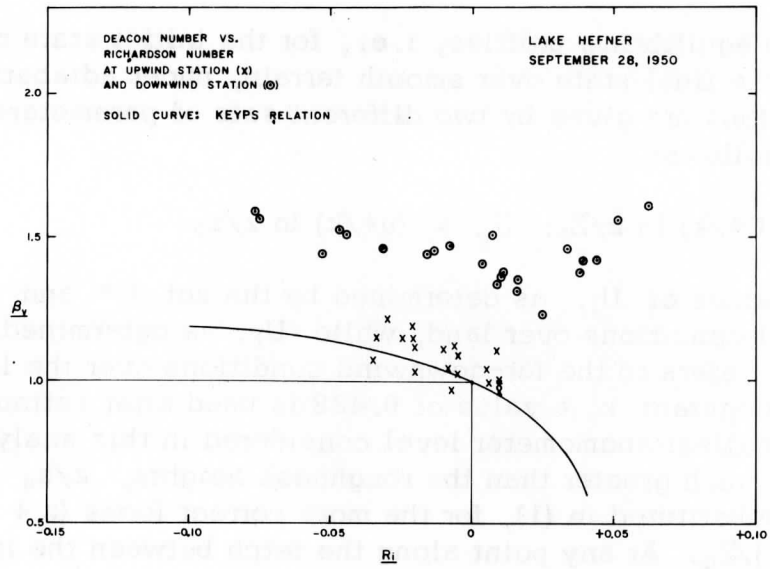

Fig. 1. Deacon number versus Richardson number for upwind and downwind station on Lake Hefner during a full diurnal cycle. The curve illustrates the theoretical "KEYPS" relation.

the wind speeds significantly, as will be seen in Section 10. Thus, the first problem will be to construct an adiabatic wind profile which is representative of equilibrium conditions over the water. This is equivalent to an extrapolation to a large fetch downwind, using the observed wind data after the effect of thermal structure has been eliminated.

Tentatively it will be assumed that surface roughness as well as friction velocity are uniform over the entire lake surface. This assumption is an oversimplification since it is often observed that the surface characteristics of the lake change downwind in connection with currents, upwellings, and/or the development of waves. However, only this assumption makes it possible to say that a neutral profile below the 4-m level at the downwind station will be representative of any other neutral profile, in these lowest air layers, at any fetch beyond this station.

4. Model Characteristics

The two equilibrium profiles, i.e., for the initial state over rough terrain and the final state over smooth terrain, under adiabatic surface layer conditions are given by two different sets of parameters of the log-law as follows:

$$U_I = (U^*/k) \ln z/Z_0; \quad U_F = (u^*/k) \ln z/z_0 \tag{1}$$

where the values of U_I, as determined by the set U^* and Z_0, pertain to the initial conditions over land, while U_F, as determined by the set u^* and z_0, refers to the far-downwind conditions over the lake. For the Karman constant k, a value of 0.428 is used after Lettau (1961). Since the smallest anemometer level considered in this analysis was numerically much greater than the roughness heights, z/z_0 and z/Z_0 have been substituted in (1), for the more correct forms $(z + z_0)/z_0$ and $(z + Z_0)/Z_0$. At any point along the fetch between the initial and final states it is assumed the wind profile is in some state of continuous transition. The initial and final wind profiles are functions of z only. The transition profiles $u = u(x, z)$ are a function of both x and z. The problem is to express this function $u(x, z)$.

With the aid of equation (1), a dimensionless transition function $\psi(x, z)$ is defined by

$$\psi \equiv \frac{\Delta u}{\Delta U} \equiv \frac{u - U_I}{U_F - U_I} \tag{2}$$

where $u = u(x, z)$ refers to the same height as U_I and U_F. This identity implies that $\psi = 0$ at $x = 0$ (i.e., at the line of roughness discontinuity). As u approaches U_F at large fetches, ψ goes to unity. Following the classical lines of a "similarity" solution, the profile changes with fetch can be described by saying that ψ must be a function of a new independent, dimensionless variable $\zeta \equiv z/Z$. Z has dimensions of length and is a monotonically increasing function of x; furthermore Z is proportional to the height of the internal boundary layer. This last condition suggests that when $\psi = 1$, ζ is small in comparison with unity, while for $\psi = 0$, ζ is large in comparison with unity.

In a tentative, semi-empirical approach to the interpolation problem, ψ was approximated by negative exponential functions which meet the above criteria, such as

$$\psi = e^{-\zeta}; \quad \text{or} \quad \psi = e^{-\zeta^2}. \tag{3}$$

The first, simple exponential form was discarded because it resulted in an unrealistic rapid rate of increase in Z with distance close to the upwind shore. The second, or Gaussian form emphasizes a continuous, gradual change of the profile downwind. The model implies an asymptotic approach to the upwind shearing stress at large heights downwind and also a gradual change in shearing stress with height without a discontinuity at the top of the internal boundary layer.

5. Computation of Equilibrium Profiles at Upwind and Downwind Stations

For the empirical determination of the transition function over Lake Hefner, it would have been ideal if adiabatic wind profiles were observed simultaneously at both stations. However, none of the measured temperature profiles showed truly adiabatic conditions, and Richardson numbers were normally of opposite sign at the two stations. An estimate of adiabatic profiles with no change in stratification was derived by interpolation in the following way, involving somewhat tedious procedures.

The upwind data were analyzed to obtain the set Z_0 and U^*, with the aid of a scheme for the diabatic surface layer described by Dalrymple, Lettau, and Wollaston (1966) and illustrated by Stearns and Lettau (1963). Accordingly, the value of Z_0 was obtained using the equation

$$\log Z_0 = \log(z + D) + 0.43(\Phi - \phi/\alpha), \qquad (4)$$

where ϕ is the diabatic influence function defined as

$$\phi = (k(z+d)\,\partial v/\partial z)/\sqrt{\tau_0/\rho}\ .$$

The integral diabatic influence function Φ is defined by

$$\Phi = \int_0^z (z+d)^{-1}(\phi - 1)dz$$

where d is the zero plane displacement which equals $D - Z_0$; α is the profile contour number which is a function of height defined by

$$\alpha = \Delta \log V/\Delta \log (z + D) \qquad (5)$$

Since $D \ll z$, a displacement height was considered insignificant in this analysis.

Roughness values were computed using β's at 400 cm and 800 cm for all eight profiles of the diurnal period. An average for the upwind site was obtained by averaging 16 values of $\log Z_0$ and resulted in $Z_0 = 4.92 \pm 1.27$ cm. This value appears to agree with independent estimates of the aerodynamic roughness of open prairie country (as for the surroundings of Lake Hefner, in Oklahoma).

Using the same diabatic surface-layer model a value for the friction velocity was also obtained using the following expression

$$U^* = k\alpha V/\phi \qquad (6)$$

As before an average of sixteen values was taken resulting in $U^* = 69 \pm 8.7$ cm/sec. The equilibrium profile over land thus obtained is shown as part of Figure 4.

A plot of Richardson numbers at the upwind versus downwind station shows the inverse relationship between stability over land and lake; see Figure 2a. The diurnal trend in temperature stratification has a distinct effect on the wind differences between the upwind and downwind stations, namely a greater or lesser degree of divergence

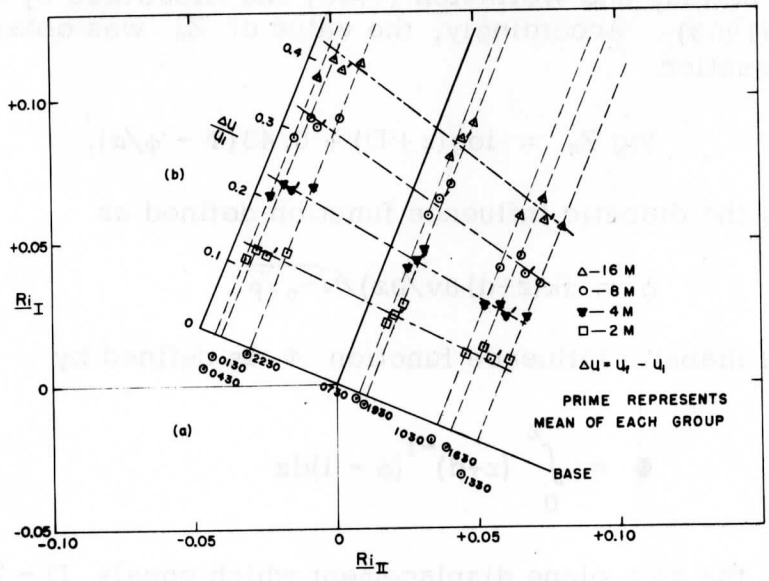

Fig. 2. (a) Stability at upwind station ($\underline{Ri}_I$) vs. stability at downwind station ($\underline{Ri}_{II}$) for eight 3-hour periods during September 28, 1950.

(b) Superposition of a new graph onto Fig. 2a, indicating wind differences between downwind and upwind stations during diabatic and adiabatic periods at four levels.

as the air accelerates over the lake. It was with this in mind that another graph (2b) was superimposed on Figure 2a. A base line approximating the slope of the $\underline{Ri}_I$ versus $\underline{Ri}_{II}$ points, was drawn through the origin. Dashed lines perpendicular to the base line were drawn through each time period on the original graph.

Wind speed differences between the upwind and downwind stations were computed at each level (16, 8, 4, 2m) for the eight three-hourly averages. These differences $(u - U_i)$ divided by the upwind speed U_i, are plotted as the ordinate in the superimposed graph. The abscissa represents time from 0130 to 1330 going left to right and 1330 to 2230 going back to the left again.

Three clusters of points are found. The first, going from left to right, represents inversion conditions over land and lapse over the lake. The second group represents slight lapse conditions over land and slight inversion over the lake. The third group indicates strong lapse over land and strong inversion over the lake. A straight line was fitted to the means of each group representing the four levels.

A new line was then drawn perpendicular to the base line through the origin (or, zero-zero of the Richardson number scales); this line can be thought of as representing the adiabatic case common to both sites. Points were read from the graph at the intersection of the new adiabatic line and the four height curves. These values were assumed to represent $\Delta u/U_I = (u-U_I)/U_I$ for the simultaneous adiabatic condition. Since the upwind adiabatic profile has already been computed, it is now possible to obtain Δu at the four levels in question; and, with the aid of equation (2), the adiabatic value of the transition function ψ.

For an array of assumed Z values, ζ^2 and ψ were calculated for the four levels using equation (3). Then ΔU was calculated with the aid of the Δu's obtained in the previous section and equation (2). Final U_F values were then computed as $\Delta U + U_I = U_F$. When a profile refers to neutral conditions, velocity differences from level to level must vary linearly with corresponding differences in ln z. Consequently since all the levels in this analysis are double heights, differences in U_F must be constant between all four instrument levels, and this criterion permits us to derive a "best value" of Z through trial and error.

For the fetch of 2 km at the downwind station, the value of Z thus obtained was 35 m. It should be noted that the basis for the estimation of Z hinges critically not only on the choice of relations (3) but also upon the representativeness of Figure 2b. Unfortunately there are too many degrees of freedom in fitting the four straight lines to the

"cluster means." Thus the values of $\Delta u/U_I$ read off the graph for the adiabatic condition could easily vary at least by $\pm$ 2 percent. Although this amount may seem small, it was found that changing the $\Delta u/U_I$ values, in the same direction, at the 2 and 16 m levels by one percent only, the best estimate of Z did change by 15 percent, which means five meters, if not more. However, improvements will be possible only when more detailed and representative observational data are available with an increased number of stations over both land and water surfaces.

Having found a representative downwind adiabatic wind profile, the roughness parameter of the lake was implicitly determined; z_0 turned out to equal 0.235 cm. The values estimated by Harbeck and Marciano (1954) ranged from 0.5 cm to 1.2 cm; they used only the lower three anemometer levels, and averages for 98 near-adiabatic cases. Their z_0-values increased directly with increasing windspeed at the 8 m level, suggesting perhaps that the roughness may be related to increasing wave height over the center of Lake Hefner. With a windspeed (at 8 m) of 1000 cm/sec, Marciano and Harbeck obtained a value of 0.94 cm for z_0, while in this analysis z_0 = 0.235 cm for the same wind condition. To a certain extent the difference can be explained by the use of k = 0.428 (Harbeck and Marciano used k = 0.40). However, it must be mentioned here that in computing z_0, Harbeck and Marciano assumed fully developed flow at the downwind station. It has been shown here that such an assumption is not valid, and may very likely lead to errors.

The computed friction velocity of 52.6 cm/sec is within 10 percent of the value 49.9 cm/sec given by Harbeck and Marciano for a 10m/sec wind at 8 m. A plot of the downwind equilibrium profile is included in Figure 4.

6. Mass Continuity and Vertical Motion

It is assumed on the scale of this analysis that density changes are negligible, since ΔT_{max} is never more than 3 °C per 2 km. This gives a value for the density disturbance of less than 10^{-5} g/cm^3, and the equation of mass continuity can be written as

$$w_z = -u_x - v_y \qquad (7)$$

where subscripts denote differentiation with respect to the indicated cartesian coordinate. If ζ is defined as before,

$$w_z = w_\zeta/Z, \quad \text{or} \quad Z w_z = w_\zeta. \qquad (8)$$

Remembering also that Z = Z(x)

$$\zeta_x = - Z_x \zeta / Z. \tag{9}$$

Now consider equation (2), which upon differentiation with respect to x produces

$$u_x = \psi_x \Delta U, \quad \text{or} \quad Z u_x = Z \psi_x \Delta U. \tag{10}$$

Therefore, equation (7) may be rewritten as

$$w_\zeta = -Z \psi_x \Delta U - v_y Z. \tag{11}$$

Differentiation of the Gaussian transition function ψ with respect to x gives

$$\psi_x = -2 \zeta_x \zeta \psi, \tag{12}$$

so that

$$Z \psi_x = -2Z\zeta_x \zeta \psi = 2Z_x \zeta^2 \psi. \tag{13}$$

The continuity equation (11) now transforms into

$$dw = -2 Z_x \zeta^2 \psi \Delta U \, d\zeta - v_y Z \, d\zeta \tag{14}$$

The negative vertical velocities which result from divergence in the lower layers must somehow be compensated for in the upper layers, or an unrealistic, finite vertical velocity at any large height will result. Let us assume that in the atmospheric flow considered the compensation in the upper layers is the result of convergence in the y-direction. As a consequence of this assumption it is found that the mean vertical velocity first increases (from the boundary value of $\overline{w}$ equal to zero at the surface) to a maximum of $\overline{w}$ in the middle layers, and then decreases to zero again at some large value of ζ, say in excess of $\zeta = 3$.

It is convenient to incorporate the v-component by making the special assumption that

$$v_y Z = Z_x \zeta^2 \Delta U \frac{d(\psi \zeta)}{d\zeta} \tag{15}$$

Thus the integral of equation (14) becomes

$$\overline{w} = -Z_x \zeta^3 \psi \Delta U \tag{16}$$

Hence if equation (16) is totally differentiated, equation (14) is obtained under the above assumption.

With the aid of this special model, the vertical velocity satisfies the boundary conditions of $\overline{w} = 0$ at the surface where $\zeta = 0$, and $\overline{w} = 0$ at large heights ($H \approx 3Z$) where $\psi = 0$ since $\zeta >> 1$. This implies a maximum $\overline{w}$ at about $\zeta = \sqrt{3/2}$. In this analysis, with $Z = 35$ m at the downwind station, $\overline{w}_{max} = -0.830$ cm/sec at a height of 40 m ($\zeta = 1.14$).

In order to facilitate a clearer understanding of the foregoing discussion, a three-dimensional schematic diagram of a volume of air between the upwind shoreline and downwind station at Lake Hefner is shown in Figure 3. The volume is represented by a semicylindrical cutaway which is not drawn to scale for purposes of simplicity and clarity. The upwind and downwind profiles are depicted, with the cross-hatched area on the downwind profile representing the amount of horizontal divergence in the x-direction. This divergence gives rise to the increasing vertical velocities indicated in the center of the cutaway. However, instead of increasing further toward the top of the volume, the vertical velocity decreases due to the assumed compensating convergence of air in the y-direction.

Equation (16) indicates that the vertical velocity at a point x along the fetch is directly dependent on Z_x (that is, the derivative of Z with respect to x), a numerical parameter which is obtained through momentum

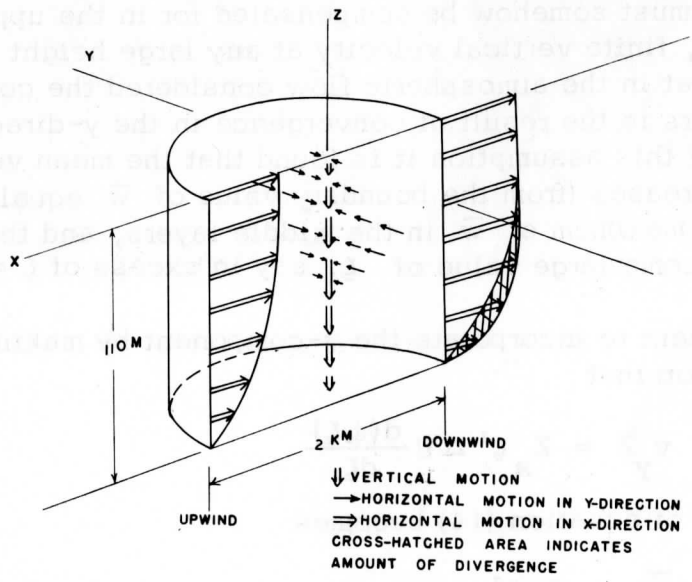

Fig. 3. A generalized schematic diagram (not drawn to scale) of the actual airflow and assumed compensating airflow between upwind and downwind station at Lake Hefner.

considerations discussed in the following section. Z_x not only permits computation of vertical velocities but, when known at various x, also permits the calculation of Z with fetch by direct numerical integration of Z_x with respect to x. Hence, the gradual change of the wind profile from the upwind shore to the final shape over the lake can be completely described.

7. Momentum Continuity and Determination of Z(x)

Assuming two-dimensional mean flow and no external accelerations or pressure gradient force and $\rho \approx$ const, then on the vertical scale considered here the continuity equation for x-momentum may be written

$$(uw)_z = -(uu)_x \tag{17}$$

If the instantaneous velocities are represented as means plus turbulent departures (as indicated by overbars and primes), after cross-multiplication of terms and averaging,

$$(\overline{u'w'})_z = -(\bar{u}\,\bar{w})_z - (\bar{u}\,\bar{u})_x - (\overline{u'u'})_x \tag{18}$$

The last term can be assumed negligibly small compared to the other terms. Thus, the characteristic balance equation may finally be written

$$(\overline{u'w'})_z = -(\bar{u}\,\bar{w})_z - 2\,\bar{u}_x\bar{u} \tag{19}$$

where $(-\overline{u'w'})$ is the Reynolds stress which corresponds to U^{*2} over land and u^{*2} over water, respectively. It is postulated that the mean flow is and remains strictly horizontal and uniform at a certain vertical distance above the interface, i.e., at levels $z \geq H$. This implies that $\bar{w} = 0$ at $z \geq H$ since $\psi \approx 0$. Tentatively, it was found sufficient to employ, as a working hypothesis, $H \approx 3Z$. This restriction in height has the obvious advantage that the vertical variation of Reynolds stress can be neglected in the initial wind profile over the land as well as in the final equilibrium profile, but of course, not below $z = H$, during transition.

Thus, with $\bar{u} = \bar{w} = 0$ at $z = 0$ and $\bar{w} = 0$ at $z \geq H$, integrating the momentum balance equation (19) between $z = 0$ and $z = H$ gives

$$[\overline{u'w'}]_0^H = -2\int_0^3 Z\,\bar{u}_x\bar{u}\,d\zeta. \tag{20}$$

It is considered that at and beyond the top of the internal boundary layer, the actual wind corresponds to the upwind conditions (i.e., $(\overline{-u'w'})_H = U^{*2}$), while near the surface the actual profile will already be adjusted to the final downwind profile (i.e., $(\overline{-u'w'})_0 = u^{*2}$). Thus it follows from equation (20) that

$$2 \int_0^H Z \bar{u}_x \bar{u} \, d\zeta = U^{*2} - u^{*2} = (U^* - u^*)(U^* + u^*) \qquad (21)$$

which implies a value for the integral which is constant for the given overall wind conditions. Upon combining equations (3), (9), and (12) with equation (18),

$$2Z_x \int_0^H \zeta^2 \psi \Delta U (U_I + \psi \Delta U) d\zeta = U^{*2} - u^{*2} \qquad (22)$$

Therefore, for any given Z, the value of Z_x may be obtained by numerical integration of equation (22). For example, when Z = 35 m, the integration produces $Z_x = 0.0168$. This Z_x-value was employed to compute vertical velocities as discussed in the previous section; this Z_x will be used also to estimate the change of the wind profile structure with fetch, i.e., the growth of the internal boundary layer produced by the change in roughness.

8. Growth of the Internal Boundary Layer

Elliott's (1958) mathematical model for the growth of the internal boundary layer under adiabatic conditions would correspond to $Z \sim x^{0.8}$. Specifically, in Elliott's model

$$h = a x^n z_0^{1-n}; \quad n = 0.8; \quad a = 0.86 \qquad (23)$$

where h denotes the height of the internal boundary layer, and z_0 is the roughness parameter of the surface over which the modification takes place. The exponent n = 4/5 agrees with values obtained experimentally in independent fluid dynamics experiments. Elliott pointed out that the growth of the boundary layer thickness was not dependent on wind speed, which contrasts with results of turbulent boundary layer development studies in wind tunnels.

In Panofsky and Townsend's (1964) model, the thickness (d) increases to infinite values with increasing distance, as does Elliott's according to equation (23). They considered the following expression

$$S = \ln (Z_0/z_0)/(-1 + \ln d/z_0) \qquad (24)$$

which, in the present notation appears to be identical with $(U^*-u^*)/U^*$. Using values estimated for Lake Hefner, a calculation of d was made with $U^* = 69$ cm/sec, $u^* = 52.6$ cm/sec; $Z_0 = 4.92$ cm; $z_0 = 0.235$ cm which resulted in $S = 0.24$, whereupon equation (24) yields a thickness of $d = 800$ m. This appears to be nearly the height of the planetary boundary layer, and obviously is unrealistic. It would be more natural to expect, especially with the relatively long fetches involved in this analysis, that at some finite distance downwind the boundary layer thickness will approach some final value.

It was seen in the preceding section that Z(x) could be attained through momentum continuity considerations. If a sufficient number of pairs of Z_x, Z values are obtained, numerical integration with respect to x will produce Z(x). With Z_x calculated for Z - values of 35, 30, 25, 20, 15, and 10 m, such a numerical integration showed that Z varied nearly linearly with x. In other words, an approximate constant value $Z_x = 0.015 \pm .001$ was obtained.

9. Intermediate Wind Profiles

Having established a relation between Z and fetch, intermediate profiles between the upwind and downwind equilibrium profiles were constructed and are illustrated in Figure 4. This scheme suggests that there is a rather quick adjustment of the wind in the lowest four meters. Gradually the intermediate profiles approach the characteristics of the initial (or, the undisturbed) flow at the top of the internal boundary layer where the shearing stress becomes equal to the value of the initial flow. At a fetch of 2 km the wind profile curvature resembles that of the profiles plotted from observed Lake Hefner data. This supports the conclusion that the observed profile at the barge station of Lake Hefner expresses a state of significantly incomplete adjustment.

Super (1964) studied air mass modification over Lake Mendota and obtained wind profiles from 0.8 to 2.8 m above the lake at various fetches between 0.25 and about 5.0 km. The dashed lines in Figure 5 illustrate Super's results under near adiabatic conditions with the aid of the ratio of the mean wind speed to the mean wind speed at a height of 2.8 m and fetch of 2.25 km.

In contrast to the prairies around Lake Hefner, the surroundings of Lake Mendota are wooded hillsides, built-up areas, intermingled with a few fields. This makes the estimate of an initial wind profile very difficult.

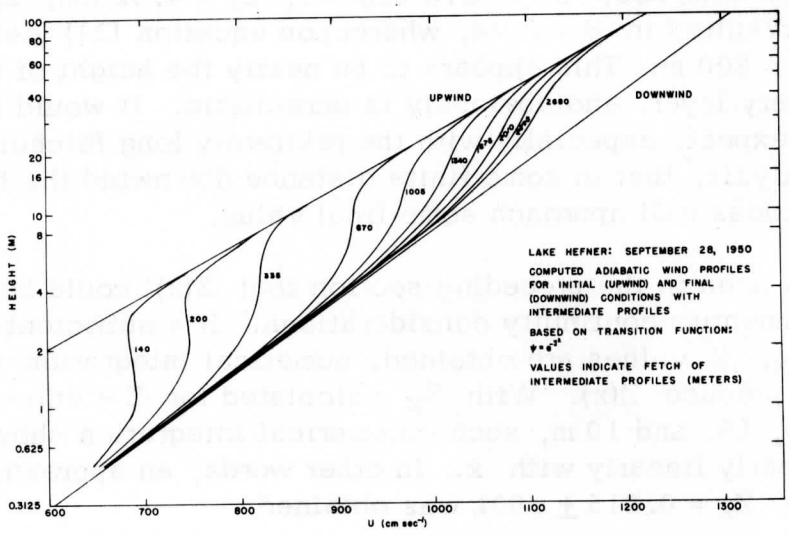

Fig. 4. Calculated upwind and downwind equilibrium wind profiles and intermediate profiles computed from interpolation model $\psi = e^{-\zeta^2}$.

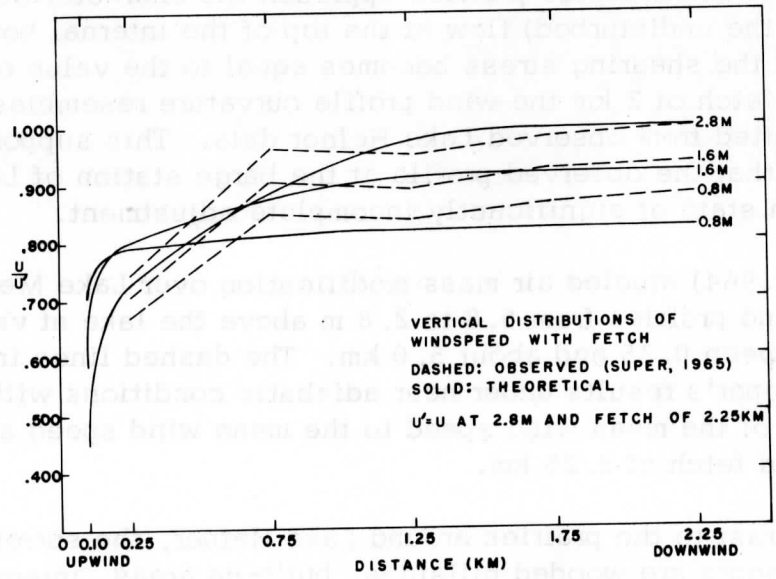

Fig. 5. Observed vertical wind distribution with fetch (Super) compared with theoretical model curves computed using Z_0 = 50 cm; z_0 = 0.235 cm; V_g = 11.5 m/sec.

For comparison with Super's experimental values, the solid curves in Figure 5 indicate the variation of wind with fetch as predicted by the interpolation theory for a geostrophic wind of 11.5 m/sec, Z_0 = 50 cm, and z_0 = 0.235 cm. Note that this Z_0 is about ten times as large as for the surroundings of Lake Hefner, to account for rougher terrain around Lake Mendota. A noticeable difference between the two sets of curves is the rapid speed increase from 0.25 km to 0.75 km in the observed case. The theory also predicts that with decreasing height the acceleration becomes very small so that there is nearly complete profile adjustment in the lowest meter beyond a fetch of 250 m.

One feature of the theoretical curves, which is not supported by observations, is the relative maximum or reversal of speed increase with height, at fetches less than 500 m. This was seen in Figure 4 where at lower levels the profiles show greater speeds than higher up. Although such S-shaped profiles may occasionally occur, they are not very likely. The theoretical model predicts this to occur at distances less than 0.5 km for the given V_g, Z_0, and z_0. However, this is hardly probable, and the "short-fetch" theories of Elliott or Panofsky and Townsend appear to be more realistic for the first 500 meters from the shoreline.

Physically, it might be possible to explain the difference in accelerations between the two sets of curves in Figure 5 by irregularities in the surface discontinuity which could greatly alter wind accelerations over the lake. Here it was assumed that z_0 was uniform over the lake surface, while in reality z_0 probably increases with fetch.

10. Influence of Thermal Stratification on Wind Profile Modification

Figure 2a illustrated the inverse relationship of stability between the upwind and downwind stations. Typically, over land lapse conditions prevail during the day and inversion at night, in contrast to daytime stability and lapse at night over the lake. This illustrates the known moderation of microclimates near lake shores since the water stores heat at daytime, as a result of high thermal admittance, and releases it at night.

During the entire diurnal period under study the air was accelerating as it encountered the smoother surface of Lake Hefner. Following continuity requirements, negative vertical velocities (subsidence) resulted from this divergence of air flow. An attempt was made to investigate the diurnal trend in the magnitude of subsidence over the lake.

Smoothed values of the vertical and horizontal windspeeds at 16 m were used to compute the ratio $(\bar{w}/\bar{u})_{16}$ where $\bar{u}$ is an average between the upwind and downwind stations. These ratios are listed in Table 1.

Table 1

Diurnal Variation of Vertical Velocity at the 16 m Level Above Lake Hefner (on September 28, 1950) as Evidenced by the Ratio of $(\bar{w}/\bar{u})_{16}$

Time (CST)	$\bar{w}_{raw}$ (cm/sec)	$\bar{w}_{smooth}$ (cm/sec)	$\bar{u}_{smooth}$ (cm/sec)	$(\bar{w}/\bar{u})_{16}$ ($\times 10^{-3}$)
0130	-1.486	-1.273	865	-1.47
0430	-1.038	-1.218	905	-1.34
0730	-1.131	-1.134	928	-1.22
1030	-1.233	-1.126	966	-1.16
1330	-1.014	-1.199	991	-1.20
1630	-1.349	-1.177	936	-1.25
1930	-1.169	-1.271	875	-1.45
2230	-1.294	-1.316	860	-1.53

A diurnal variation, although small, appears to be significant in the values of $(\bar{w}/\bar{u})_{16}$. A minimum occurs at 1030 hours and a maximum twelve hours later at 2230. The higher values of $(\bar{w}/\bar{u})_{16}$ are associated with the period (from 10:00 PM to 5:00 AM) when advection was from a stable to unstable regime. Correspondingly, lower values of $(\bar{w}/\bar{u})_{16}$ coincide with the period of transition from instability over land to a stable stratification over the lake (between 10:00 AM and 5:00 PM).

Figure 6 illustrates a possible explanation for this $\bar{w}$ cycle as suggested by diabatic surface layer theory (Lettau, 1962). Fully developed synthetic wind profiles for a given geostrophic speed of V_g = 15 m/sec for the adiabatic cases are shown by solid lines for upwind station (Z_0 = 5 cm) and downwind station (z_0 = 0.05 cm). The two friction velocities were computed with the aid of geostrophic drag coefficients, using the surface-Rossby number as a scaling factor for predicting ground drag from the horizontal pressure gradient field. Inversion and lapse profiles are shown for both stations as dashed and dot-dashed curves respectively. During the night the upwind station is under the inversion regime and wind speeds are less than during the neutral period, while the downwind station is under lapse conditions with speeds greater than those of the downwind neutral profile. Therefore

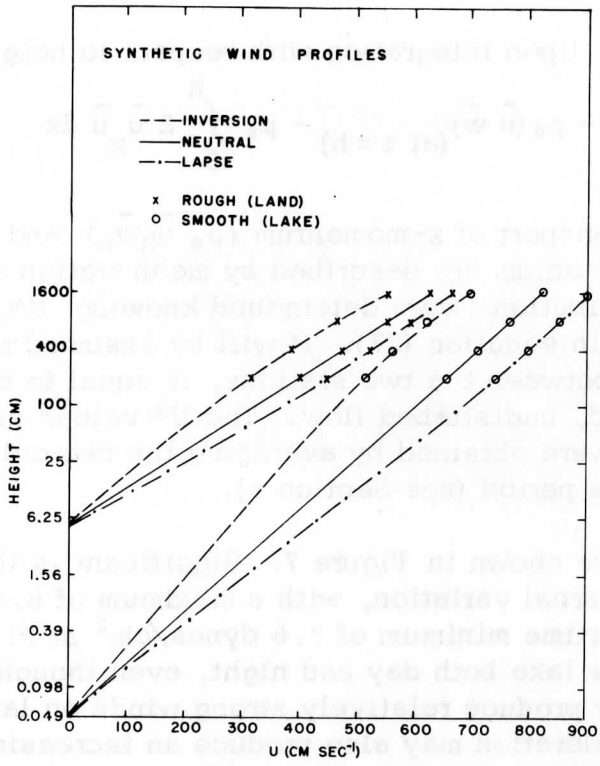

Fig. 6. Synthetic adiabatic and diabatic wind profiles for upwind land surface (Z_0 = 5 cm) and downwind lake surface (z_0 = 0.05 cm).

the divergence is strongest at night, thus producing a greater vertical velocity. Correspondingly, during the day, the divergence has a minimum value. Thus, it can be shown quantitatively how the thermal stratification affects the horizontal wind speed which in turn alters the amount of divergence and consequently the subsidence above the water. However, it is re-emphasized here that the thermal structure is not solely responsible for the transient shape of the wind profiles over the lake.

11. Momentum Budget

Momentum budgets between the upwind and downwind stations for the eight time periods were constructed using the x-momentum continuity equation (19) rewritten as

$$\rho_0 [2 \bar{u} \bar{u}_x + (\bar{u} \bar{w})_z] = \tau_z \qquad (26)$$

where $\tau = -\rho \overline{u'w'}$. Upon integration with respect to height

$$\tau_0 = \tau_{(\text{at } z=h)} - \rho_0 (\bar{u}\,\bar{w})_{(\text{at } z=h)} - \rho_0 \int_0^h 2\,\bar{u}_x \bar{u}\, dz \qquad (27)$$

The vertical transport of x-momentum ($\rho_0\ \bar{u}_h \bar{w}_h$) and the horizontal divergence of x-momentum are described by mean motion components. The eddy-flux contributions were determined knowing U*, with τ_0 becoming the residue in equation (27). It will be assumed that the shearing stress at 16 m between the two stations, is equal to the shearing stress of the upwind, undisturbed flow. The U* values used in the budgeting problem were obtained by averaging the two calculated U* values for each time period (see Section 5).

Four budgets are shown in Figure 7. Significant is that τ_0 over the lake shows a diurnal variation, with a maximum of 6.5 dynes/cm^2 at 1330, and a nighttime minimum of 3.6 dynes/cm^2 at 0130. The wind accelerates over the lake both day and night, even though lapse conditions during the day produce relatively strong winds on land. The daytime downwind acceleration may also produce an increasing z_0 with fetch. Thus, the diurnal variation of τ_0 illustrates the strong influence of Richardson number on the process of air mass modification.

Although the τ_0 variation is apparently real, the actual values associated with the eddy-flux in Figure 7 are somewhat questionable chiefly because there is some doubt as to whether the shearing stress at 16 m is, in fact, the same as the upwind shearing stress. More likely it is less, since the flow at 16 m shows some adjustment to the water surface, at least theoretically (see Figure 4). In view of this, the surface stress values should be lower.

12. Conclusion

Assuming that both upwind and downwind equilibrium wind profiles can be estimated, it has been shown that an interpolation model offers a possible approach to the problem of wind profile modification. Admittedly, the possible choices of transition functions are numerous, and the Gaussian form selected for this analysis was rather arbitrary. Improved observations of simultaneous upwind and downwind neutral profiles over land and lake are highly desirable. The thermal effect on wind profile modification had been already clearly demonstrated in Super's work on Lake Mendota, however, a complete description of profile modification, including mechanical influences, was not possible because upwind (land) data was lacking due to the fact that the surroundings of Lake Mendota are aerodynamically too complicated. This

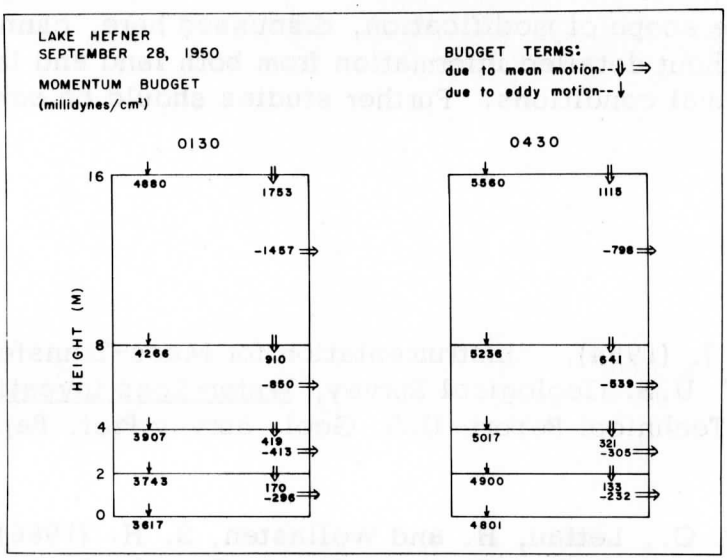

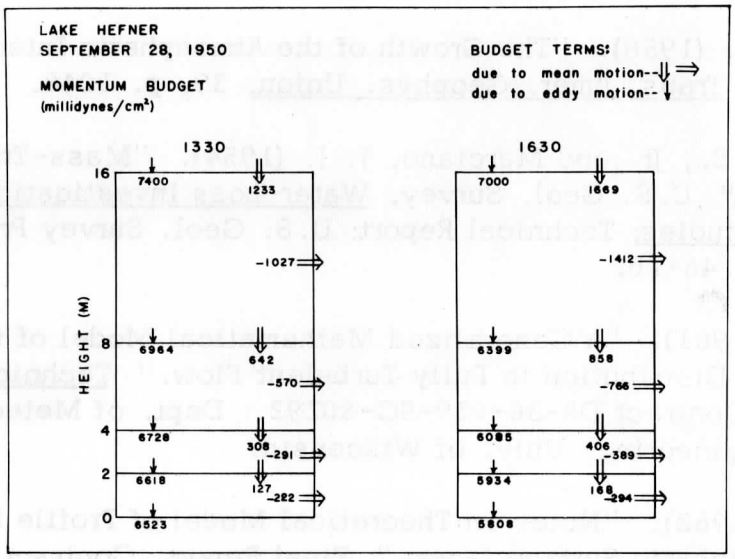

Fig. 7. Momentum budgets between upwind and downwind stations centered at four 3-hour periods during September 28, 1950.

study took into account the mechanical effects on profile modification and primarily dealt with the adiabatic case. It should be quite apparent that the entire scope of modification, discussed here, cannot be fully described without detailed information from both land and lake surfaces under all thermal conditions. Further studies should be conducted with this in mind.

References

Anderson, L. J. (1954). "Instrumentation for Mass-Transfer and Energy Budget." U.S. Geological Survey, Water-Loss Investigations—Lake Hefner, Technical Report: U.S. Geol. Survey Prof. Paper 269, pp. 35-45.

Dalrymple, P. C., Lettau, H. and Wollasten, S. H. (1966). "South Pole Micrometeorology Program: Part 2, Data Analysis." Antarctic Research Series, Vol. 9, pp. 13-57. Amer. Geoph. Union, Washington, D.C.

Elliott, W. P. (1958). "The Growth of the Atmospheric Internal Boundary Layer." Trans. Amer. Geophys. Union, 39, p. 1048.

Harbeck, G. E., Jr. and Marciano, J. J. (1954). "Mass-Transfer Studies." U.S. Geol. Survey, Water-Loss Investigation, Lake Hefner Studies: Technical Report: U.S. Geol. Survey Prof. Papers 269, pp. 46-70.

Lettau, H. (1961). "A Generalized Mathematical Model of the Mean-Velocity Distribution in Fully Turbulent Flow." Technical Report No. 3, Contract DA-36-039-SC-80292. Dept. of Meteorology and Civil Engineering, Univ. of Wisconsin.

Lettau, H. (1962). "Notes on Theoretical Model of Profile Structure in the Diabatic Surface Layer." Final Report, Contract DA-36-039-SC-80282 (USEPG, Fort Huachuca, Arizona) Univ. of Wisconsin, pp. 195-226.

Panofsky, H. A. and Townsend, A. A. (1964). "Change of Terrain Roughness and the Wind Profile." Quart. Jour. of the Roy. Meteorol. Soc., 90, p. 147.

Stearns, C. R. and Lettau, H. (1963). "Report on Two Wind Profile Modification Experiments in Air Flow over the Ice of Lake Mendota." Annual Report, Contract DA-36-039-AMC-00878 (USEPG, Fort Huachuca, Arizona) Univ. of Wisconsin, pp. 115-138.

Super, A. B. (1964). "Preliminary Results of an Air Mass Modification Study over Lake Mendota." Annual Report, Contract DA-36-039-AMC-00876 (USEPG, Fort Huachuca, Arizona) Univ. of Wisconsin, pp. 1-21.

Scanner's note:

This page is blank.

3

Wind Disturbance by a Vertical Cylinder in the Atmospheric Surface Layer

Walter F. Dabberdt
University of Wisconsin, Madison

ABSTRACT:

The velocity distribution in the neighborhood of a cylindrical obstacle was measured over the frozen surface of Lake Mendota, Madison, Wisconsin. Reductions in wind speed of six percent are noted upwind and greater than forty percent downwind. Cross-wind increases of five percent and more occur. The upwind isotach pattern is fairly well represented by the potential solution. The more complex downwind pattern is asymmetrical about the centerline. Large vertical components of the velocity are observed.

1. Introduction

Errors are often encountered in the measurement of the wind velocity which are a result of the mast or tower used to support the sensing instruments. The first phase of an experimental investigation of the so-called "tower effect" was conducted during the winter of 1965. A cylindrical obstacle, representative of a simple and uncluttered tower, was erected on the frozen surface of Lake Mendota. The velocity distribution in the vicinity of the "tower" was measured under the nearly ideal flow conditions which prevail over the smooth ice surface. Utilizing the results and experience gained from this study, a second phase was undertaken the following summer at Brookhaven National Laboratory, Upton, New York. The effects of their 420 ft meteorology tower, "Ace," were studied (Dabberdt, 1968).

2. Observational Site

Lake Mendota is located in south-central Wisconsin and has a surface area of approximately 40 km^2. Its surface is usually frozen four months of the year. The observational site was located 500 m north of Second Point (see Fig. 1). Only those wind directions which provided a minimum undisturbed fetch over the ice of 2000 m were used. This enabled the establishment of a representative wind profile in accordance with Lettau's (1959) suggested rule of thumb—that the undisturbed fetch be at least fifty times the height of the highest measuring level.

Five 55- gallon oil drums were vertically stacked to provide a cylindrical tower. The simulated tower had a diameter of 56 cm and was approximately 5 m high. At close view each drum had several surface discontinuities; three ribs around each drum protruded 1.3 cm as did the bung, 7 cm in diameter. Four guy wires held the tower in place and prevented oscillation in the wind. The tower was painted white so as to reduce differential heating between it and the surrounding ice surface (Fig. 2).

Seventeen Thornthwaite anemometers were used. The signals were sent to a junction box at the site where they were amplified and relayed to the Meteorology Instrument Building at Second Point. There the signals were recorded on electromechanical and electronic counters. A 720 cm bar was fitted with thirteen anemometers and mounted horizontally on a movable stand (Fig. 2). Crosswind profiles at any of four heights—40, 80, 160, and 320 cm—were then made. Comparisons were made to correct for possible anemometer errors arising from: (1) anemometer interaction, (2) inherent instrument differences, and/or (3) sag of the supporting bar. A conventional mast was used to measure vertical wind profiles.

3. Results

The horizontal wind profiles were nondimensionalized by taking the percentage of the individual velocities to a reference value obtained at the same height on the remote vertical mast. Isopleth diagrams were constructed (Figs. 3-6).

The upwind patterns are quite symmetrical about the centerline. A region of relatively low velocity exists forward of the cylinder; this is a manifestation of the forward stagnation point. Howarth (1953) states that the velocity near this point is a linear function, c, of distance, x, given by:

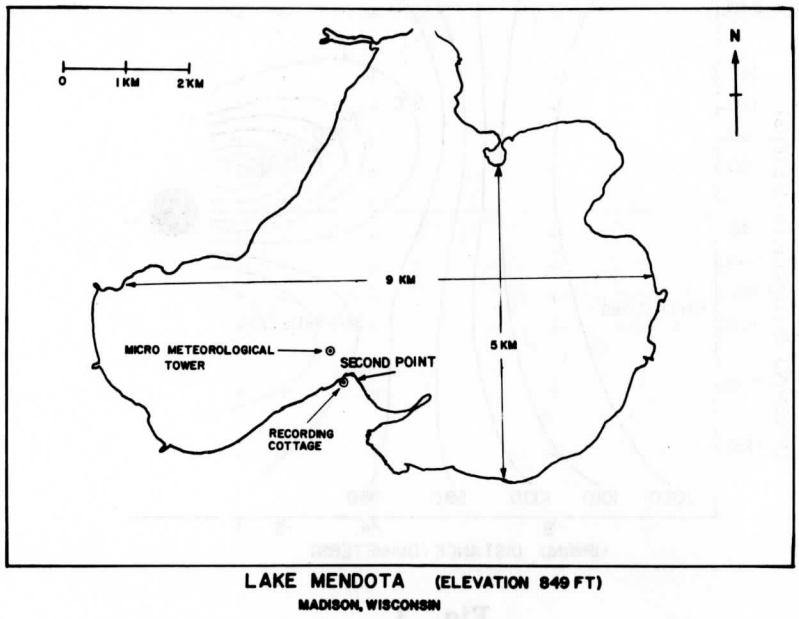

Fig. 1. Lake Mendota, Madison, Wisconsin

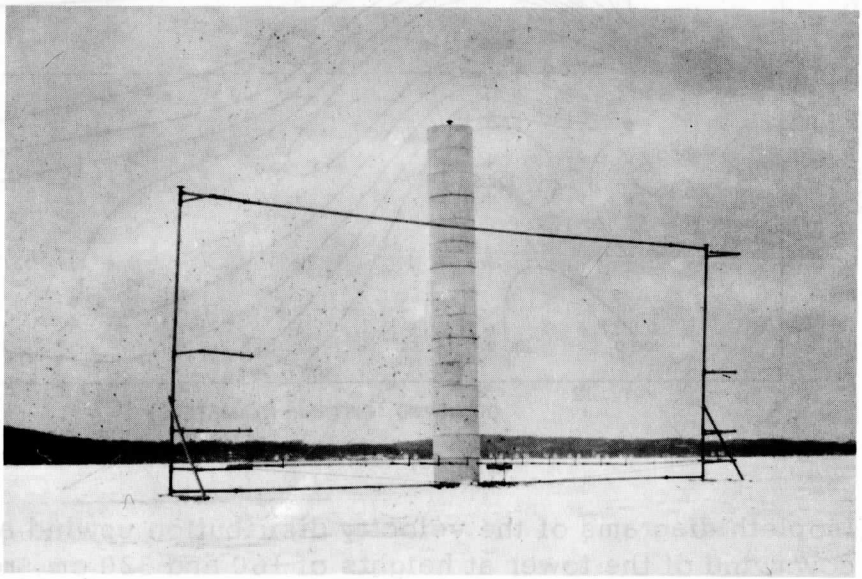

Fig. 2. Horizontal wind profile mast and simulated tower, Lake Mendota.

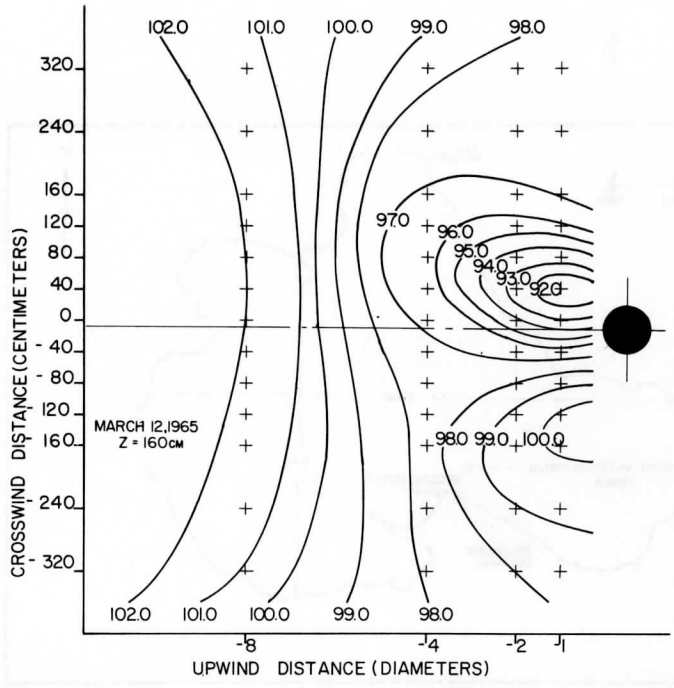

Fig. 3

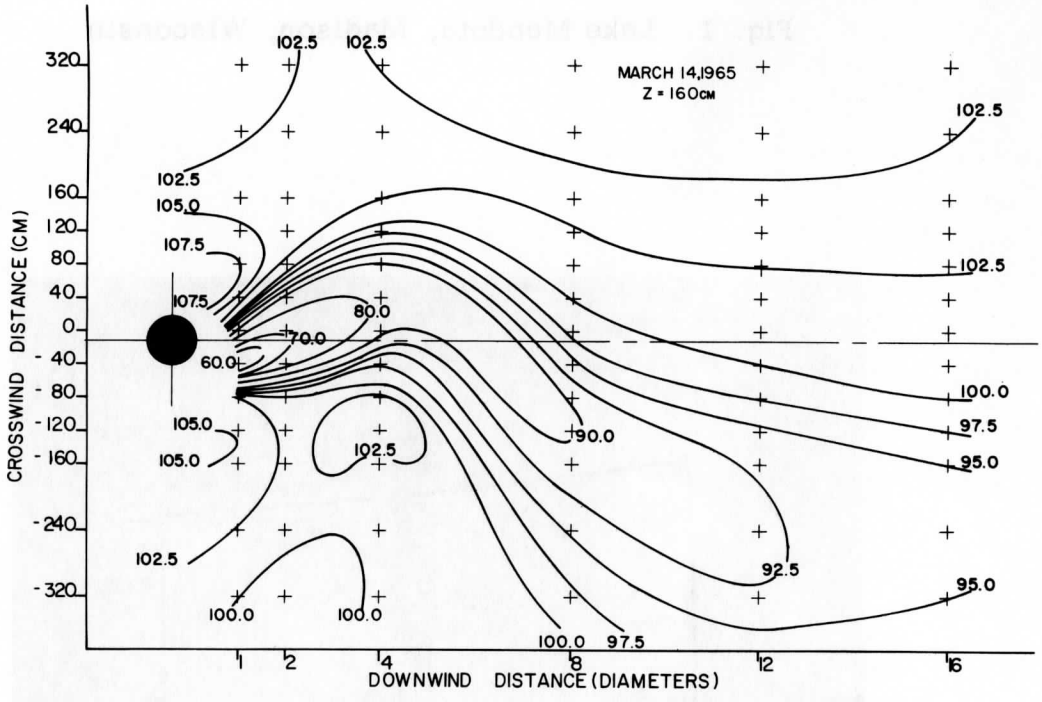

Fig. 4

Figs. 3–6. Isopleth diagrams of the velocity distribution upwind and downwind of the tower at heights of 160 and 320 cm, respectively. The isopleths are lines of constant values of the ratio of test to reference speeds, given as percentages. The lateral positions are given in cm, those longitudinal in tower diameters.

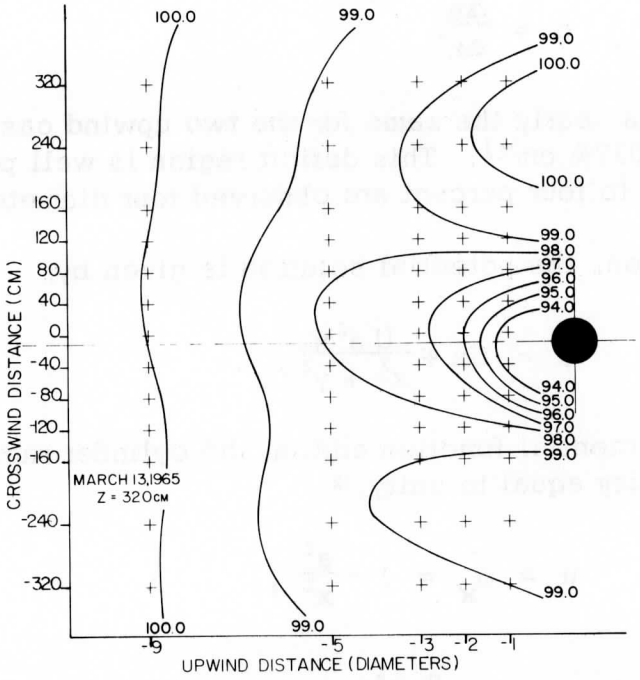
100.0
99.0
99.0
100.0
100.0
99.0
98.0
97.0
96.0
95.0
94.0
94.0
95.0
96.0
97.0
98.0
99.0
99.0
MARCH 13,1965
Z = 320cm
CROSSWIND DISTANCE (CM)
320
240
160
120
80
40
0
-40
-80
-120
-160
-240
-320
100.0
99.0
-9
-5
-5
-3
-2
-1
UPWIND DISTANCE (DIAMETERS)

Fig. 5

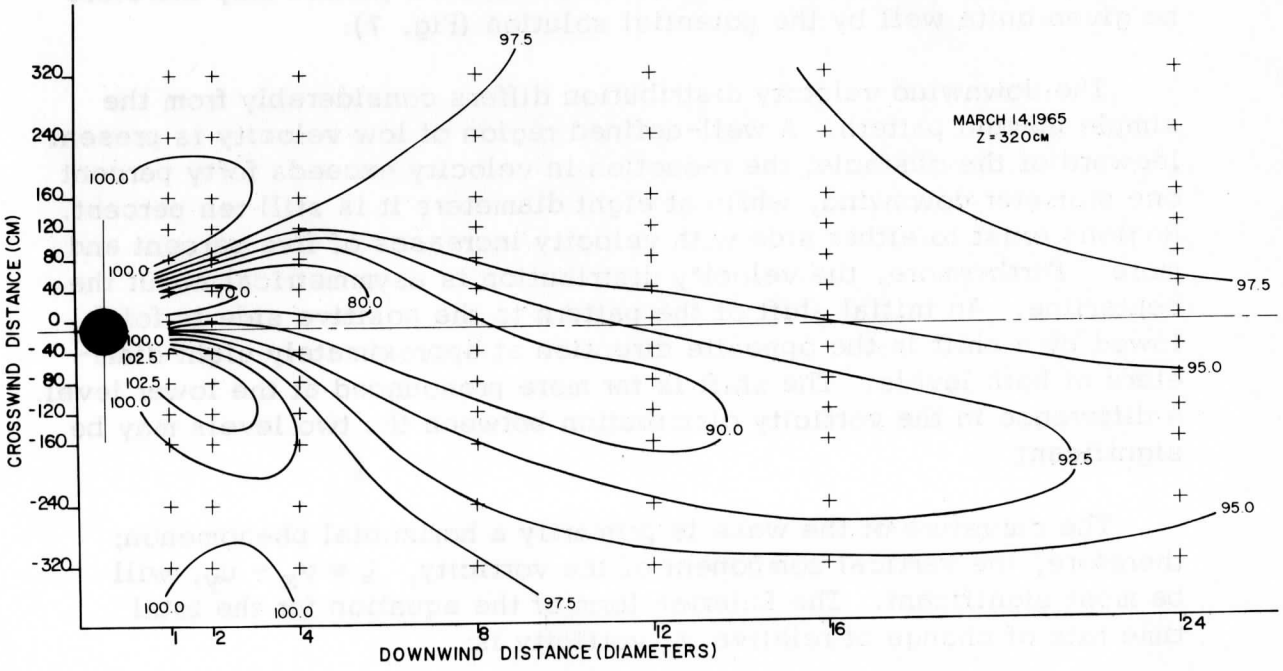
97.5
MARCH 14,1965
Z = 320cm
100.0
100.0
97.5
95.0
90.0
92.5
95.0
97.5
100.0
102.5
102.5
100.0
100.0
100.0
CROSSWIND DISTANCE (CM)
320
240
160
120
80
40
0
-40
-80
-120
-160
-240
-320
1
2
4
8
12
16
24
DOWNWIND DISTANCE (DIAMETERS)

Fig. 6.

$$c = \frac{\Delta u}{\Delta x}. \tag{1}$$

The value of c is nearly the same for the two upwind cases and is approximately 0.037% cm^{-1}. This deficit region is well pronounced; reductions of two to four percent are observed four diameters upwind.

For comparison, the potential solution is given by:

$$\phi = Ux + \frac{U a^2 x}{x^2 + y^2}, \tag{2}$$

where ϕ is the potential function and a the cylinder radius. Setting the ambient velocity equal to unity, *

$$u = \phi_x = 1 - \frac{a^2}{x^2}, \tag{3a}$$

and

$$u_x = 2a^2 x^{-3}. \tag{3b}$$

Although the linear function of Howarth differs considerably, observation shows that beyond two diameters upwind the two solutions yield similar results. The general shape of the upwind pattern may therefore be given quite well by the potential solution (Fig. 7).

The downwind velocity distribution differs considerably from the simple upwind pattern. A well-defined region of low velocity is present leeward of the obstacle; the reduction in velocity exceeds forty percent one diameter downwind, while at eight diameters it is still ten percent. Regions exist to either side with velocity increases of five percent and more. Furthermore, the velocity distribution is asymmetrical about the centerline. An initial shift of the pattern to the positive side is followed by a shift in the opposite direction at approximately eight diameters at both levels. The shift is far more pronounced at the lower level. A difference in the vorticity distribution between the two levels may be significant.

The curvature of the wake is primarily a horizontal phenomenon; therefore, the vertical component of the vorticity, $\zeta \equiv v_x - u_y$, will be most significant. The Eulerian form of the equation for the total time rate of change of relative ζ vorticity is:

$$\frac{d\zeta}{dt} = -\zeta(u_x - v_y) - (w_x v_y - w_y u_z) - (\alpha_x p_y - \alpha_y p_x) + (\vartheta v_{zz} - \vartheta u_{zz}), \tag{4}$$

*Subscripts denote partial differentiation with respect to the subscripted value.

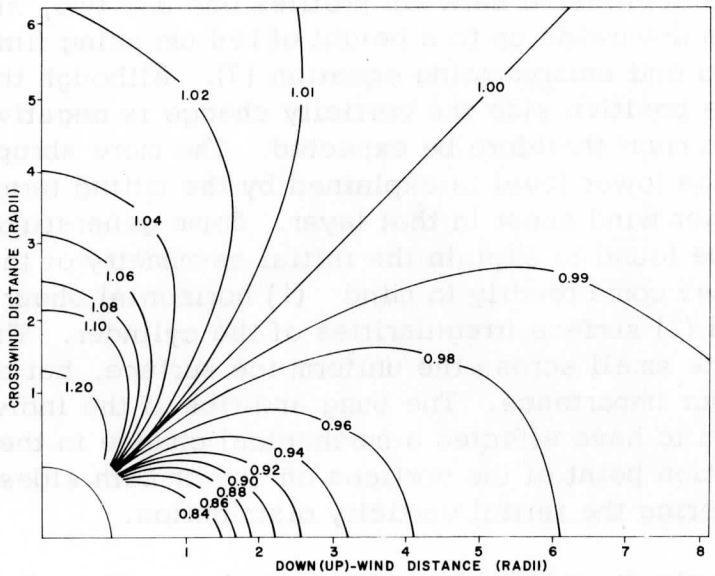

Fig. 7. Nondimensional velocity distribution about a circular cylinder as given by the potential solution.

where α is the specific volume, ϑ the kinematic coefficient of viscosity, and p, the pressure. The third (solenoidal) term on the right is negligibly small. The fourth (friction) term may also be disregarded as a first approximation upon considering $u_z > u_{zz}$, etc. The curvature may then be explained by the first (divergence) and/or second (tilting) terms. As a further simplification, terms incorporating v and its derivatives may be considered small with respect to u and w. Equation (4) now reduces to:

$$\frac{d\zeta}{dt} = u_x u_y + u_z w_y. \tag{5}$$

Under the imposed restrictions the continuity equation for an incompressible fluid reduces to:

$$u_x = - w_z. \tag{6}$$

Inserting the dynamic boundary condition of zero velocity at the surface, w may be estimated at height z by:

$$w = - \int_0^z u_x dz. \tag{7}$$

Equation(5) was evaluated between profiles one and two, and two and four diameters downwind up to a height of 160 cm using finite difference techniques and incorporating equation (7). Although the initial shift is toward the positive side the vorticity change is negative and clockwise rotation must therefore be expected. The more abrupt shift of the pattern at the lower level is explained by the tilting term which reflects the stronger wind shear in that layer. Some generating mechanism must still be found to explain the initial asymmetry of the horizontal profile. Two come readily to mind: (1) horizontal shear of the ambient flow, and (2) surface irregularities of the cylinder. The first is most likely quite small across the uniform ice surface, but the second may be of major importance. The bung and ribs of the individual drums are believed to have effected a mechanical change in the location of the separation point of the vortices on one or both sides of the cylinder, thus altering the initial vorticity distribution.

The vertical velocity was computed across the profile. Several large values were present in the immediate vicinity of the cylinder (Table 1). These were later confirmed by visual observations. Smoke grenades were released upwind of the tower and a 16 mm movie camera in the wake photographed the plume. The smoke was observed to spiral and rise in the lee of the cylinder (Fig. 8).

The strong vertical motion is a direct consequence of the effects of friction, both at the cylinder and ice surfaces. Convergent spiral vortices are continually shed at the cylinder surface. A positive vertical velocity at the vortex center follows from the consideration of three-dimensional mass continuity. Furthermore, friction at the ice surface induces further convergence.

The drag coefficient of the cylinder was computed through a numerical integration of the velocity deficit across the wake. Values range from 0.21 to 0.31 over a corresponding Reynolds number range of 2.26 to 3.44×10^5. This variation is illustrated in Fig. 9 along with values obtained by Roshko (1954) from wind tunnel data.

4. Conclusions

Reductions in wind speed of up to six percent are noted upwind and greater than forty percent downwind. Increases of five percent and more occur to the sides. The upwind isotach pattern is fairly well represented by the potential solution. The complex downwind pattern is asymmetrical about the centerline. This asymmetry is the result of surface irregularities of the cylinder. The vertical velocity in the lee of the cylinder is of the same order of magnitude as the horizontal

Fig. 8. Smoke plume passing a circular cylinder of 56 cm diameter. The smoke is being emitted from a smoke grenade on the ice surface. The wind speed at height of 2m is about 1 m sec^{-1}.

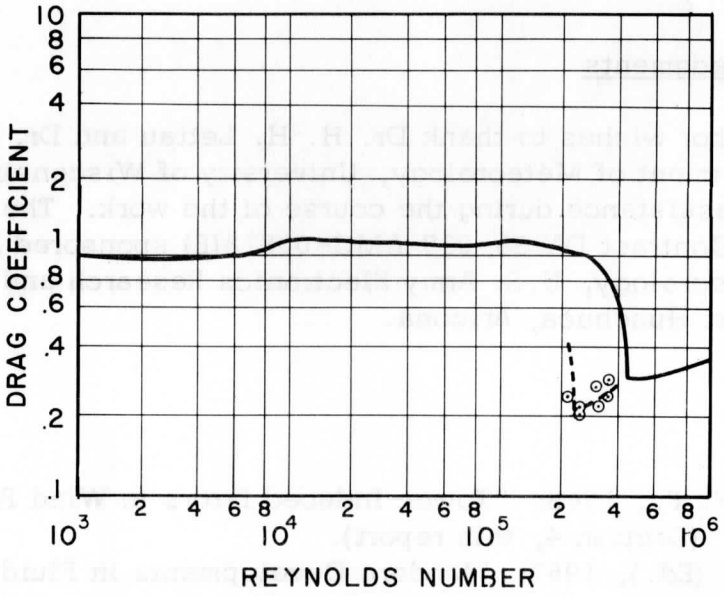

Fig. 9. Variation of the drag coefficient of a circular cylinder with the Reynolds number. The solid curve is from data given by Roshko (1954). The points and dashed curve are from values computed over the ice surface.

Table 1. Mean values of the vertical component of the velocity, w, downwind of the simulated tower, March 14, 1965, for the layer between the surface and 160 cm. W is expressed as a percentage of the horizontal component of the ambient velocity, U_0. The mean value of U_0 is approximately 5m/sec. The crosswind positions are given as distances from the centerline in cm.

Crosswind Position (cm)	Mean W 1-2 Diam.	Mean W 2-4 Diam.
+160	+ .0511	+ .0069
+120	+ .0891	+ .0719
+ 80	+ .1480	+ .2079
+ 40	+ .6028	+ .0715
0	+ .5031	- .2355
- 40	- .9888	- .1255
- 80	+ .0594	- .0183
-120	+ .1048	- .0293
-160	+ .0854	- .0276

component. The cylinder drag coefficient ranges from 0.21 to 0.31 for Reynolds numbers of 2.26 to 3.44×10^5.

5. Acknowledgments

The author wishes to thank Dr. H. H. Lettau and Dr. C. R. Stearns of the Department of Meteorology, University of Wisconsin, for their advice and assistance during the course of the work. The work was done under Contract DA-36-039-AMC-00878(E) sponsored by the Department of Meteorology, U. S. Army Electronics Research and Development Activity, Fort Huachuca, Arizona.

References

Dabberdt, W. F., 1968: "Tower-Induced Errors in Wind Profile Measurements," (Section 4, this report).

Howarth, L. (Ed.), 1953: "Modern Developments in Fluid Dynamics, High Speed Flow," Vol. II, Oxford: The Clarendon Press, 790-793.

Lettau, H. H., 1959: "Research Problems in Micrometeorology," Final Report, Contract No. DA-36-039-SC-80063, University of Wisconsin.

Roshko, A., 1954: "On the Development of Turbulent Wakes from Vortex Streets," NACA Technical Report No. 1191.

4

Tower-Induced Errors in Wind Profile Measurements

Walter F. Dabberdt
University of Wisconsin, Madison

ABSTRACT:

An investigation of the effect of a meteorological tower on the measurement of wind speed was conducted at Brookhaven National Laboratory. Reductions up to 35 percent occur in the wake. The distribution of the velocity deficit in the wake is nearly Gaussian; corrections based on this distribution have improved wind data in a trial case. A slight dependence on atmospheric stability was detected; the deficit appears to be independent of the wind speed.

1. Introduction

Errors in the measurement of wind velocity are often encountered which are a result of the effect of the mast or tower used to support the sensing instruments. Although this so-called "tower effect" presents a major problem with regard to the measurement of unbiased wind data, there have been few adequate published investigations of this phenomenon. Especially sparse are investigations conducted under atmospheric conditions, i.e., exclusive of wind tunnel studies.

An investigation of this effect was conducted at Brookhaven National Laboratory, Upton, New York. The 420-foot meteorology tower at the site was instrumented and detailed measurements of the horizontal wind speed were obtained at seven positions. This approach has the advantage over wind tunnel studies that the effects of wind shear and density stratification are brought into play.

2. Velocity Distribution in the Turbulent Wake

Following the discussion of Schlichting (1955), the mean motion in the wake of a cylindrical obstacle may be considered steady-state, horizontal, and without a pressure gradient. The equation of motion is then

$$u\frac{\partial u}{\partial x} = \frac{1}{\rho}\frac{\partial \tau}{\partial y} - v\frac{\partial u}{\partial y}, \tag{1}$$

where τ is the turbulent shearing stress and u and v are the longitudinal and lateral velocity components, respectively. Schlichting obtains a solution of (1) through similarity concepts which is valid for large downstream distances. The distribution of the velocity deficit, $u' = U - u$, is given by:

$$u' = \frac{0.17}{\beta} U \left(\frac{c_d d}{x}\right)^{1/2} \left[1 - \left(\frac{y}{b}\right)^{3/2}\right]^2 \tag{2}$$

where U is the ambient velocity of the fluid, d is the cylinder diameter, b the width of the wake, c_d the drag coefficient, and β a constant. β must be derived empirically; Schlichting gives a value of 0.18.

Comparison between this theoretical distribution and results obtained by Schlichting in the wind tunnel shows excellent agreement. The solution is valid at values of $(x/c_d d)$ greater than 50. At the transition between laminar and turbulent flow, c_d has a value between 0.2 and 0.4. Therefore, the solution may be valid for some cases at distances as small as ten diameters.

Schlichting's solution (Eq. 2) can be very nearly approximated by a Gaussian distribution. Lin (1954) takes a different approach to the problem and obtains a similar velocity distribution

$$u \sim \exp\left(-\frac{1}{2}\eta^2\right), \tag{3}$$

where η is an independent variable given by $y(U/2\vartheta x)^{1/2}$; ϑ is the kinematic coefficient of viscosity. It is, therefore, not unreasonable to expect a Gaussian-type velocity distribution in the wakes of certain meteorological towers.

3. Experimental Site

Brookhaven National Laboratory is located in east-central Long Island. The terrain is fairly flat; the maximum surface height variation is approximately 5 m over a 500 m radius. The vegetation is primarily scrub oak and pine 8 to 11 m high; there are several large grass fields at the site (Fig. 1). Singer and Nagle (1962) have given a detailed description of the site.

The tower under investigation was the 128 m Ace Tower, which is used for meteorological data collection. It is an equitriangular structure 5.5 m on a side with an open steel framework. Booms housing wind and temperature sensors are mounted at heights of 5.5, 11.3, 22.9, 45.7, 91.4, 108.2, and 125.0 m. A different level was chosen for the study so as to be completely free of any interference with existing equipment; Dabberdt (1964) has shown such effects to be highly significant. The 30.5 m level was chosen; it is representative of the general tower structure. Three rectangular aluminum booms ($0.05 \times 0.15 \times 6.10$ m) were mounted approximately 120 degrees apart. Two three-cup anemometers were mounted on each boom (Fig. 2), one 2.74 m and the other 5.49 m from the tower. The outer position corresponded to those of aerovanes at the "normal" levels. At the test level two cables extend to a smaller tower 274 m away. A motor-driven traveler fitted with an anemometer was designed to move along these cables. All anemometers were calibrated in the Brookhaven wind tunnel both before and after their use on the tower.

Hourly vertical temperature and velocity profiles were obtained from Brookhaven's existing sampling system, "Punchy." This has been thoroughly described by Mazzarella and Kohl, Brown (1959), and Singer and Nagle (1962).

4. Data Reduction

The wind and averaged Punchy data were used to compute various scale and shape factors, in addition to nondimensional velocity ratios. The calculations were made on IBM 7094 and CDC 3600 electronic digital computers.

The gradient Richardson number, Ri, provides a measure of atmospheric stability. Values were computed and analyzed for each run for layers between 0 and 11.3 m, and 22.9 and 45.7 m. The gradient Richardson number is defined as

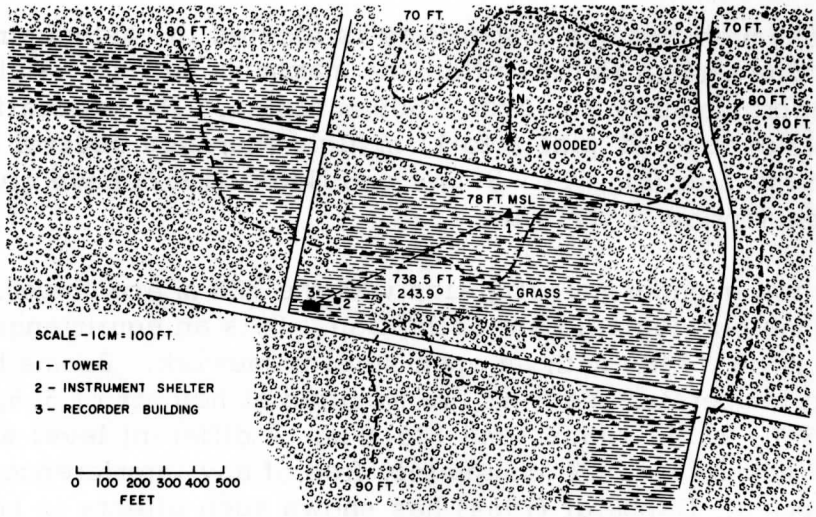

(a)

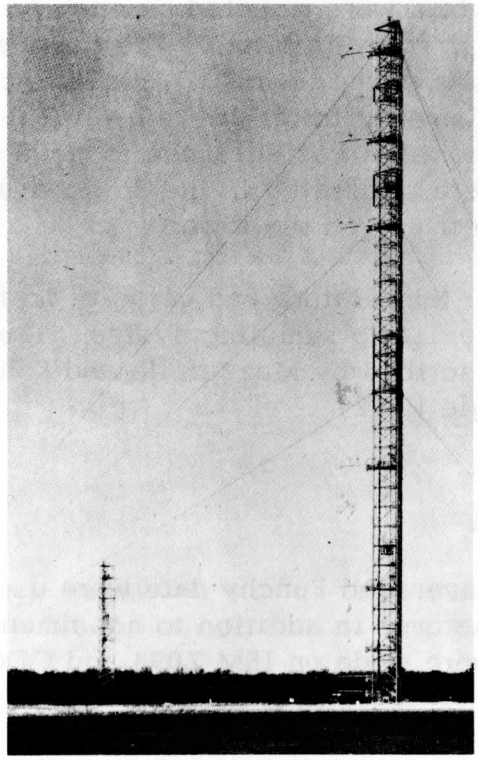

(b)

Fig. 1. (a) The topography of the field site at Brookhaven National Laboratory showing the location of (b) Ace Tower (courtesy BNL.

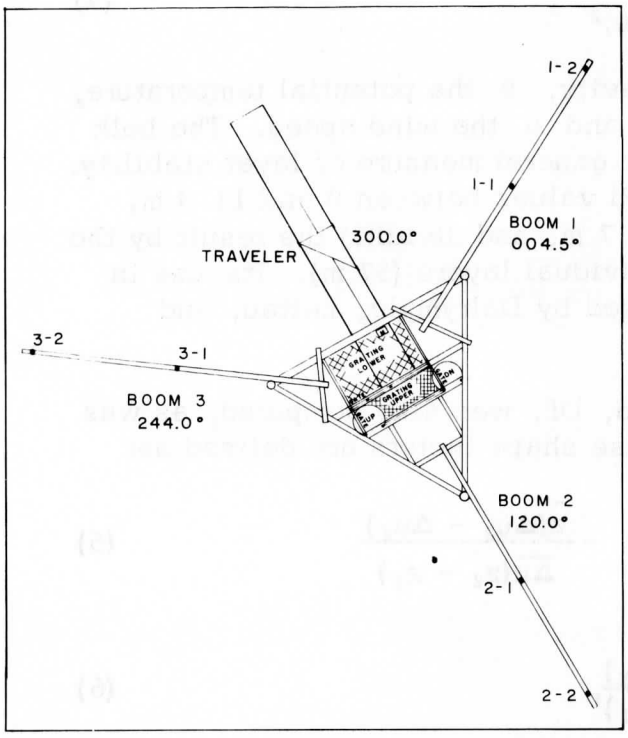

Fig. 2. Working level for the study, 30.5 m, showing the relative positioning of booms, anemometers, and traveler.

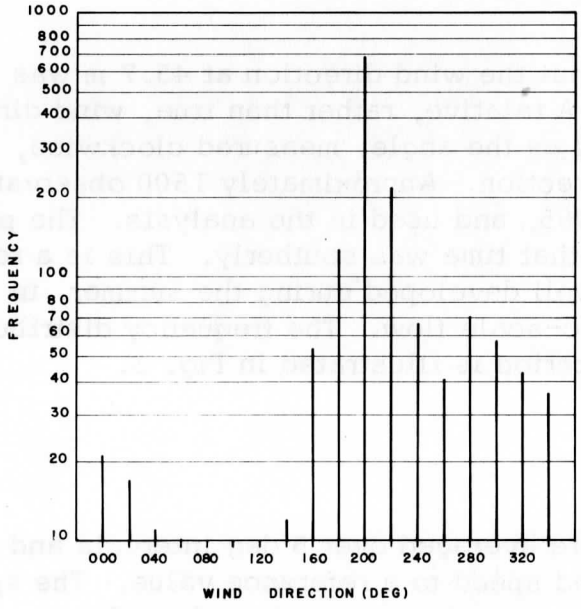

Fig. 3. Wind direction frequency distribution over 12 min periods and 20 deg intervals for the period 6 to 16 August 1965, at Brookhaven National Laboratory.

$$Ri \equiv \frac{g}{\bar{T}} \frac{\Delta\theta\Delta z}{(\Delta u)^2} , \qquad (4)$$

where g is the acceleration of gravity, θ the potential temperature, z the height, T the temperature, and u the wind speed. The bulk Richardson number, A Ri, is a more general measure of layer stability. It was calculated by summing the Ri values between 0 and 11.3 m, 11.3 and 22.9 m, and 22.9 and 45.7 m, and dividing the result by the sum of the mean heights of the individual layers (57 m). Its use in climatic analysis has been discussed by Dalrymple, Lettau, and Wollaston (1963).

The Deacon number for the wind, DE, was also computed, as was the "power law" exponent, p. These shape factors are defined as:

$$DE \equiv -\frac{\partial \log(\Delta u/\Delta z)}{\partial \log z} \cong -\frac{\bar{z}(\Delta u_2 - \Delta u_1)}{\overline{\Delta u}(z_2 - z_1)} \qquad (5)$$

and,

$$p \equiv \frac{\partial \log u}{\partial \log z} \cong \frac{\log(u_2/u_1)}{\log(z_2/z_1)}, \qquad (6)$$

where subscripts refer to heights and the overbar denotes a mean value for the layer.

It was assumed that the wind direction at 45.7 m was equal to that measured at 30.5 m. A relative, rather than true, wind direction was used. This is defined as the angle, measured clockwise, between the booms and the true direction. Approximately 1500 observations were made during August 1965, and used in the analysis. The predominant wind direction during that time was southerly. This is a result of the sea breeze which is well developed during the summer, in addition to the prevailing synoptic-scale flow. The frequency distribution of wind direction during that period is illustrated in Fig. 3.

5. Results

The wind data were averaged over 5 deg intervals and calculated as the ratio of the wind speed to a reference value. The speed of the outer, most upwind anemometer was used as the reference. Figures 4-9 are hodographs of the distribution of these ratios with the true wind direction. Reductions up to 35 percent are consistently noted in the downstream sectors. These occur through an arc of approximately 60 deg. Increases, on the other hand, up to 19 percent occur when the flow is along the tower sides. These may partially reflect some bias of the reference as its relative wind direction increases.

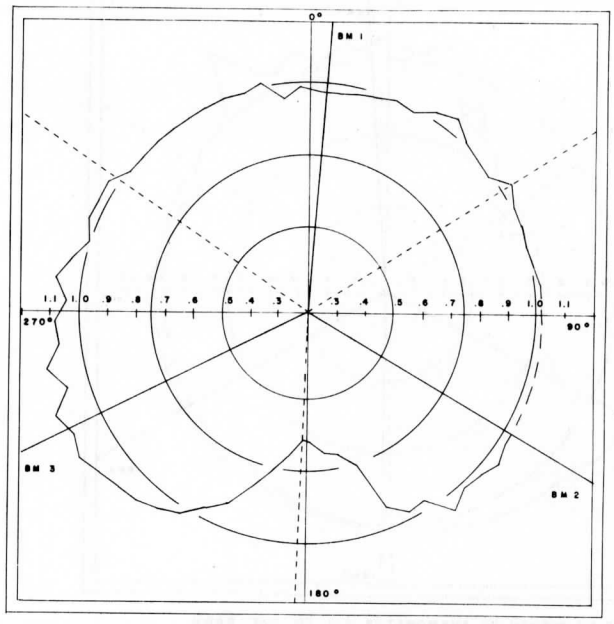

RATIO OF SPEEDS OF ANEMOMETER 1-1 TO THE BOOM REFERENCE ANEMOMETER AS A FUNCTION OF THE WIND DIRECTION.

Fig. 4

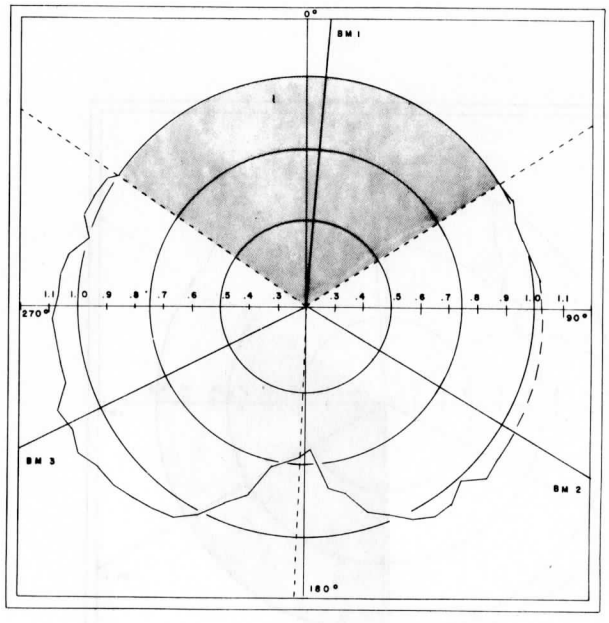

RATIO OF SPEEDS OF ANEMOMETER 1-2 TO THE BOOM REFERENCE ANEMOMETER AS A FUNCTION OF THE WIND DIRECTION.

Fig. 5

Figures 4-9. Hodographs of the velocity distribution about Ace Tower at six positions for the period 6 to 16 August 1965. The shaded areas indicate those arcs for which the outer anemometer served as the reference.

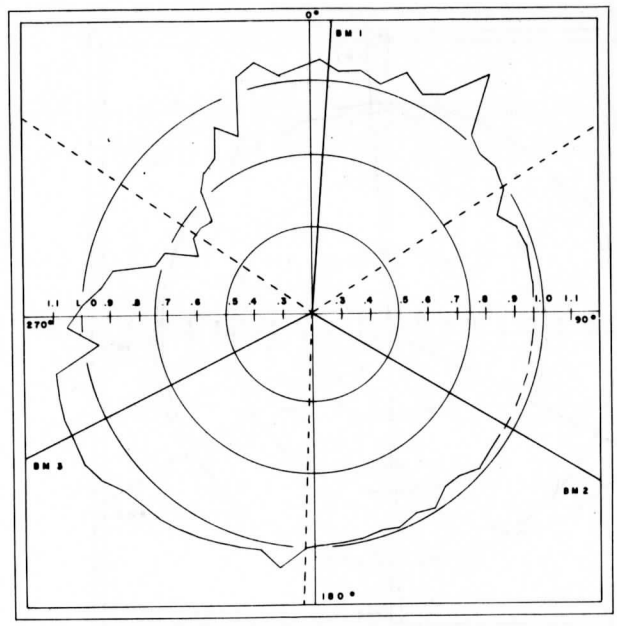

RATIO OF SPEEDS OF ANEMOMETER 2-1 TO THE BOOM
EFERENCE ANEMOMETER AS A FUNCTION OF THE WIND DIRECTION.

Fig. 6

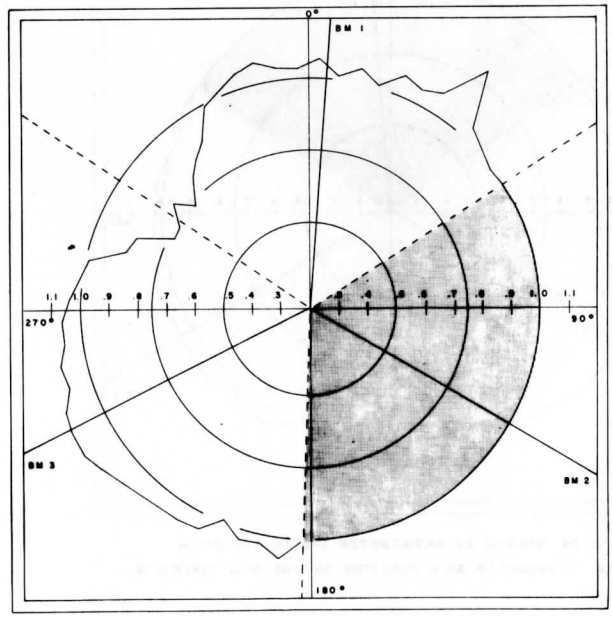

RATIO OF SPEEDS OF ANEMOMETER 2-2 TO THE BOOM
REFERENCE ANEMOMETER AS A FUNCTION OF THE WIND DIRECTION

Fig. 7

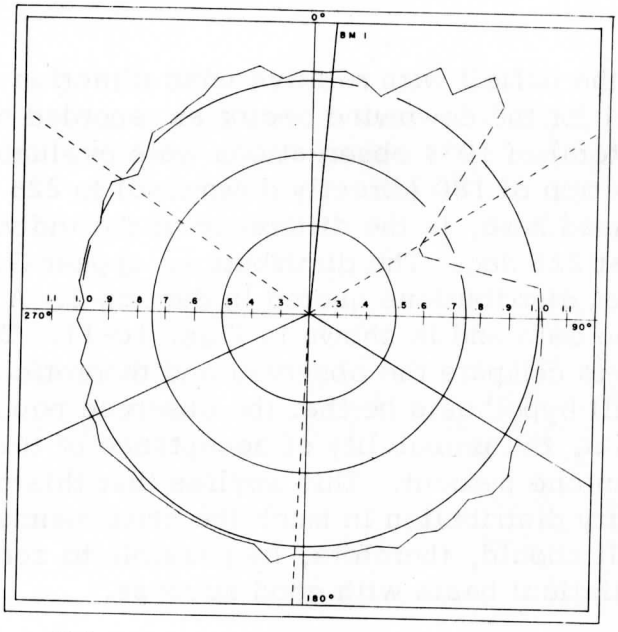

RATIO OF SPEEDS OF ANEMOMETER 3-1 TO THE BOOM REFERENCE ANEMOMETER AS A FUNCTION OF THE WIND DIRECTION.

Fig. 8

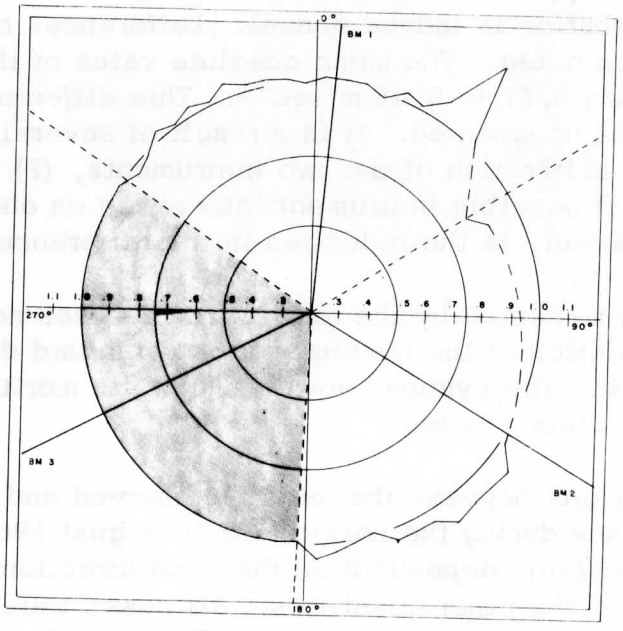

RATIO OF SPEEDS OF ANEMOMETER 3-2 TO THE BOOM REFERENCE ANEMOMETER AS A FUNCTION OF THE WIND DIRECTION.

Fig. 9

The variation of the deficit with relative wind direction was investigated in greater detail for the downwind sector as recorded by anemometers 1-1 and 1-2. A total of 1034 observations were evaluated over a range of relative direction of 180 (directly downwind) to 225 deg. The velocity deficit, as used here, is the difference of the individual ratios from the mean value at 225 deg. The distributions appear Gaussian, as were the theoretical distributions quoted in Section 2. A normal curve was fitted to the data and is shown in Figs. 10-11. The chi-square test was used to compare the observed and theoretical distributions. Letting the null hypothesis be that the observed population is not a part of the normal, the probability of acceptance of this hypothesis is very much less than one percent. This implies that this complicated tower effects a velocity distribution in much the same manner as does a circular cylinder. It should, therefore, be possible to correct downwind values on a statistical basis with good success.

A test of this premise was made. Two booms, approximately 120 degrees apart, are used to measure hourly values of the wind speed at the 45.7 m level. During the period 6 to 10 August, the predominant wind direction was such that one of the booms was consistently in the upwind sector while the other was downwind. Mean corrections over 5-degree intervals were applied to the downwind values under the assumption that the distribution is indeed normal. Differences from the upwind values were then noted. The mean absolute value of this difference was reduced from 0.57 to 0.45 m sec^{-1}. This difference is still quite large, but not unexpected. It is a result of several other factors; (1) the lack of calibration of the two instruments, (2) the long sampling period, and (3) possible instrument interaction on one of the booms. Important, however, is the reduction in the difference.

The wind speed as measured by the remote traveler was not used in the analysis. Oscillation of the system induced standard deviations too large for acceptance. The system, however, has its merits and may prove practical for other studies.

Statistical correlations between the various observed and computed parameters for 1034 cases during the period 6 to 16 August 1965, show the velocity ratio to be highly dependent on the wind direction and relatively independent of the other quantities. All cases were within a range of relative direction of 180 to 225 deg. The linear correlation coefficient between the ratio and the relative direction is 0.852. The partial correlation coefficients between these two parameters, holding various scale and shape factors constant, depart less than 0.003 from this value. The partial correlation coefficient between the ratio and Richardson number, eliminating the effect of direction, is -0.101. Increased mixing in the atmosphere is a direct consequence of a decrease

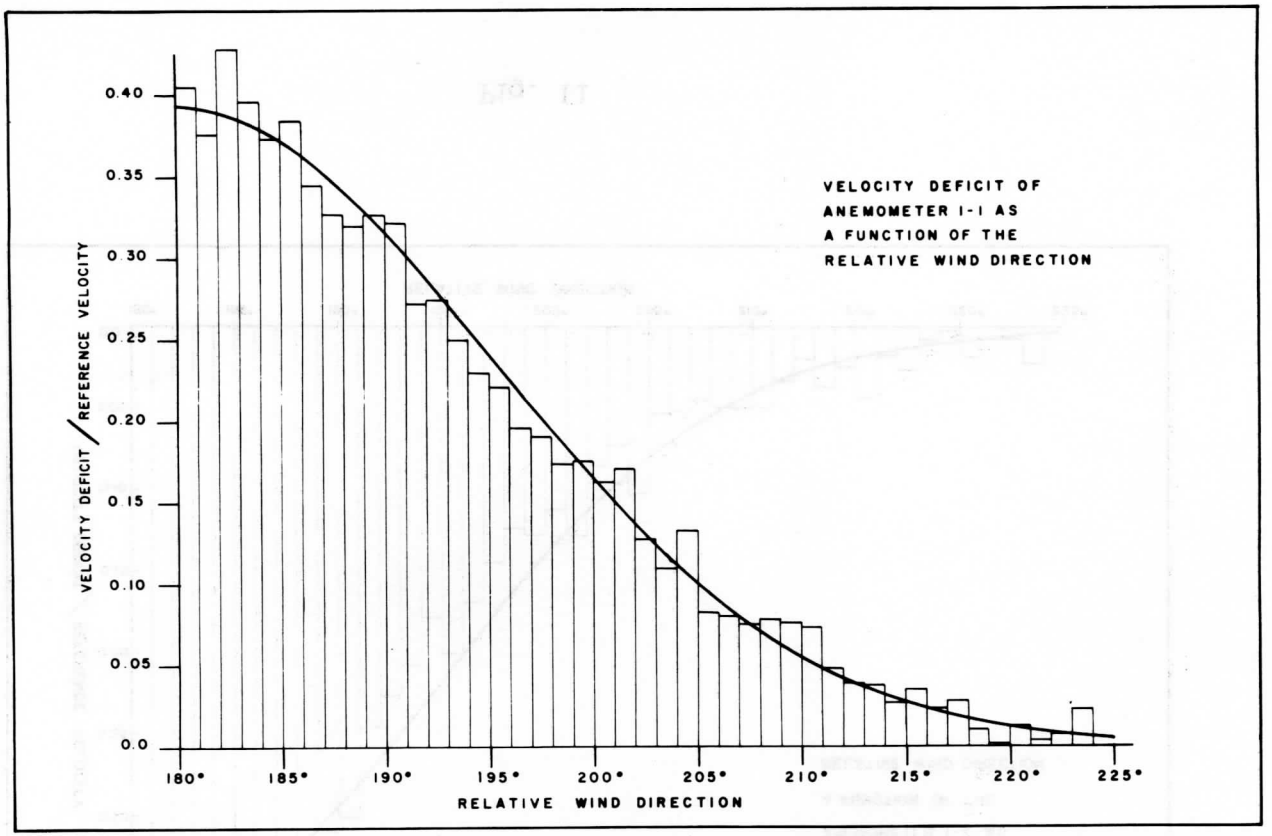

Fig. 10

Figs. 10-11 (see next page). Distribution of the velocity deficit in the wake of Ace Tower as a function of the relative wind direction. The deficit is defined here as the difference of the individual velocity ratios and that at 225 deg (relative). The relative direction is the angle, measured clockwise, between the boom and the true wind direction. The solid curve is the normal curve fitted to the data.

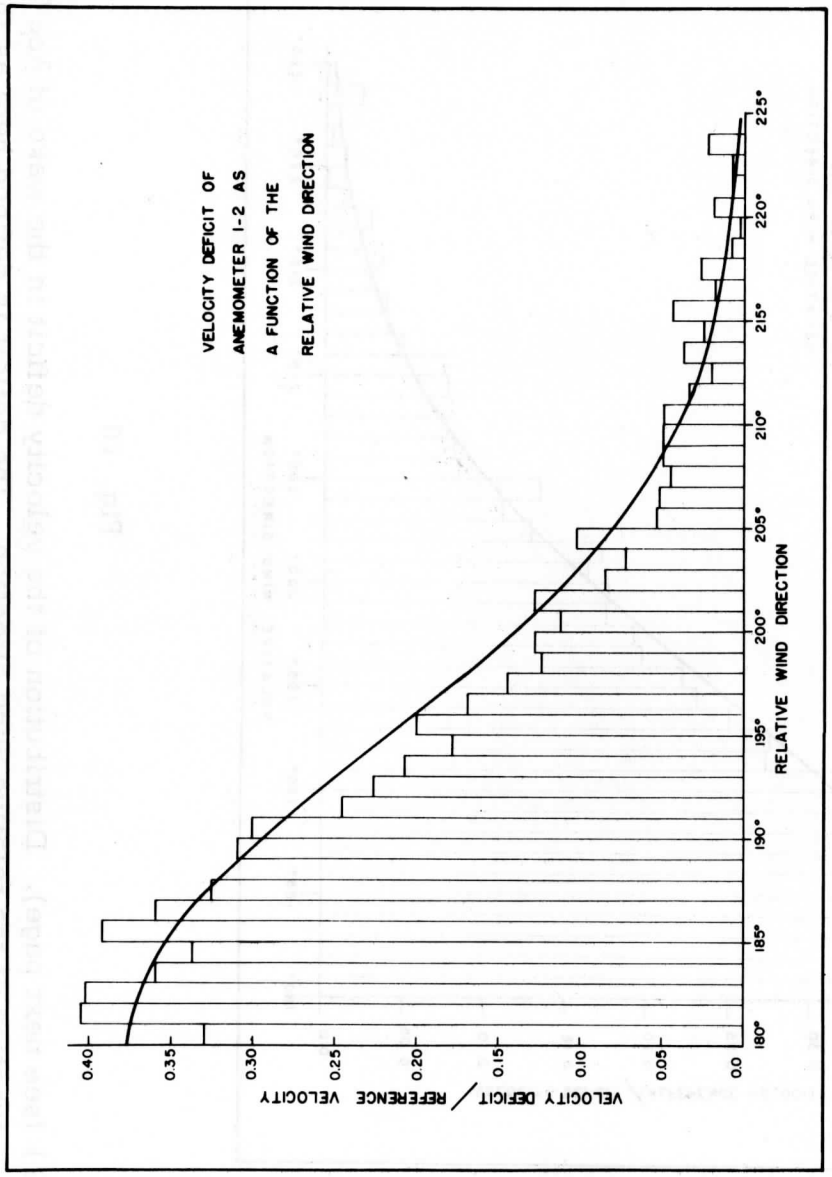
VELOCITY DEFICIT OF
ANEMOMETER 1-2 AS
A FUNCTION OF THE
RELATIVE WIND DIRECTION
VELOCITY DEFICIT / REFERENCE VELOCITY
0.0
0.05
0.10
0.15
0.20
0.25
0.30
0.35
0.40
180°
185°
190°
195°
200°
205°
210°
215°
220°
225°
RELATIVE WIND DIRECTION

Fig. 11

in stability. Therefore, an increase in the speed or, in other words, a decrease in the deficit can be expected. While the magnitude of this term is not as statistically meaningful as that for direction, its sign is consistent with theory. This effect can be expected to increase as the surface is approached.

This study clearly shows that the downwind velocity distribution is nearly Gaussian. Some effect of the stability of the air, as given by scale factors such as the Richardson number, has been detected. No dependence on wind speed was ascertained as this would require extensive study of individual anemometer characteristics. Wind speed is not, however, thought to play a major role provided the flow is consistently in one regime, i.e., turbulent.

6. Conclusions

Decreases in the wind speed up to 35 percent are noted downwind of the tower with increases up to 19 percent along the sides. The deficit region extends through an arc of approximately 60 deg and is well represented by a Gaussian distribution. Corrections of the wind speed based on this distribution reduced the error in a trial case. A slight dependence on atmospheric stability was detected. No effect of wind speed was observed.

7. Acknowledgments

The author wishes to thank Dr. H. H. Lettau and Dr. C. R. Stearns of the Department of Meteorology, University of Wisconsin, and M. E. Smith, R. E. Brown, and the members of the Meteorology Group, Brookhaven National Laboratory for their advice and assistance during the course of the work.

8. Bibliography

Brown, R , 1959: "An Automatic Data Collecting System," J. of Geophys. Res., 64, 2369-2372.

Dabberdt, W. F., 1964: "Anemometer-Aerovane Interaction," [Memorandum, Brookhaven National Laboratory, N.Y.]

Dalrymple, P., H. Lettau, and S. Wollaston, 1963: "South Pole Micrometeorology Program, Part II: Data Analysis," Technical Report ES-7, Quartermaster R and E Center, Natick, Mass.

Lin, C. C., 1954: "On Periodically Oscillating Wakes in the Oseen Approximation," Studies in Mathematics and Mechanics (presented to R. von Mises), 170-176, Academic Press, N.Y.

Mazzarrella, D. A. and D. K. Kohl: "Temperature Measurements on a 420-foot Tower," [Meteorology Group, Brookhaven National Laboratory, N.Y.]

Schlichting, H., 1955: Boundary Layer Theory, Pergamon Press, N.Y.

Singer, I. and C. Nagle, 1962: "A Study of the Wind Profile in the Lowest 400 Feet of the Atmosphere," Final Report, Contract No. R-61-5-SC-01-91, Brookhaven National Laboratory, N.Y.

5

Application of Lettau's Theoretical Model of Thermal Diffusion to Soil Profiles of Temperature and Heat Flux

Charles R. Stearns
University of Wisconsin, Madison

ABSTRACT:

Diurnal cycles of soil temperatures and heat flux measured on the Pampa de La Joya, Peru, are analyzed harmonically. A theory of thermal diffusion put forth by Lettau (1962) is used to determine the relative calibration of the soil heat flux plates and the relative depth intervals between the flux plates in comparison to the soil temperature profile. The absolute value of the soil heat flux is based on the allowed range of values for the volumetric heat capacity or soil density.

Introduction

One of the problems associated with the determination of the heat budget at the air-earth interface is the measurement of the heat flux into soil. The soil temperature integral method utilizing the change in soil heat storage with respect to time together with an average volumetric heat capacity of the soil profile (Lettau, 1957) has often been used to determine the soil heat flux. This method requires a measurement of the volumetric heat capacity of the soil usually involving the removal of a soil sample which may not be representative of the place where the soil temperature profile is being measured.

An alternative method would be to use a soil heat flux plate such as is described by Deacon (1950) where the output signal is proportional to the soil heat flux provided the "in situ" calibration is known. The theory of heat flux plates has been adequately explained by Portman (1958) and Philip (1961) so that the construction of the heat flux plate can be such as to minimize the design errors. Both of the above authors discussed the calibration errors which may arise due to

differences in conductivity between the medium and the soil flux plate. A common method of calibrating heat flux plates is to place them in a medium such as sand through which a known heat flux is maintained (Deacon, 1950). Then placing the calibrated heat flux plates in another medium of different and unknown conductivity will alter the calibration of the heat flux plate.

Philip (1961) pointed out that one of the major difficulties with the heat flux plate when used in the soil is the degree of thermal contact between the soil and the flux plate. Poor thermal contact could result in an underestimation of the soil heat flux by as much as 50 percent.

The unknown errors in flux plate "in situ" calibration due to the uncertainty about the degree of thermal contact and the ratio of flux plate to medium conductivity makes it desirable to check the flux plate calibration after installation in the soil.

The purpose of this paper is to apply a theory of thermal diffusion developed by Lettau (1962) to determine the relative calibration of soil heat flux plates at several depths in the soil and finally, the soil heat fluxes based on an assumption about the possible range of soil densities. The successful application of the theory requires that soil temperature and heat flux be determined simultaneously at several depths in the soil over several cycles of insolation.

Harmonic Analysis Theory

The method of calculating the soil thermal characteristics such as volumetric heat capacity, conductivity, diffusivity and admittance is based entirely on Lettau's(1962) theoretical model of thermal diffusion.

The soil temperature and heat flux are assumed to be harmonic functions of the form

$$T(t) = T_m + \sum A_n \cos(\omega nt - \alpha_n) \quad (1)$$

$$F(t) = F_m + \sum B_n \cos(\omega nt - \beta_n) \quad (2)$$

where $T(t)$ and $F(t)$ are the temperature (deg C) and the heat flux (ly/sec) respectively, T_m and F_m are the mean temperature and heat flux for the period under consideration, A_n and B_n are amplitudes of the n^{th} harmonic of temperature and heat flux respectively, α_n and β_n are the respective phase angles of the n^{th} harmonic, and $\omega = 2\pi/P$ where P is the period of time for the first harmonic. $2\pi n/P$ is then the frequency in radians/sec of the n^{th} harmonic.

Differentiation of equation (1) with respect to time and depth yields

$$\dot{T}(t) = \dot{T}_m - \omega n \sum [a_n \sin(\omega nt - \alpha_n) \tag{3}$$

$$T'(t) = T'_m + \sum [A_n' \cos(\omega nt - \alpha_n) + A_n \alpha_n' \sin(\omega nt - \alpha_n)] \tag{4}$$

Differentiation of equation (2) with respect to depth yields

$$F'(t) = F'_m + \sum B_n' \cos(\omega nt - \beta_n) + B_n \beta_n' \sin(\omega nt - \beta_n)]. \tag{5}$$

The basic equation of continuity in the absence of heat sources or sinks in the medium is

$$F'(t) = -C \dot{T}(t) \tag{6}$$

where C is the volumetric heat capacity (ly $cm^{-1} K^{-1}$). Fourier's law is the second basic equation which is

$$F(t) = - \lambda T'(t) \tag{7}$$

where λ = heat conductivity (ly $sec^{-1} K^{-1}$ cm). Let $\gamma_n = \alpha_n - \beta_n$ which is the difference in phase angle between the temperature and the heat flux wave for the n^{th} harmonic. Substitution of $\alpha_n = \gamma_n + \beta_n$ in equation (3) yields

$$\dot{T}(t) = - \sum \omega n A_n \sin(\omega nt - \gamma_n - \beta_n). \tag{8}$$

By use of a trigonometric identity for the sum of two angles one obtains

$$\dot{T}(t) = \sum -\omega n A_n [\sin(\omega nt - \beta_n) \cos \gamma_n - \cos(\omega nt - \beta_n) \sin \gamma_n]. \tag{9}$$

By substituting equation (4) and (9) into (7) and dropping the summation sign on the assumption that the n^{th} harmonic of the heat flux wave determines the n^{th} harmonic of the temperature wave, one obtains

$$B_n' \cos(\omega nt - \beta_n) + B_n \beta_n' \sin(\omega nt - \beta_n)$$

$$= \omega nC A_n [\sin(\omega nt - \beta_n) \cos \gamma_n - \cos(\omega nt - \beta_n) \sin \gamma_n]. \tag{10}$$

When

$$\omega nt - \beta_n = 0, \pi$$

then

$$B_n' = -C\,\omega n\, A_n \sin \gamma_n \tag{11}$$

and when $\omega nt = \beta_n = \pi/2,\ 3\pi/2$

we have that

$$B_n \beta_n' = C\,\omega n\, A_n \cos \gamma_n. \tag{12}$$

From equations (11) and (12) the two equally valid expressions now available for calculating the volumetric heat capacity of the soil are

$$C = -\frac{B_n'}{\omega n\, A_n \sin \gamma_n} = \frac{B_n \beta_n'}{\omega n\, A_n \cos \gamma_n} \tag{13}$$

With equation (2), the substitution of $\beta_n = \alpha_n - \gamma_n$, and the use of a trigonometric identity one obtains that

$$F(t) = \sum B_n[\cos(\omega nt - \alpha_n)\cos \gamma_n - \sin(\omega nt - \alpha_n)\sin \gamma_n]. \tag{14}$$

By the use of equation (7), after dropping the summation sign, one obtains

$$B_n[\cos(\omega nt - \alpha_n)\cos \gamma_n - \sin(\omega nt - \alpha_n)\sin \gamma_n]$$

$$= -\lambda[A_n' \cos(\omega nt - \alpha_n) + A_n \alpha_n' \sin(\omega nt - \alpha_n)]. \tag{15}$$

Then at

$$\omega nt - \alpha_n = 0, \pi$$

$$B_n \cos \gamma_n = -\lambda A_n' \tag{16}$$

and at

$$\omega nt = \alpha_n = \pi/2,\ 3\pi/2$$

$$B_n \sin \gamma_n = \lambda A_n \alpha_n' \tag{17}$$

From equations (16) and (17), the two expressions now available for calculating the heat conductivity of the medium are

$$\lambda = -\frac{B_n \cos \gamma_n}{A_n'} = \frac{B_n \sin \gamma_n}{A_n \alpha_n'} \tag{18}$$

The most nearly correct values for λ and C will be taken as the average of the two possible relationships. From equations (13) and (18) the thermal diffusivity ($\kappa = \lambda/C$, cm^2/sec) which controls the downward propagation speed of the temperature wave and the thermal admittance ($\mu = (\lambda C)^{1/2}$, ly K^{-1} $sec^{-1/2}$) which controls the ratio of heat flux and temperature amplitude may be determined.

$$\kappa = \frac{\lambda}{C} = \frac{A_n B_n \left[\frac{\sin \gamma_n}{A_n \alpha_n'} - \frac{\cos \gamma_n}{A_n'}\right]}{\frac{1}{\omega n}\left[\frac{B_n \beta_n'}{\cos \gamma_n} - \frac{B_n'}{\sin \gamma_n}\right]} \tag{19}$$

$$\mu^2 = \lambda C = \frac{B_n}{\omega n A_n} \cdot \frac{\left[\frac{\sin \gamma_n}{A_n \alpha_n'} - \frac{\cos \gamma_n}{A_n'}\right]^2 \cdot \left[\frac{B_n \beta_n'}{\cos \gamma_n} - \frac{B_n'}{\sin \gamma_n}\right]^2}{} \tag{20}$$

Experimental Setup

Lettau's theory was applied to data collected on the Pampa de La Joya, Peru during July, 1964. A description of the region, the purpose of the expedition and the measurements made have been discussed by Stearns (1967). Mean annual rainfall is virtually zero.

The desert sand in which the soil temperature and heat flux transducers were buried has been studied by Finkel (1959) and S. Hastenrath (personal communication, 1965). Table 1 gives the size distribution of two sand samples taken by Hastenrath. Sample 1 is from a 2 to 5 cm layer, and sample 2 from the 0 to 2 cm layer in an area where the soil sensors were buried. 40 cm was selected as the greatest depth at which temperature measurements would be made because the amplitude of the diurnal wave would be reduced to $< 1/1000$ of its surface value. Five temperature differences were measured in the soil between the following levels, -40 to -20, -20 to -10, -10 to -5, -5 to -2, and -2 to -0.5 cm, using 4-junction thermopiles potted in 3mm diameter aluminum tubing 30 cm long. The correct spacing of the aluminum tubes was secured and maintained by two plexiglass spacers in which holes were

drilled just a fraction of a mm larger than the aluminum tube and at the correct relative depth. The -40 cm temperature was measured by a 1N 2326 diode thermometer. A 1 cm scale projected above the -0.5 cm temperature probe so that the depth below the sand surface to the nominal -0.5 cm level could be verified after burial. The plexiglass spacers were positioned at each end of the tubes.

Table 1. Size distribution by weight percentage for two sand samples from the desert floor of the Pampa de La Joya, Peru.

	Sieve size, microns								
Sample No.	>500	500 to 250	250 to 177	177 to 125	125 to 104	104 to 74	74 to 62	<62	bulk density, gm/cm^3
1	28.00	12.6	11.1	17.5	11.9	7.0	5.5	5.6	1.41
2	17.1	6.5	8.4	27.2	15.4	8.8	3.1	4.1	1.39

The soil heat flux transducers consisted of 25.4 by 76.2 by 1.3 mm glass microscope slides with 100 turns of No. 36 constantan wire tightly wound around the 25.4 × 1.3 mm dimension with each turn spaced 0.6 mm apart along the 76.2 mm dimension. The constantan wire was electroplated with copper along the 25.4 mm edge to a depth of between 10 and 15 mm until the resistance of the wire had dropped from around 200 ohms to about 120 ohms. The result is a series of copper constantan junctions located along the surface of the glass slide with alternate junctions on opposite sides of the slide. The temperature differences across the narrow dimension of the glass slide will be measured by the thermopile. Leads are soldered to the copper plated constantan turn at each end of the glass slide and the entire slide is varnished with glyptal to insulate the wires from the soil and to improve the thermal contact between the glass and the thermocouples.

The two heat flux transducers were electrically connected in series so that the signals were additive, then buried on opposite sides of the soil temperature profile at nominal depths of -7.5, -15 and -30 cm, and the -0.5 cm flux plates were buried approximately 50 cm away from the soil temperature profile.

Analysis of Data

Harmonic analysis was applied to three diurnal periods commencing 0940 July 9, 1800 July 10 and 1800 July 11, 1964, of 10 minute mean soil temperatures and heat fluxes. The -40.0 cm temperature was not analyzed as the sensing system was not accurate enough to detect any diurnal variation. Some missing data was filled in by linear interpolation between the end points.

The calibration of the soil heat flux plates was initially based on the temperature integral method of determining the soil heat flux at the -0.5 cm level. The volumetric heat capacity for the sand of the Pampa de La Joya, Peru is based on Hastenrath's measurements of the bulk density of the sand which was about 1.40 gms/cm^3 and the heat capacity for granite rock of 0.188 cal/gm per deg C as given in the Handbook of Chemistry and Physics (1955). The resulting volumetric heat capacity is 0.263 cal/gm^3 per deg C assuming the sand is derived from granite rock.

Tables 2 and 3 present the results of the harmonic analysis of the soil temperatures and heat flux. The results are also presented graphically in Figs. 1, 2, 3 and 4. The natural logarithm of the temperature amplitude as a function of phase angle in Fig. 1 provides a basis for an estimate of the quality of the soil temperature profile system. The slope of 1:1 is characteristic of a uniform conductor; that is, heat capacity and conductivity in the medium are independent of depth. On this basis, the first and second harmonic of soil temperature indicate only small departures from a uniform conductor. The third harmonic of the temperature is not to be trusted as the amplitudes are very small. The soil heat flux results, graphically shown in Fig. 2 as the natural logarithm of heat flux amplitude versus phase angle, reveals that the -0.5 cm flux plate departs somewhat from the 1:1 line for n = 1 and 2, and also that the third harmonic is erratic which is to be expected. The departure of the -0.5 cm heat flux amplitude from the 1:1 slope, in view of the good agreement for the soil temperature profile, suggests that the calibration of the -0.5 cm flux plate relative to the -7.5, -15.0 or -30.0 cm flux plates is open to question, that there is an error in the relative depth of the flux plates or there may be a difference in the soil heat flux at the location of the -0.5 cm flux plate. All three factors could be influencing the value of the -0.5 cm flux plate.

Figures 3 and 4 graphically present the phase angle versus depth for temperature and heat flux respectively. Phase angle is plotted against depth rather than the natural logarithm of the amplitude because the former is independent of calibration and can be used with confidence to determine if the medium diffusivity is uniform provided the depths

TABLE 2. Results of harmonic analysis of the soil temperature at nominal depths (cm) for three diurnal periods on the Pampa de La Joya, Peru, during July 1964. The period mean (A_0, deg C), the amplitude (A_n, deg C) and phase angle ($_n$, radians) for n = 1, 2, 3 may be used to reconstruct the temperature, A(t), at a given time t (hrs from local midnight) as $A(t) = A_0 + \sum_{n=1} A_n \cos(\omega nt - \alpha_n)$ where $\omega = 2\pi/24$ and n is the order of the harmonic.

Depth	Diurnal Period	Period Mean	n = 1 Amplitude	n = 1 Phase	n = 2 Amplitude	n = 2 Phase	n = 3 Amplitude	n = 3 Phase
-0.1	I	19.40	20.54	3.462	9.17	0.276	0.78	3.365
	II	18.57	20.53	3.370	8.82	0.153	1.69	2.436
	III	19.67	21.70	3.400	9.55	0.266	1.83	2.874
	3 Period mean	19.21	20.92	3.410	9.18	0.232	1.43	2.892
-0.5	I	19.45	18.95	3.530	8.19	0.363	0.68	3.499
	II	18.69	18.95	3.440	7.88	0.243	1.45	2.536
	III	19.71	20.11	3.480	8.55	0.365	1.50	2.981
	3 Period Mean	19.28	19.33	3.483	8.50	0.324	1.21	3.006
-2.0	I	19.52	15.02	3.752	5.95	0.668	0.49	3.972
	II	18.93	15.10	3.668	5.70	0.554	0.93	2.929
	III	19.66	16.04	3.700	6.33	0.627	0.98	3.457
	3 Period Mean	19.37	15.39	3.706	5.99	0.633	0.80	3.453
-5.0	I	19.53	9.94	4.174	3.31	1.249	0.27	4.676
	II	19.18	10.07	4.099	3.13	1.146	0.46	3.620
	III	19.56	10.62	4.106	3.71	1.242	0.52	4.338
	3 Period Mean	19.42	10.21	4.126	3.38	1.212	0.41	4.211
-10.0	I	19.58	5.37	4.830	1.36	2.170	0.12	5.649
	II	19.44	5.51	4.758	1.27	2.090	0.15	4.720
	III	19.54	5.65	4.746	1.60	2.070	0.29	5.438
	3 Period Mean	19.50	5.51	4.778	1.41	2.110	0.19	5.069
-20.0	I	19.76	1.52	6.128	0.24	4.019	0.01	2.100
	II	19.84	1.55	6.021	0.22	3.975	0.03	2.022
	III	19.80	1.52	6.029	0.23	3.839	0.02	1.176
	3 Period Mean	19.80	1.53	6.059	0.23	3.945	0.02	1.766

I Diurnal Period beginning 0940 EST July 9, 1964
II Diurnal Period beginning 1800 EST July 10, 1964
III Diurnal Period beginning 1800 EST July 11, 1964

TABLE 3. Results of harmonic analysis of the soil heat flux as determined by the soil flux plates (-0.5, -7.5, -15, -30 cm depth) and temperature integral method (0.0 cm depth) for three diurnal periods on the Pampa de La Joya, Peru during July 1964. The period mean (B_0, ly/min), the amplitude (B_n, ly/min), and phase angle (β_n, radians) for n = 1, 2, 3 may be used to reconstruct the heat flux, B(t) at a given time t (hrs from local midnight) as

$B(t) = B_0 + \sum_{n=1}^{3} B_n \cos(\omega nt - \beta_n)$ where $\omega = 2\pi/24$ and n is the order of the harmonic.

Depth (cm)	Diurnal Period	Period Mean	n = 1 Amplitude	n = 1 Phase Angle	n = 2 Amplitude	n = 2 Phase Angle	n = 3 Amplitude	n = 3 Phase Angle
0.0	I	0.0022	0.131	2.751	0.0805	5.756	0.0106	2.453
	II	-0.0075	0.1375	2.751	0.0814	5.563	0.0074	0.680
	III	0.0030	0.1367	2.719	0.0831	5.786	0.0209	2.202
	3 Period Mean	-0.0007	0.1358	2.740	0.0817	5.702	0.0130	1.762
-0.5	I	0.0009	0.1390	2.750	0.0866	5.857	0.0014	2.672
	II	-0.0040	0.1377	2.658	0.0816	5.772	0.0190	2.050
	III	0.0025	0.1396	2.724	0.0819	5.939	0.0221	2.169
	3 Period Mean	-0.0002	0.1388	2.700	0.0834	5.823	0.0142	2.297
-7.5	I	0.0019	0.0592	3.725	0.0244	0.958	0.0021	4.544
	II	-0.0017	0.0599	3.637	0.0233	0.860	0.0034	3.624
	III	-0.0012	0.0627	3.671	0.0257	0.947	0.0047	4.071
	3 Period Mean	-0.0003	0.0606	3.677	0.0245	0.924	0.0034	4.080
-15	I	-0.0003	0.0222	4.738	0.0063	2.364	0.0007	0.532
	II	-0.0013	0.0227	4.678	0.0059	2.282	0.0008	5.813
	III	-0.0012	0.0230	4.667	0.0074	2.333	0.0014	5.993
	3 Period Mean	-0.0009	0.0226	4.695	0.0065	2.326	0.0010	6.207
-30.	I	-0.0025	0.0037	0.556	0.0009	4.363	0.0002	2.770
	II	-0.0020	0.0037	0.404	0.0008	4.309	0.0001	0.293
	III	-0.0021	0.0031	0.490	0.0011	4.220	0.0001	1.832
	3 Period Mean	-0.0022	0.0035	0.517	0.0009	4.297	0.0001	1.632

I Diurnal period beginning 0940 EST July 9, 1964
II Diurnal period beginning 1800 EST July 10, 1964
III Diurnal period beginning 1800 EST July 11, 1964

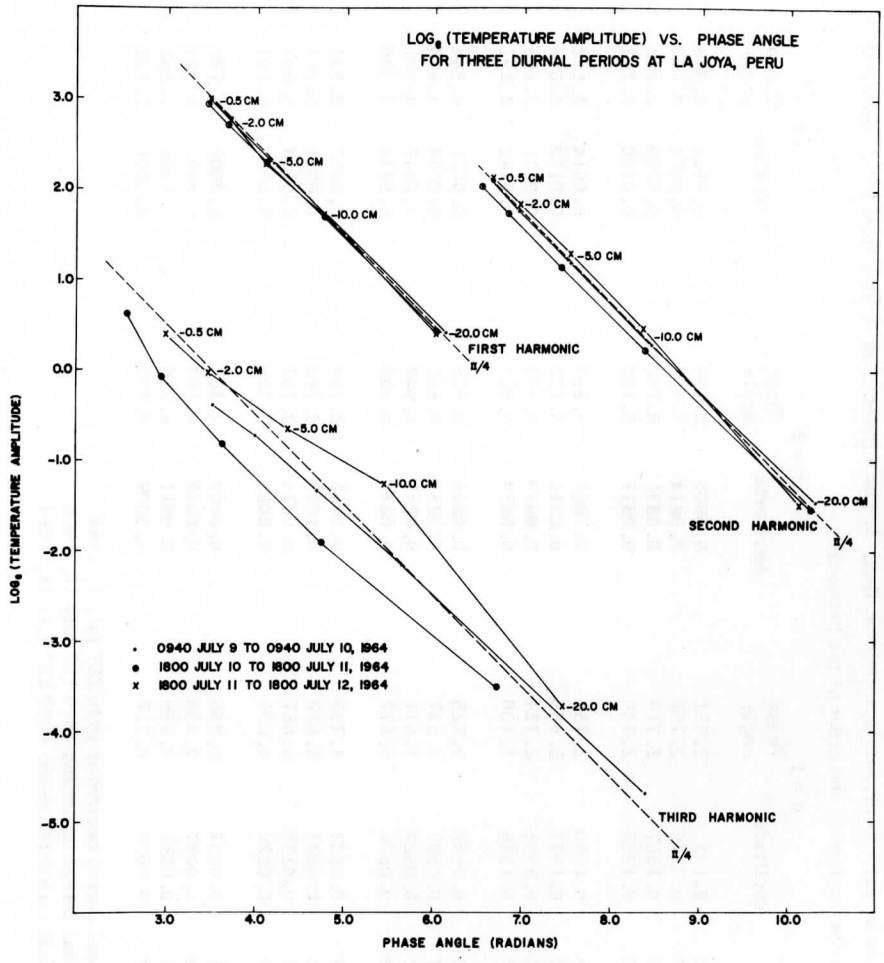

Fig. 1. The natural logarithm of soil temperature amplitude as a function of phase angle at the indicated depths for the first three harmonics for three diurnal periods on the Pampa de La Joya, Peru. The 1:1 slope (dashed line) is characteristic of a homogeneous conductor where $\gamma = \pi/4$.

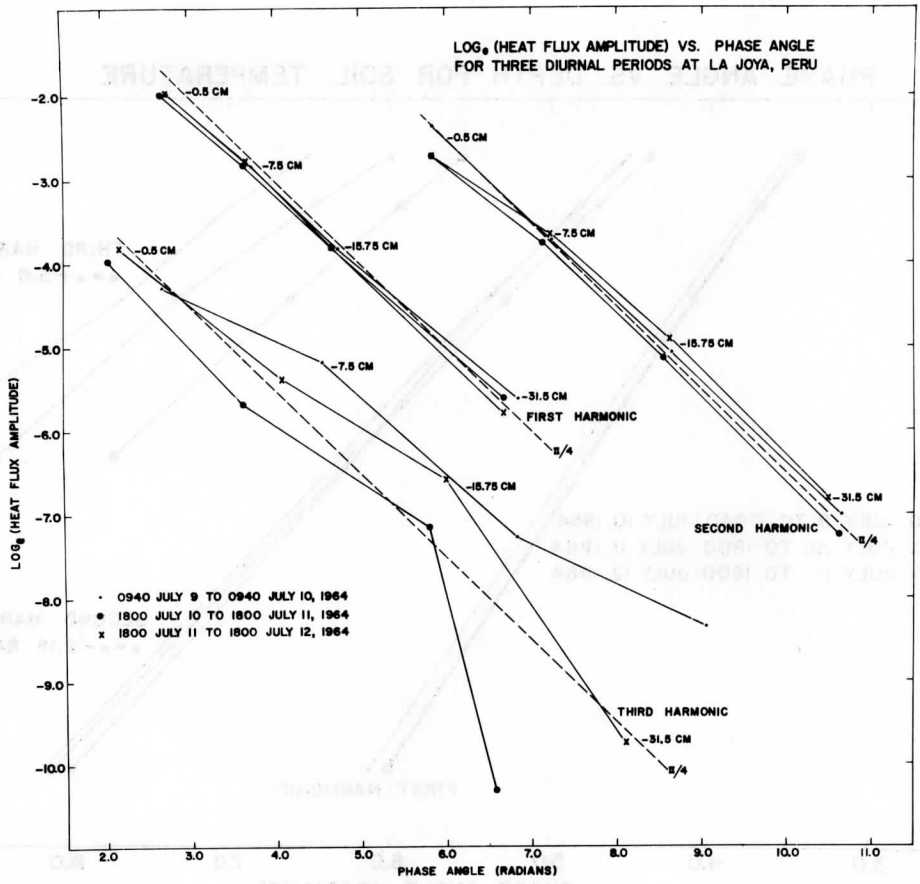

Fig. 2. The natural logarithm of soil heat flux amplitudes (uncorrected) as a function of phase angle at the indicated depths for the first three harmonics for three diurnal periods on the Pampa de La Joya, Peru. The 1:1 slope (dashed line) is characteristic of a homogeneous conductor where $\gamma = \pi/4$.

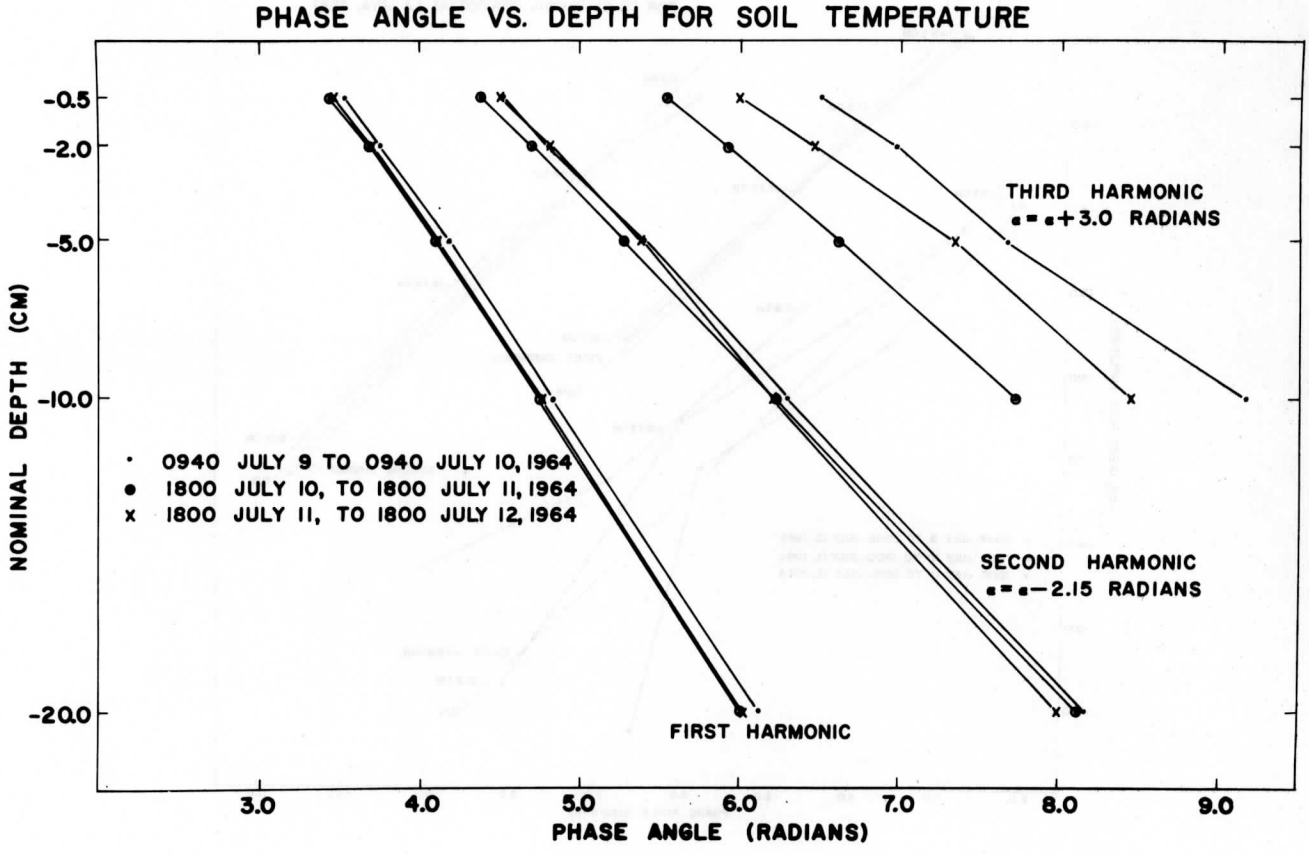

Fig. 3. Phase angle of soil temperature as a function of depth in the soil for the first three harmonics for three diurnal periods on the Pampa de La Joya, Peru. The second and third harmonics are displaced from their true value for clarity.

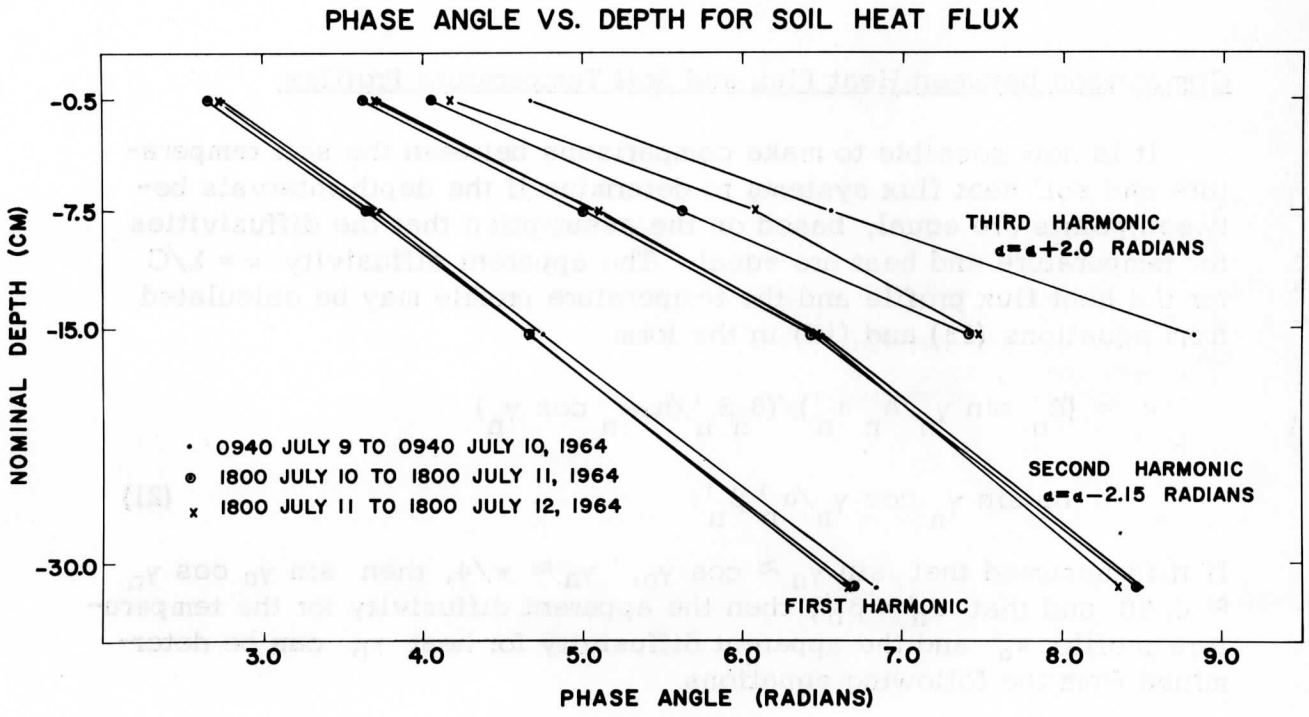

Fig. 4. Phase angle of soil heat flux as a function of depth for the first three harmonics for three diurnal periods on the Pampa de La Joya, Peru. The second and third harmonics are displaced from their true value for clarity.

are correct. The slight curvature indicates the possibility of a higher thermal diffusivity near the surface.

Due to the more numerous levels at which the soil temperature was measured plus the greater reliability in the calibration of the temperature sensors, the temperature amplitudes and phase angles were interpolated to the nominal levels at which the soil heat fluxes were measured assuming that the diffusivity was constant between the two points used.

Comparison between Heat Flux and Soil Temperature Profiles

It is now possible to make comparisons between the soil temperature and soil heat flux systems to determine if the depth intervals between points are equal, based on the assumption that the diffusivities for temperature and heat are equal. The apparent diffusivity $\kappa = \lambda/C$ for the heat flux profile and the temperature profile may be calculated from equations (13) and (18) in the form

$$\kappa = (B_n \sin \gamma_n / A_n \alpha_n') / (B_n \beta_n' / n\omega A_n \cos \gamma_n)$$

$$= n\omega \sin \gamma_n \cos \gamma_n / \alpha_n' \beta_n'. \qquad (21)$$

If it is assumed that $\sin \gamma_n \approx \cos \gamma_n$, $\gamma_n \approx \pi/4$, then $\sin \gamma_n \cos \gamma_n \approx 0.50$ and that $\alpha_n' = \beta_n'$, then the apparent diffusivity for the temperature profile κ_α and the apparent diffusivity for heat κ_β can be determined from the following equations

$$\kappa_\alpha = 0.5\, n\omega / (\alpha_n')^2$$

$$\kappa_\beta = 0.5\, n\omega / (\beta_n')^2. \qquad (22)$$

The equality of the depth intervals will be determined by making $\alpha' = \beta'$ or $\kappa_\alpha = \kappa_\beta$. The value of $\gamma_n = \alpha_n - \beta_n$ will be preserved over the depths of the profile as being $\pi/4$. Table 4 presents the diffusivities determined using the nominal depth intervals and the depth intervals for β which make $\alpha' = \beta'$.

Table 4. Diffusivity (κ, cm^2/sec) calculated over the indicated depth differences ($z_2 - z_1$, cm) and the corrected depth differences (Δz_β, cm) which will make $\alpha' = \beta'$ using the means of three 24 hour periods for the first harmonic.

$z_2 - z_1 = \Delta z$	$\kappa_\alpha \times 10^3$	$\kappa_\beta \times 10^3$	Δz_β
7.5 - 0.5 = 7.0	1.91	1.85	7.1
15 - 7.5 = 7.5	2.18	1.97	7.9
30 - 15 = 15	2.25	1.91	16.3

The value of Δz_β is the depth difference which will make $\kappa_\alpha = \kappa_\beta$ when calculated by equation (22). Accordingly, based on the assumption that the -0.5 cm flux plate is at -0.5 cm or is at the same depth in the soil as the -0.5 cm temperature probe, the actual depths of the soil flux plates are determined to be -0.5, -7.6, -15.5 and -31.8 cm. The phase angle rather than the amplitude is used to estimate a depth correction because the phase angle is independent of the calibration factor for either the temperature or the heat flux in the soil.

The comparison of diffusivities calculated for heat flux amplitude and for phase angle could be used to obtain an estimate of the relative calibration of the heat flux plates in the soil. From equation (13) and (18), assuming that $\gamma = \pi/4$, we have that

$$\kappa_B = n\omega \sin^2 \gamma_n / (B_n'/B_n)^2 \qquad (23)$$

where κ_B is the diffusivity calculated from the amplitude of the heat flux. The assumption is now made that $\kappa_\beta = \kappa_B$ with the results presented in Table 5.

The same procedure can be followed with the temperature amplitude and phase angle. The results are presented in Table 6 illustrating that the ratio A_c'/A_u' varies from 0.96 to 1.0 while B_c/B_u varies from 0.85 to 1.0. The ratio for other than the -0.5 cm flux plate varies from 0.85 to 0.89 and is comparable to the variation over the temperature profile which tests the validity of the assumption that $\gamma = \pi/4$ and/or experimental error.

The relative calibration factors for the soil heat flux plates could decrease with depth because the greater weight of the soil above pressing against the flux plates could improve the thermal contact between the soil and the flux plate resulting in a larger signal from the

Table 5. Uncorrected soil heat flux amplitude (B_u, ly/sec), corrected heat flux amplitude relative to -0.5 cm heat flux amplitude (B_c, ly/sec) and the ratio B_c/B_u at corrected flux plate depth (z, cm) for the first harmonic (n = 1) of the mean of three 24-hr periods on the Pampa de La Joya, Peru. The assumption is that $\kappa_B = \kappa_\beta$ or that $\beta' = -B'/B$ and $\gamma = \pi/4$.

z	B_u	B_c	B_c/B_u
- 0.5	0.002313	0.002313	1.0
- 7.6	0.001010	0.000879	0.872
-15.5	0.000377	0.000334	0.885
-31.8	0.000058	0.000049	0.845

Table 6. Uncorrected soil temperature amplitude (A_u, deg C), corrected soil temperature amplitude (A_c, deg C) at nominal soil depth (z, cm), for n = 1 of the mean of three 24 hour periods on the Pampa de La Joya, Peru. The assumption is that $\kappa_A = \kappa_\alpha$ or that $\alpha' = -A'/A$ and $\gamma = \pi/4$.

z	A_u	A_c	A_c/A_u
- 0.5	19.33	19.33	1.00
- 7.5	7.50	7.34	0.978
-15	2.90	2.79	0.961
-30	0.42	0.41	0.978

flux plate for the same heat flow in the soil or a larger calibration factor expressed as mv/ly/sec.

The conductivity of the flux plate is approximately 0.002 ly/sec per deg C/cm, while the soil of the Pampa de La Joya has a conductivity of approximately 0.0006 ly/sec per deg C/cm, which is a ratio of 3 between the thermal conductivity of the flux plate to the soil so that the flux plate approaches a "thermal short circuit" for the soil. According to Philip (1961) and Portman (1958), with a ratio of flux plate conductivity to soil conductivity of 3, the flux plate should indicate about a 15 percent higher heat flux than the true heat flux in the soil. This does not consider the effect of air gaps around the flux plate which will tend to reduce the indicated heat flux. If the pressure of the soil improves the thermal contact between the flux plate and the soil, then the -0.5 cm flux plate should have the poorest thermal contact and thus the same calibration factor will indicate less than the actual heat flow.

This is evident in Table 5 where the ratio B_c/B_u is approximately 0.87 below the -0.5 cm level while assumed to be 1 at the -0.5 cm level.

The establishment of the absolute value of the heat flux requires an assumption about the volumetric heat capacity or, assuming a specific heat for the soil, the soil density. Experimental packing of a soil sample from the Pampa de La Joya, Peru shows that with little effort the density can be increased to 1.75 gm/cm^3 but not beyond this value. Chudnovsky (1962) also agrees with the maximum density of 1.75 gm/cm^3 for quartz sand. Assuming a specific heat for granite rock of 0.188 cal/gm per deg C (which appears to be the source material for much of the soil on the Pampa de La Joya, Peru), an upper limit for the volumetric heat capacity of 0.329 cal/cm^3 per deg C is obtained while for a minimum soil density of 1.40 gm/cm^3 the minimum volumetric heat capacity is 0.263 cal/cm^3 per deg C.

The calibration of the heat flux plates and thus the flux of heat into and out of the soil may be determined in terms of the allowed values of the soil density or heat capacity. That is, the soil cannot be denser than 1.75 gm/cm^3 nor lighter than 1.40 gm/cm^3.

Table 7 presents values of the thermal diffusivity, thermal admittance, thermal conductivity, volumetric heat capacity and soil density using the heat fluxes corrected according to Table 5. The resulting soil density varies from 1.7 gm/cm^3 at -0.5 cm to 1.52 gm/cm^3 at -15 cm, well within the allowed range of soil densities.

Table 8 gives values of the volumetric heat capacity and the soil density for each of the diurnal periods. During the first diurnal period the soil density varies from 1.75 gm/cm^3 at -0.5 cm to 1.52 gm/cm^3 at -15 cm for the first harmonic which should be considered the most accurate although the agreement between the first and the second harmonic is rather good showing less variation than with depth.

The values of soil density show a variation with respect to time and depth being a maximum near the surface, then decreasing with depth. At the surface the soil density decreases with respect to time while there is a corresponding but slight increase in soil density at -15 cm. When the sensors were installed in the soil, the closer spacing of the sensors near the surface resulted in greater mechanical packing of the sand, so the decrease in soil density with time at -0.5 cm may indicate a slight relief from the initial packing of the sand with the possibility of an increase in the packing of the sand to a depth due to natural settling.

Table 7. Thermal diffusivity (κ, cm^2/sec), thermal admittance (μ, ly/deg per $sec^{1/2}$), volumetric heat capacity (C, cal/cm^3 per deg C), heat conductivity (λ, cal/cm^2 sec per deg/cm), and soil density (ρ, gm/cm^3) at three soil depths (z, cm) for the first two harmonics (n, cycles/24 hr) of the mean amplitudes and phase angles for three 24-hr periods on the Pampa de La Joya, Peru, during July 1964).

z(cm):	-0.5		-7.5		-15	
n :	1	2	1	2	1	2
$\kappa \times 10^3$:	1.76	1.81	2.19	2.28	2.21	2.49
μ 10^2 :	1.34	1.36	1.41	1.39	1.36	1.35
$C \times 10^1$:	3.20	3.19	3.01	2.89	2.89	2.71
λ 10^4 :	5.63	5.77	6.58	6.58	6.38	6.75
ρ :	1.70	1.70	1.60	1.54	1.52	1.51

Table 8. Volumetric heat capacity (C, cal/cm^3 per deg C) and soil density (ρ, gm/cm^3) for the three 24 hr periods (I, beginning 0940 EST July 9; II, beginning 1800 EST July 10; III, beginning 1800 EST July 11, 1964) for the first two harmonics (n, cycles/24 hrs) at indicated depths (z, cm).

z :		-0.5		-7.5		-15	
n :		1	2	1	2	1	2
C :	I	0.330	0.337	0.302	0.300	0.286	0.265
C :	II	0.324	0.328	0.301	0.306	0.286	0.274
C :	III	0.300	0.295	0.299	0.263	0.295	0.279
ρ :	I	1.75	1.79	1.61	1.59	1.52	1.41
ρ :	II	1.72	1.74	1.60	1.63	1.52	1.46
ρ :	III	1.59	1.57	1.59	1.40	1.57	1.49

The resulting range of soil densities are well within the allowed densities. However, they are definitely near the upper limit of soil densities, but if the soil density was 1.4 gm/cm^3 at -15 cm rather than 1.57 gm/cm^3, the estimated calibration factor for the soil heat flux plates would be 10 percent low. It should be pointed out that the settling of the soil could also result in an increase in the thermal contact between the heat flux plate and the soil which would appear as a fictitious increase in the soil density.

Some curvature is present in the diffusivity profile for temperature which will not be reflected in the diffusivity profile for heat as the heat flux plates were not installed at close intervals near the surface. Table 9 presents values of diffusivity calculated from the temperature profile over the depth intervals where actual measurements were made for a comparison between the two methods of determining the diffusivity.

Table 9. Soil diffusivity (κ_A, cm^2/sec) calculated from temperature amplitude (A_n, deg C) and soil diffusivity (κ_α, cm^2/sec) calculated from phase angle (α_n, radians) over the nominal depth intervals (z, cm) and soil diffusivity (κ_β, cm^2/sec) determined by the phase angle (β_n, radians) of the soil heat flux over the nominal depth differences (z', cm) for the mean amplitudes and phase angles of three 24 hr periods.

z_1	z_2	$\kappa_A \times 10^3$	$\kappa_\alpha \times 10^3$	z_1'	z_2'	$\kappa_\beta \times 10^3$
- 0.5	- 2.0	1.65	1.57			
- 2.0	- 5.0	1.86	1.94	- 0.5	- 7.5	1.91
- 5.0	-10.0	2.13	2.39	- 7.5	-15.0	2.18
-10.0	-20.0	2.21	2.21	-15	-30	2.25

For comparison purposes, values of λ, κ and C for sand from two literature sources together with values for the Pampa de La Joya, Peru are presented in Table 10. Geiger's values represent orders of magnitude while Chudnovski's values were carefully determined experimentally.

Based on Philip's (1961) equation for the error in the heat flux due to a ratio of three between the conductivity of the flux plate to the medium, the flux plate will indicate 10 percent higher heat flux in the medium. The above calibration factor must then be increased to 4.7 mv per ly/min which may be compared to the value of 4.6 mv per ly/min determined from the temperature and heat flux profile in the soil presented above. Selecting the lower limit for the soil density would increase the calibration factor for the flux plates to about 5.1 mv per ly/min.

The -0.5 cm flux plate calibration of 3.9 mv per ly/min when compared to the other flux plates in the soil indicates an error, which may be due to air gaps of -12 percent in the meter. That is, the air gaps at the surface of the meter result in an underestimation of the heat flux in the medium which is within the range of errors suggested by Philip (1961).

Table 10. Values of thermal conductivity (λ, ly/sec per deg C/cm), thermal diffusivity (κ, cm^3/sec) and volumetric heat capacity (C, cal/cm^3 per deg C) for the Pampa de La Joya, Peru, in comparison with values for sand by Geiger (1953) and Chudnovsky (196) for Quartz sand.

	Pampa de La Joya, Peru	Geiger	Chudnovski
$\lambda \times 10^4$	5.6 - 6.8	4.0	6.2 - 11.2
$\kappa \times 10^3$	1.6 - 2.4	1.3	2.2 - 2.5
$C \times 10^1$	2.6 - 3.3	3.0	2.1 - 3.1

Summary

Assuming that the conductivity of the flux plate is 0.002 ly/sec per deg C/cm and that the plate is 0.13 cm thick, then 1.08 deg C temperature difference across the flux plate corresponds to a heat flux of 1 ly/min. If there are 100 copper-constantan thermocouple junctions across the glass plate, then the signal corresponding to a heat flux of 1 ly/min would be 4.3 mv per ly/min. This is comparable to Deacons (1950) value of 1.2 mv per ly/min for 30 thermojunctions which corresponds to 4.0 mv for 100 junctions across the flux plate. Deacon describes his method of calibration which is an absolute method not depend-end on a guess at the thermal conductivity of a particular piece of glass but could be in error due to uncertainties about the thermal contact between the calibrating medium (sand) and the flux plate.

The initial guess at the flux plate calibration at -0.5 cm as described earlier resulted in 3.9 mv per ly/min for each plate, which is 10 percent less than the calibration based on the conductivity of glass. The corrected calibration factor for the flux plates below -0.5 cm would amount to an average of about 4.6 mv per ly/min.

Conclusions

The application of Lettau's theory of thermal diffusion to the results of harmonic analysis of soil temperature and heat flux profiles provides a method for determining the relative calibration of a set of heat flux plates used in a profile in dry soil. A test is possible to determine the relative depths of the soil heat flux plates and the soil temperature profile provided the phase angle between heat flux and temperature amplitudes is $\pi/4$ radians. The absolute value of the soil heat flux plate calibration is determined from the allowed range of soil density

assuming a specific heat for the soil which is constant throughout the depth of measurement.

The technique would have greater usefulness if it could be applied to soils with moisture present in varying amounts and abrupt changes in conductivity. It is doubtful that the results would be as satisfactory as were obtained on the Pampa de La Joya, Peru. It is possible that if soil heat flux and temperature sensors were placed at the obvious discontinuities in the soil profile as well as other levels that the effect of the conductivity discontinuity could be minimized.

Acknowledgments

I gratefully acknowledge the guidance of Dr. H. H. Lettau in applying his theoretical approach to the soil temperature and heat flux profiles. The trip to the Pampa de La Joya was financed by the Center for Climatic Research, Dr. R. A. Bryson, Director under Grant No. GP-444 from the National Science Foundation, Washington, D.C. The data processing and analysis was carried out under funds provided by Contract DA AMC 28-043-66-G24 from the U.S. Army Meteorological Research Office, Fort Huachuca, Arizona. Professor C. B. Tanner and associate Marcel Fuchs provided helpful and appreciated criticism of the manuscript.

References

Chudnovskii, F. A., Heat transfer in the soil, National Science Foundation, Washington, D. C., 1962.

Deacon, E. L., The measurement and recording of the heat flux into the soil, Q.J.R., Met. Soc., 76, pp. 479-483, 1950.

Finkel, H. J., The barchans of southern Peru, Journal of Geology, Vol. 67, pp. 614-647, 1959.

Geiger, R., The Climate Near the Ground, Harvard University Press, Cambridge, Massachusetts, 1950.

Handbook of Chemistry and Physics (Charles P. Hodgman, Ed.), Chemical Rubber Publishing Co., Cleveland, Ohio, 1955.

Lettau, H. H., Computation of heat budget constituents of the earth/air interface, Exploring the Atmosphere's First Mile, Vol. 1, Lettau and Davidson, Eds.), Pergamon Press, Inc., New York and London, Sec. 7.4, pp. 328-366, 1957.

Lettau, H. H., A theoretical model of thermal diffusion in non-homogeneous conductors, Gerl. Beitr. Geophys., 71/5, pp. 257-271, 1962.

Philip, J. R., The theory of heat flux meters, J. Geoph. Res., 66, 571-579, 1961.

Portman, Donald J., Conductivity and length relationships in heat-flow transducer performance, Transactions of the American Geophysical Union, Vol. 39, No. 6, pp. 1089-1094, 1958.

Stearns, C. R., Micrometeorological studies in the coastal desert of southern Peru, Ph.D. Thesis, Dept. of Meteorology, University of Wisconsin, Madison, Wisconsin, 1967.

6

Three-Dimensional Turbulence in Unidirectional Mean Flow

Heinz H. Lettau
University of Wisconsin, Madison

ABSTRACT:

The coupling between mean and fluctuating velocities in fully developed turbulence is investigated, first in general, and then with special consideration of unidirectional mean shear flow past a solid boundary. Eulerian equivalents of three-dimensional eddy displacements are defined which are shown to possess important properties of isotropy; Reynolds-averaging of them results in variances and covariances which yield—in addition to the conventional (or lateral) length-scale of wall-turbulence, and the Karman constant—a set of longitudinal length-scales, also another constant for which the name "Laufer constant" is proposed, and a new rationale for Prandtl's kinematic relation between mean shear and friction velocity. Literature data on nondimensional variances of turbulent fluctuations in the center-region of a two-dimensional channel, as well as in the vicinity of the earth/air interface (as related to micrometeorological wind profiles in adiabatic surface layers) are investigated and interpreted with the aid of the new model. Closed mathematical solutions for the complete profile of normalized root-mean-square values of both, down-stream and cross-stream components of fluctuating velocities are then derived; computed theoretical distributions are compared with the empirical results of detailed measurements reported by Laufer (1950) in a two-dimensional channel. In an appendix, certain results of the application of the new concepts to the free turbulence of a steady two-dimensional jet are summarized.

1. Background Information

In two preceding notes—Lettau (1964), (1966)—a new hypothesis of vorticity-transfer in turbulent flows was introduced, in order to specify nonconservation (adaption) of properties along eddying fluid paths. The concept was based on an implicit formulation of three-dimensional eddy displacements, and resulted in the definition of Eulerian longitudinal length-scales of turbulence as an important supplement to the conventional (or lateral) length-scale of mean shear flow. In the second note, the practical value of the new concept was demonstrated by its application to free turbulence in a two-dimensional jet. In more detail, and with emphasis on root-mean-square values of fluctuating velocities, this type of free turbulence was also the subject of the author's presentation at the IUGG-IUTAM International Symposium on Boundary Layers and Turbulence, in September of 1966, at Kyoto, Japan. It was shown that in free turbulence the Eulerian equivalents of eddy displacements satisfy perfectly the classical requirements of isotropy, in spite of definite anisotropy of velocity fluctuations. The present note is concerned with root-mean-squares of fluctuating velocities in "wall turbulence" when the nomenclature proposed by Hinze (1959) is accepted. It will also be demonstrated that the previously inductively developed new concepts of eddy displacements are capable of rationalization.

Employing conventional notation (e.g., α = specific volume of the fluid, p = pressure, g = gravity, etc.) the Navier-Stokes equations, in instantaneous form and after application of the standard Reynolds bar-operation, are,

$$(1a) \qquad D\underset{\rightarrow}{V}/Dt = -\alpha \nabla p - \underset{\rightarrow}{k} g + \nu \nabla^2 \underset{\rightarrow}{V}$$

$$(1b) \qquad \overline{D\underset{\rightarrow}{V}/Dt} = -\alpha \nabla p - \underset{\rightarrow}{k} g + \nu \nabla^2 \bar{\underset{\rightarrow}{V}}$$

where the three-dimensional velocity vector has a mean and a fluctuating part,

$$(2) \qquad \underset{\rightarrow}{V} \equiv \bar{\underset{\rightarrow}{V}} + \underset{\rightarrow}{V}' \equiv \underset{\rightarrow}{i}(\bar{u} + u') + \underset{\rightarrow}{j}(\bar{v} + v') + \underset{\rightarrow}{k}(\bar{w} + w').$$

On the left-hand side of (1) the individual derivative expresses a time-change following the instantaneous motion of a fluid particle,

$$(3) \qquad D(\ )/Dt \equiv \partial(\ )/\partial t + \underset{\rightarrow}{V} \cdot \nabla(\ ).$$

For convenience, a corresponding derivative following the mean motion is defined by the symbolic identity,

$$(4) \qquad d(\ )/dt \equiv \partial(\ )/\partial t + \bar{\underset{\rightarrow}{V}} \cdot \nabla(\ ) \equiv D(\ )/Dt - \underset{\rightarrow}{V}' \cdot \nabla(\ ).$$

The significant difference is that only in (4) the average of the derivative equals the derivative of the average, that is to say,

$$\overline{d(\ )/dt} = d(\bar{\ })/dt,$$

while in (3), with the aid of (4),

$$(5a) \qquad D\bar{\underset{\rightarrow}{V}}/Dt \equiv d\bar{\underset{\rightarrow}{V}}/dt + \underset{\rightarrow}{V}' \cdot \nabla\bar{\underset{\rightarrow}{V}} \neq \overline{D\underset{\rightarrow}{V}/Dt} \equiv d\bar{\underset{\rightarrow}{V}}/dt + \overline{\underset{\rightarrow}{V}' \cdot \nabla\underset{\rightarrow}{V}'},$$

whereupon another useful identity results,

$$(5b) \qquad D\underset{\rightarrow}{V}'/Dt \equiv -\underset{\rightarrow}{V}' \cdot \nabla\bar{\underset{\rightarrow}{V}} - d\bar{\underset{\rightarrow}{V}}/dt + D\underset{\rightarrow}{V}/Dt.$$

The Navier-Stokes equation for the mean state can now be contrasted with the departure flow equation as follows,

$$(6) \qquad d\bar{\underset{\rightarrow}{V}}/dt = -\overline{\underset{\rightarrow}{V}' \cdot \nabla\underset{\rightarrow}{V}'} - \overline{\alpha \nabla p} - \underset{\rightarrow}{k}\, g + \nu \nabla^2 \bar{\underset{\rightarrow}{V}},$$

$$(7) \qquad D\underset{\rightarrow}{V}'/Dt = \overline{\underset{\rightarrow}{V}' \cdot \nabla\underset{\rightarrow}{V}'} - \underset{\rightarrow}{V}' \cdot \nabla\bar{\underset{\rightarrow}{V}} - (\alpha \nabla p - \overline{\alpha \nabla p}) + \nu \nabla^2 \underset{\rightarrow}{V}'.$$

The significant difference is that after another Reynolds-averaging of all members, none in (6) is changed, while all in (7) vanish. The term $\overline{\underset{\rightarrow}{V}' \cdot \nabla\underset{\rightarrow}{V}'}$ appears with the opposite sign in both equations and therefore seems to represent direct "coupling" between mean and eddy flow. On the right-hand side of the departure equation (7), the three members following the "coupling term" will be referred to as "eddy transfer term," "pressure fluctuation term," and "viscous term," respectively. One result of the following discussions will be that not the so-called "coupling term" but the eddy transfer term in (7) is most important for the understanding of relationships between eddy and mean states.

2. Restrictive Conditions

Up to this point the developments are well known and universally valid. Further discussions will be restricted to eddy sizes of that particular subrange of the eddy spectrum which contributes dominantly to total energy of mechanical turbulence and which, simultaneously, can and will be most important as well as efficient, for eddy transfer processes. Turbulence is normally generated mechanically by pressure gradient forces in relatively large-scale disturbances, but is dissipated by viscosity in relatively small-scale disturbances. Hence, at sufficiently high Reynolds numbers

an intermediate class of disturbances is known to exist called the inertial subrange of the whole spectrum. Presumably, eddy transfer is most efficiently brought about by eddies of sizes somewhere in the transition region between inertial and energy-input subranges. A relatively clear-cut delineation of such subranges, however, can be expected only when the disturbances are unaffected by fluid compressibility as well as diabatic processes. Therefore, let us rule out, at least for the introductory discussions, the case of convective type turbulence. Namely, in truly free convection there is no mean motion so that (6) would reduce to the statement of mean hydrostatic equilibrium while (7) would express the total acceleration as the sum of merely two terms, with the pressure fluctuation term then being interpretable as a "buoyancy term."

The tentatively imposed restrictions can be summarized by saying that the discussion will be concerned mainly with flow conditions which cause other terms on the right-hand side of (7) to be sufficiently small in comparison with the eddy transfer term. Since turbulence can exist in steady states of one-dimensional mean flow (with or without pressure gradient forces, and with relatively weak mean shear) it can certainly be justified from the mean equation (6) that the coupling term can be as small as the possibly vanishing $d\underset{\rightarrow}{\bar{V}}/dt$; in any case, the derivative $d\underset{\rightarrow}{\bar{V}}/dt$ must be small in comparison with the absolute magnitude of the strongly fluctuating $D\underset{\rightarrow}{V}'/Dt$. Consequently, if the Reynolds number is sufficiently large, to make the eddies of interest too small for significant pressure effects yet still too large for significant viscous dissipative effects, equation (7) may be reformulated by singling out the remaining, and therefore dominant, eddy-transfer term,

$$(8) \qquad D\underset{\rightarrow}{V}'/Dt \equiv -\underset{\rightarrow}{V}' \cdot \nabla\underset{\rightarrow}{\bar{V}} + \underset{\rightarrow}{a}\,.$$

The magnitude of the vector of acceleration $\underset{\rightarrow}{a}$ in the defining identity (8) will be small in comparison with that of the total acceleration, as well as that of the eddy transfer term. An explicit sum for $\underset{\rightarrow}{a}'$ would follow from a comparison with (7) but does not need to be spelled out.

3. The New Theoretical Model of Turbulence

The vorticity-transfer concept introduced by the earlier notes was based on a fluctuating three-dimensional vector (defined at any instant of time anywhere in the turbulent fluid) which has the dimension of length,

$$(9a) \qquad \underset{\rightarrow}{r}' \equiv \underset{\rightarrow}{i}x' + \underset{\rightarrow}{j}y' + \underset{\rightarrow}{k}z'; \quad \text{with } \overline{\underset{\rightarrow}{r}'} = 0.$$

This eddy displacement vector is a point-value and describes an Eulerian equivalent of fluctuating trajectories of the fluid particles. Previously, the defining identity for $\underrightarrow{r}'$ was derived in an inductive manner involving both, curl and divergence of the two vectors $\underrightarrow{\bar{V}}$ and $\underrightarrow{r}'$, with an explicit formulation of $\underrightarrow{V}'$. Taking a more direct approach let $\underrightarrow{r}'$ be implicitly defined by

$$\text{(9b)} \qquad \underrightarrow{V}' \equiv D\underrightarrow{r}'/Dt; \quad \text{with } \overline{\underrightarrow{V}' \cdot \nabla \underrightarrow{r}'} = 0.$$

The supplementary statement in (9b) is due to the fact that the Reynolds average of $\underrightarrow{V}'$ must vanish. Simultaneously with (9b) let us define a vector $\underrightarrow{b}'$, which will be of the nature of a correction term, in the following identity

$$\text{(9c)} \qquad \underrightarrow{V}' \equiv -\underrightarrow{r}' \cdot \nabla \underrightarrow{\bar{V}} + \underrightarrow{b}'.$$

After taking the total time derivative of (9c), and consideration of (9b), a relationship between the correction term $\underrightarrow{b}'$ and the vector of acceleration $\underrightarrow{a}$ in (8) results,

$$\text{(10a)} \qquad D\underrightarrow{V}'/Dt = -\underrightarrow{V}' \cdot \nabla \underrightarrow{\bar{V}} - \underrightarrow{r}' \cdot \nabla (D\underrightarrow{\bar{V}}/Dt) + D\underrightarrow{b}'/Dt,$$

$$\text{(10b)} \qquad \underrightarrow{a} = -\underrightarrow{r}' \cdot \nabla (D\underrightarrow{\bar{V}}/Dt) + D\underrightarrow{b}'/Dt.$$

It follows from a discussion in Lettau (1964) that $\underrightarrow{b}'$ in (9c) could be zero only if momentum were perfectly conserved along fluctuating trajectories. Such perfect degree of conservation is accepted in the models of kinetic theory of gases, and applies along the "free path" between discrete molecular encounters, because the speed of the molecular unrest is independent of mean or macroscopic fluid motion and perpetual as long as the temperature remains unchanged. In turbulence there would be no Reynolds stress in unidirectional shear flow if $\underrightarrow{b}'$ were zero in (9c). It shall be demonstrated that the previous discussions—Lettau (1964, 1966)—concerning coexisting tendencies of adaption as well as conservation of fluid properties (such as vorticity) along eddying or fluctuating trajectories, are equivalent to the statement that $\underrightarrow{b}'$ in (9c) must be finite. In order to rationalize the previously intuitive concepts and to specify the nonvanishing $\underrightarrow{b}'$ mathematically, the following identity of vector calculus is useful, where $\underrightarrow{A}$ and $\underrightarrow{B}$ denote two arbitrary three-dimensional vectors,

$$\text{(11)} \qquad -2\underrightarrow{B} \cdot \nabla \underrightarrow{A} \equiv \underrightarrow{A} \times [\nabla \times \underrightarrow{B}] + \underrightarrow{B} \times [\nabla \times \underrightarrow{A}] - \underrightarrow{B}(\nabla \cdot \underrightarrow{A})$$

$$+ \underrightarrow{A}(\nabla \cdot \underrightarrow{B}) - \nabla \times [\underrightarrow{A} \times \underrightarrow{B}] - \nabla(\underrightarrow{A} \cdot \underrightarrow{B}).$$

The substitution of $\underset{\rightarrow}{r}'$ for $\underset{\rightarrow}{B}$ and $\bar{\underset{\rightarrow}{V}}$ for $\underset{\rightarrow}{A}$ in (11) will show that each of the following relations corresponds to a definite but different specification of the vector $\underset{\rightarrow}{b}'$ in (9c),

$$(12a) \qquad \underset{\rightarrow}{V}' \approx \frac{1}{2} \underset{\rightarrow}{r}' \times [\nabla \times \bar{\underset{\rightarrow}{V}}],$$

$$(12b) \qquad \underset{\rightarrow}{V}' \approx \frac{1}{2} \{\underset{\rightarrow}{r}' \times [\nabla \times \bar{\underset{\rightarrow}{V}}] + \bar{\underset{\rightarrow}{V}} (\nabla \cdot \underset{\rightarrow}{r}')\},$$

$$(12c) \qquad \underset{\rightarrow}{V}' \approx \frac{1}{2} \{\underset{\rightarrow}{r}' \times [\nabla \times \bar{\underset{\rightarrow}{V}}] + \bar{\underset{\rightarrow}{V}} (\nabla \cdot \underset{\rightarrow}{r}') + \bar{\underset{\rightarrow}{V}} \times [\nabla \times \underset{\rightarrow}{r}']\}.$$

With the exception of the factor $1/2$ and certain changes in sign (two features which can be shown not to affect the basic principle of the arguments) the sequence of relations (12a) to (12c) reflects the gradual development of the author's vorticity-transfer-and-adaption hypothesis from 1964 to 1966, in the previously intuitive manner. It appears possible that these formulations (12) could apply selectively to different turbulence types. Nevertheless, the really decisive step was the introduction of the first term which is common to all relations (12). Namely, (12a) expresses already the two important coexisting tendencies of conservation as well as adaption of vorticity, which can be evidenced by taking the curl of (12a). For the discussion of the resulting two main terms, reference is made to Lettau (1964).

Taking as a basis the relatively general form (12c), the expression for $\underset{\rightarrow}{b}'$ according to (9c) and (11) will be as follows,

$$(13) \qquad \underset{\rightarrow}{b}' = \frac{1}{2} \{\nabla \times [\bar{\underset{\rightarrow}{V}} \times \underset{\rightarrow}{r}'] + \nabla (\bar{\underset{\rightarrow}{V}} \cdot \underset{\rightarrow}{r}') + \underset{\rightarrow}{r}' (\nabla \cdot \bar{\underset{\rightarrow}{V}})\}$$

The last term on the right-hand side of (13) is certainly small, and could have been incorporated, rather than in (13), on the right-hand side of any of the equations (12) as was actually suggested in Lettau (1967), for reasons of symmetry. Upon consideration of (9b), the curl of the vector product and the gradient of the scalar product formed by the pair of vectors $\bar{\underset{\rightarrow}{V}}$ and $\underset{\rightarrow}{r}'$ may be finite but sufficiently uniform to the effect that the individual derivative $D\underset{\rightarrow}{b}'/Dt$ and, consequently, $\underset{\rightarrow}{a}$ in (10a) as well as (8), is negligibly small. However, it is not necessarily implied that (12c) is actually the last form of the sequence (12) or that (13) is the best possible choice.

Because a direct proof is difficult, it can be argued that rather than trying to justify an instantaneous form like (12c) on the basis of (13), (10b), and (8), an equally convincing but more practical procedure would be to test whether or not one of the relationships (12) predicts statistical results that either can be empirically confirmed, or must be discarded because of disagreement with reliable empirical

data reported in the literature. This alternative approach shall be used, with (12c), in the following sections.

4. Wall-Turbulence of Unidirectional Mean Shear Flow as a Test Case

For specific experimental testings of the new theory it is convenient to restrict the discussion to an elementary case of turbulent flow, for example, the steady mean fluid motion parallel to a plain wall where unidirectional mean shear occurs only perpendicular to the fluid boundary. Such conditions are realized by a variety of flow types. Examples are plane Couette flow, or flat-plate-boundary layer flow in wind tunnels, or constant-pressure-gradient flow either in a channel of uniform rectangular cross section (and of sufficient aspect ratio to suppress side-wall effects), or, in adiabatic states of the lower atmosphere (that is to say, in an adiabatic surface layer) at a sufficiently flat micrometeorological site with uniform roughness structure. The basic statistics of wall-turbulence for the last two types of unidirectional mean shear flow appear to be fairly well documented in the literature, by the independent work of a variety of authors. Concerning flow in two-dimensional wide channels, reference can be made to Laufer (1950), or the earlier experiments by Reichardt (1938) as summarized in Schlichting (1960, p. 466). Eddy structure of atmospheric surface layer flow, or measurements of wind fluctuation data, have been thoroughly reviewed in Lumley and Panofsky (1964, pp. 119 to 160).

Empirical findings will be compared with theoretical variances and covariances computed with the aid of (12c). This requires that, first of all, the characteristics of the mean flow must be specified. Here like in the following developments, let a subscript (t, x, y, or z) indicate a partial derivative with time (t) or the three spatial coordinates (x, y, z), respectively.

$$\text{(14a)} \qquad \begin{cases} \bar{\underset{\rightarrow}{V}}_t = 0; \quad \bar{\underset{\rightarrow}{V}} = \underset{\rightarrow}{i}\,\bar{u}; \quad \nabla\cdot\bar{\underset{\rightarrow}{V}} = \bar{u}_x = 0; \\ \nabla\times\bar{\underset{\rightarrow}{V}} = \underset{\rightarrow}{j}\,\bar{u}_z; \qquad \nabla^2\bar{\underset{\rightarrow}{V}} = \underset{\rightarrow}{i}\,\bar{u}_{zz}. \end{cases}$$

The summary (14a) for mean unidimensional duct flow may be compared with a corresponding set in Lettau (1967), for the free turbulence of a two-dimensional jet. For sufficiently high Reynolds numbers, wall-turbulence will be fully developed with no laminar sublayer existing nearest to the fluid boundary. This implies that, due to wall roughness, the viscous term in the mean equation (6) is negligible. The gravity term drops out when the mean flow is horizontal. With (14a), and $d\underset{\rightarrow}{V}/dt = 0$, also $\nabla\cdot\underset{\rightarrow}{V}' = 0$, equation (6) thus reduces to equality

of the x-component of the horizontal pressure gradient force and the coupling term,

$$(14b) \quad \overline{\alpha\, p_x} = \alpha\, \overline{p_x} = \overline{\underset{\rightarrow}{V}' \cdot \nabla u'} = \nabla \cdot \overline{(\underset{\rightarrow}{V}' u')} = \overline{(u'u')}_x + \overline{(v'u')}_y + \overline{(w'u')}_z .$$

Equation (14b) illustrates the well-known fact that this elementary type of turbulent flow can be generated by a pressure gradient, and is dominated by the derivatives of the Reynolds stress. There will be no dependency of averages either on x, or on y, so that the first two Reynolds stresses in (14b) can only be constant or zero. The third Reynolds stress and its z-derivative must be finite. If the pressure gradient is uniform and constant, $\overline{u'w'}$ must be linear in z. But, even though the coordinate z determines the mean shear, there is no "a priori" reason to expect that $\overline{u'w'}$ should be directly proportional, or even functionally related, to the mean shear. Such dependency could only be accepted if it would follow conclusively as a result of theory.

5. Three-dimensional Turbulence in Unidirectional Mean Flow

Consideration of (14a) in the basic theoretical relation (12c) yields

$$(14c) \quad \underset{\rightarrow}{V}' = \underset{\rightarrow}{i}\, \frac{1}{2} \{\bar{u}(x'_x + y'_y + z'_z) - \bar{u}_z z'\}$$

$$+ \underset{\rightarrow}{j}\, \frac{1}{2}\, \bar{u}(x'_y - y'_x) + \underset{\rightarrow}{k}\, \frac{1}{2} \{\bar{u}(x'_z - z'_x) + \bar{u}_z x'\}.$$

Obviously, (12c) provides a sufficient number of terms to produce, simultaneously and explicitly, all three components of the eddy velocity vector, in spite of one-dimensionality of the vector of mean flow. No similar result was achieved by other phenomenological theories of turbulence; but, doubtlessly, this feature is necessary and sufficient to develop, in closed form, and in a unified manner, all products and squares which, after Reynolds-averaging, produce the variances ($\overline{u'u'}$, $\overline{v'v'}$, $\overline{w'w'}$) as well as the covariances ($\overline{u'v'}$, $\overline{v'w'}$, $\overline{u'w'}$) of possible physical significance for any turbulent flow.

The employment of the Eulerian eddy displacement vector would hardly be worthwhile if $\underset{\rightarrow}{r}'$ and its spatial derivatives would not possess important properties of isotropy and symmetry. Lettau (1967) showed that this concerns most universally the totality of nine first-order derivatives of the eddy displacement components (that is to say, x'_x, x'_y, x'_z, y'_x, y'_y, y'_z, z'_x, z'_y, and z'_z). Isotropy requires that averages of squares are exactly equal to each other and significantly unequal to zero, while averages of any mixed products are exactly equal to zero,

$$(15a)\qquad \overline{x'_x x'_x} = \overline{x'_y x'_y} = \overline{x'_z x'_z} = \overline{y'_x y'_x} = \ldots\ldots = \overline{z'_z z'_z} > 0,$$

$$(15b)\qquad \overline{x'_x y'_y} = \overline{x'_x z'_z} = \overline{y'_y z'_z} = \overline{x'_y y'_x} = \overline{x'_z z'_x} = 0.$$

Consequently, the variances in (15a) yield one and only one positive number which, in view of (14c) shall be defined by the identity,

$$(15c)\qquad \kappa^2 \equiv \overline{x'_x x'_x}/4 \equiv \overline{z'_z z'_z}/4 \equiv \ldots$$

Hence, the component-derivatives which contribute to divergence and curl of the displacement vector in (14c) yield, after squaring and averaging,

$$(15d)\qquad \overline{(x'_x + y'_y + z'_z)^2}/4 = 3\kappa^2 \; ; \; \overline{(x'_y - y'_x)^2}/4 = \overline{(x'_z - z'_x)^2}/4 = 2\kappa^2 .$$

In addition to the products listed in (15b), another class of covariances contains a displacement component and one derivative as factors. Their averages will be subject to certain restraints which are direct consequences of the physical nature of the mean motion. In flow-states as described by (14a), it must be expected that no Reynolds-average can be a function of x or y. This implies zero-values for the following two kinds of average products, a first group involving x-derivatives,

$$(16a)\qquad \overline{x'_x x'} = \overline{x'_x z'} = \overline{y'_x x'} = \overline{y'_x z'} = \overline{z'_x x'} = \overline{z'_x z'} = 0$$

and a second group involving y-derivatives,

$$(16b)\qquad \overline{x'_y x'} = \overline{x'_y z'} = \overline{y'_y x'} = \overline{y'_y z'} = 0.$$

However, the physical nature of the flow with one-dimensional mean shear ($\bar{u}_z$ and only $\bar{u}_z$ unequal to zero) will also prescribe that products which involve z-derivatives do not vanish, so that

$$(16c)\qquad \overline{x'_z x'} \neq 0; \; \overline{y'_z y'} \neq 0; \; \overline{z'_z z'} \neq 0; \; \overline{z'_z x'} \neq 0; \; \overline{x'_z z'} \neq 0.$$

Even though the factor y'_z does not appear in (14b) the product $y'_z y'$ was included in (16c) since a finite value must also be expected for its average.

The Reynolds averages of squared components of the eddy displacement vector represents the physical basis for the rigorous definition of the longitudinal length-scale of turbulence. With minor modifications of defining equations given previously in Lettau (1966) and (1967), let

(17a) $$X^2 \equiv \overline{x'x'}/4; \qquad Y^2 \equiv \overline{y'y'}/4; \qquad Z^2 \equiv \overline{z'z'}/4.$$

The first three products in (16c) are essentially the z-derivatives of the squares in (17a). The last two products in (16c) are related to the covariance which serves as the physical basis for the definition of the lateral length-scale (ℓ) of turbulence. In a minor modification of the previous form corresponding to that of the longitudinal length-scales), let

(17b) $$\ell^2 \equiv \overline{x'z'}/4.$$

As was demonstrated at the Kyoto meetings, free turbulence appears to be distinguished by perfect isotropy of Eulerian displacement components so that $X = Y = Z$, together with $\ell = 0$, even though there is anisotropy in velocity components; namely, $\overline{u'u'} \neq \overline{w'w'}$ together with $\overline{u'w'} \neq 0$ (as opposed to $\overline{x'x'} = \overline{z'z'}$ together with $\overline{x'z'} = 0$). The characteristic difference between free turbulence and duct-flow turbulence appears to be that for the latter $\overline{u'u'} \neq \overline{w'w'}$, and $\overline{u'w'} \neq 0$ together with $\overline{x'x'} \neq \overline{z'z'}$, and $\overline{x'z'} \neq 0$. For physical interpretation it is significant that relations (17) are coupled with (16c) as follows:

(18a) $$(X^2/2)_z = X_z X = \overline{x'_z x'}/4; \qquad Z_z Z = \overline{z'_z z'}/4, \text{ etc.},$$

(18b) $$(\ell^2)_z = 2\ell_z \ell = (\overline{x'_z z'} + \overline{z'_z x'})/4.$$

In spite of lack of isotropy there will be symmetry, which leads to the following relation for the lateral length-scale in wall-turbulence,

(18c) $$\ell_z \ell = \overline{x'_z z'}/4 = \overline{z'_z x'}/4.$$

As was previously shown, further differentiation of the lateral length-scale in wall-turbulence results in a covariance expression for the Karman constant (k), so that, with the new factor of 1/4,

(18d) $$k^2 = \overline{x'_z z'_z}/4.$$

6. Predicted Variances and Covariances of Velocity Fluctuations

The above developed relations (15a) through (18c) are useful for the transformation of the products and squares of the $\underset{\rightarrow}{V}'$-components in (14c). After Reynolds-averaging the following covariances result,

(19a) $$-\overline{u'w'} = (\bar{u}_z \ell)^2 \equiv u^{*2}; \text{ where } u^* \equiv \bar{u}_z \ell = (\overline{-u'w'})^{1/2}$$

(19b) $$\overline{u'v'} = \overline{v'w'} = 0$$

Interestingly, the Reynolds stress (19a) turns out to be exactly proportional to the square of mean shear. Thus, a definite physical meaning for the friction velocity u^* as well as for the lateral length-scale ℓ is established. The result is not due to the introduction of an arbitrary working hypothesis but derives from generally formulated conditions of isotropy and symmetry of Eulerian eddy displacement components, together with the restraints imposed by the physical nature of the flow. In this respect it is highly significant to note that the products to be formed to obtain the Reynolds stress $\overline{u'w'}$, with the aid of (14c), include $\bar{u}_z\bar{u}(\overline{z'_z x'} - \overline{x'_z z'})$, which will vanish only when (18c) holds true. Such condition of symmetry should be expected for a homogeneous or quasi-homogeneous fluid, but not necessarily for unidirectional mean flow with density stratification. It should also be emphasized that for the free turbulence of a two-dimensional jet the Reynolds stress (as derived by Lettau (1966) with the aid of corresponding developments) turned out not to be a quadratic expression of mean shear.

In the historical development of fluid mechanics there were many attempts to relate Reynolds stresses to the mean motion. Details may be found in standard textbooks such as Hinze (1959), or Schlichting (1960, Chapters XIX and XX), or in source-books like that edited by Friedlander and Topper (1961). It may suffice here to recall that most of the earlier investigators, beginning with Boussinesq (about 90 years ago), attempted to build on a possible analogy between turbulent and molecular transfer processes. However, unlike molecular conductivity or viscosity, the eddy counterparts turned out not to be a property of the fluid, but depended strongly on mean-flow intensity and position relative to boundaries. This made it imperative to continue the search for empirical as well as theoretical relationships between eddy and mean states.

When reference is made to Batchelor (1953), Taylor (1921, 1935) attempted first to discard, in principle, the direct analogy to kinetic theory of gases; he introduced new statistical concepts, such as the correlation between velocities at two points, as the quantities useful to describe turbulence. Ensuing important developments are summarized by Batchelor (1953); reference can also be made to a collection of original classical papers on statistical theory, edited by Friedlander and Topper (1961). However, Batchelor (1953, p. 2) pointed out that there must occur interactions between the fluctuating and mean components of motion which are difficult to handle mathematically on the basis of Taylor's concepts, and that similar difficulties appear to prevent a successful treatment of the transport effects produced by the different

intensity of the fluctuating motion at different points. Batchelor went on to say: "There are complicated mechanical effects and we have not yet obtained a proper understanding of them. As a preliminary, it seems appropriate to consider homogeneous turbulence which has neither of the two properties mentioned above." These statements appear to be valid up to this day. Regarding more recent developments concerning interactions between mean flow and Reynolds stress, reference can be made to Phillips (1966).

In a modest way the present discussion attacks also such problems of interaction between fluctuating and mean components, and of eddy transfer. A new line of developments is followed which is not related to Taylor's but to another historical break with the unacceptable Boussinesq analogy to kinetic theory, namely that initiated by Prandtl (1925), and further on refined, with partially quite impressive results, by the Goettingen school of aerodynamicists; reference can be made to Schlichting (1960), or Hinze (1959). The important advance made by Prandtl about 40 years ago was to discard the Boussinesq ratio $-\overline{u'w'}/\bar{u}_z$ (which has the physical dimension of length times velocity), and to consider instead the ratio $-\overline{u'w'}/(\bar{u}_z)^2 \equiv (u*/\bar{u}_z)^2$. In principle, this means indeed abandonment of the primitive concept of direct proportionality between Reynolds stress and mean strain, introducing instead a type of non-Newtonian relationships into turbulence which is foreign to kinetic theory of gases. Empirically, the strictly kinematic quantity $u*/\bar{u}_z$ (which is a point value but has the physical dimension of length) can be exactly defined in a frame of Eulerian concepts; empirically it proved to be satisfactorily independent of the intensity of mean flow, at least for the more important of the elementary types of wall-turbulence. However, the term "mixing length" chosen by Prandtl was an unfortunate misnomer, and the rationale for this concept as, for example, offered in Schlichting (1960, pp. 477 to 480) cannot be convincing, for essentially two reasons. Firstly, quasi-Lagrangian concepts of turbulent "mixing" were employed in a confusing connection with the strictly Eulerian or kinematic ratio $u*/\bar{u}_z$, and secondly, Prandtl's length-scale was originally too narrowly interpreted as merely one-dimensional by giving undue preference and sole consideration to the component of eddy displacement parallel to the direction of mean shear.

With respect to these two important points it is hoped that the new lines of approach and rationalization, developed since 1964 and fortified with the present discussion leading to (19a, b) may appeal to some investigators as more satisfactory than Prandtl's original rationale. Especially, properties of isotropy may be interesting which appear if three-dimensionality of eddy displacements is taken into consideration. No restriction to homogeneous turbulence needs to be made, and not only can the Reynolds stresses be rigorously derived via a covariance which produces a somewhat complicated length such as $(\overline{x'z'})^{1/2}$, but also

the variances of velocity fluctuations via relatively simple length-scales such as $(\overline{x'x'})^{1/2}$ and $(\overline{z'z'})^{1/2}$, as shall be demonstrated below.

After squaring each of the three components in (14c) and taking the Reynolds-average, consideration of (15a) through (18c) yields

$$\overline{u'u'} = (\bar{u}_z Z)^2 + 3(\kappa \bar{u})^2, \tag{20a}$$

$$\overline{v'v'} = 2(\kappa \bar{u})^2, \tag{20b}$$

$$\overline{w'w'} = (\bar{u}_z X)^2 + 2(\kappa \bar{u})^2. \tag{20c}$$

It is assumed in (20a) and (20c) that neither $\overline{x' \nabla \cdot \underset{\rightarrow}{r'}}$ nor $\overline{z' \nabla \cdot \underset{\rightarrow}{r'}}$ are different from zero. In this respect the mechanical turbulence in channels appears to be significantly distinct from free turbulence; namely, Lettau (1966) found the product $\overline{x' \nabla \cdot \underset{\rightarrow}{r'}}$ important for the two-dimensional free jet; presumably, this is due to an actual expansion of eddies as they are carried by the free stream in the downwind direction with unimpeded growth because of the absence of ducting or restraining walls.

7. Comparison with Observational Data

Comparison of the theoretical results (20) with empirical variances will be crucial for the validity of (9b) and the ensuing formulas (12a) to (12c). Detailed profile data for the three variances in unidirectional mean motion are still relatively scarce in the available literature. The studies in channels appear to be restricted to ranges of Reynolds numbers for which turbulence will not be fully developed so that a laminar sublayer was present, which is likely to suppress velocity fluctuations near the wall. In the atmosphere, even for light winds, the Reynolds number will exceed nearly always the order of 10^6 (due to large thickness of the planetary boundary layer and fully rough interface) which rules out the presence of a laminar sublayer; but, a different setback is that only in the atmospheric surface layer (approximately, the lowest ten to twenty meters) the mean motion will be sufficiently close to unidirectional. Namely, due to the ever-present Coriolis force, atmospheric boundary layer flow shows directional changes with height so that at levels where $\bar{u}_z$ vanishes, neither $\bar{v}$ nor $\bar{v}_z$ will be zero. Furthermore it is imperative to restrict the discussion to adiabatic surface layers, because the structure of turbulence is modified by Richardson-number effects, or density stratification in cases of surface heating, or cooling.

In conclusion, it appears advisable for a first test to investigate the theoretical predictions (20) separately; namely, for a zero-shear region by comparison with measurements near the center of a channel; and, for the wall-region (or, where the limiting value of $\bar{u} = 0$ is approached due to z going to zero) by comparison with measurements in atmospheric surface layers under adiabatic conditions.

It will be convenient to transform variances into standard deviations (σ), which can readily be made dimensionless by dividing the σ-value by a reference speed. For the region with vanishing shear, the mean fluid velocity is at a maximum, or, quasi-independent of position, and serves as the proper scaling factor whereupon (20) yields, with $\bar{u}_Z = 0$,

$$\sigma(u)/\bar{u} = \kappa\sqrt{3}, \tag{21a}$$

$$\sigma(v)/\bar{u} = \sigma(w)/\bar{u} = \kappa\sqrt{2}. \tag{21b}$$

For $\bar{u}$ going to zero, with the approach to the fluid boundary, the friction velocity u* as defined in (19a) goes to u_0* which serves as the proper scaling factor, whereupon (20) yields, strictly for $\bar{u} = 0$,

$$\sigma(u)/u_0* = Z/\ell, \tag{22a}$$

$$\sigma(v)/u_0* = 0, \tag{22b}$$

$$\sigma(w)/u_0* = X/\ell. \tag{22c}$$

Equations (21) imply that $\sigma(u)/\sigma(w) = \sqrt{3/2} = 1.225$ for the center of the duct (with $\bar{u}_Z = 0$, and $u* = 0$), while according to (22), for the immediate vicinity of the wall, $\sigma(u)/\sigma(w) = Z/X$ which is the ratio of the two longitudinal length-scales defined in proportion to the variances $\overline{x'x'}$ and $\overline{z'z'}$ of the Eulerian eddy displacement components. In wall-turbulence it must be expected that $X \neq Z$. The values of the variances $\sigma(u)$ and $\sigma(w)$, for $\bar{u}_Z \neq 0$, depend also on the covariance $\overline{x'z'}$ which defines the lateral length-scale of turbulence.

From graphical illustrations of measured profiles of standard deviations in Laufer (1950), we read for average flow conditions of the two largest Reynolds numbers used, that in the center region of the rectangular channel:

$$\text{(Laufer)} \qquad \sigma(u)/\bar{u} = 0.027; \quad \text{and} \quad \sigma(v)/\bar{u} = \sigma(w)/\bar{u} = 0.022.$$

The ratio $0.027/0.022 = 1.227$ is gratifyingly close to $\sqrt{3/2} = 1.225$. From graphs illustrating Reichardt's (1938) measurements—as repro-

duced in Schlichting (1960, Fig. 18.3)—we read for the center region of the tunnel, with $\bar{u}_{max} = 100$ cm/sec,

(Reichardt) $\sigma(u)/\bar{u} = 0.043$; and $\sigma(w)/\bar{u} = 0.035$.

Again, $0.043/0.035 = 1.229$, satisfactorily close to the theoretical value of $\sqrt{3/2}$. However, the constant κ would equal 0.0156 according to Laufer's result, and 0.025 according to Reichardt's. The discrepancy could be either an effect of differences in Reynolds numbers, or more likely, as Laufer pointed out, due to an unsatisfactory aspect ratio in Reichardt's channel.

In Section 5, the constant κ was defined by the covariance (15a), which shows noteworthy similarity with the covariance-definition of the Karman constant k in (17b). Since short nomenclature will be convenient, it is proposed to refer to κ as the "Laufer constant." In summary,

(Karman constant, $k = 0.428$): $(2k)^2 = \overline{(x'_z z')}_{wall}$

(Laufer constant, $\kappa = 0.0156$): $(2\kappa)^2 = \overline{(x'_x x')}_{center} = .. = \overline{(z'_z z')}_{center}$

It appears desirable that the possibly universal nature of κ, and its representative value, be securely tested. Lettau (1966), (1967) showed that for the free turbulence in a two-dimensional jet a similar constant exists which acts as the counterpart of the Karman constant of wall turbulence. The name "Reichardt constant" was proposed; its physical significance will briefly be summarized in the "Appendix."

From the discussion in Lumley and Panofsky (1964), supplemented by oral communications with H. Panofsky during spring of 1967, it can be concluded that, in the atmospheric surface layer, standard deviations of both longitudinal and lateral-vertical components of wind fluctuations, are effectively normalized by a division through u_0*. This statement refers to experiences collected at a considerable variety of micrometeorological sites in different countries, provided that the measurements are taken sufficiently close to the ground level, and during times of the day with near neutral thermal stratification. The lateral-horizontal (or horizontal cross-wind) component, however, does not seem to be capable of normalization by dividing its value by u_0*; instead, it tends to show a significant variability from place to place. In summary,

(Panofsky)
$$\begin{cases} \sigma(u)/u_0^* = C; \qquad \sigma(w)/u_0^* = A; \\ \sigma(v)/u_0^* = \text{variable, possibly depending on surface roughness as well as distance from the ground.} \end{cases}$$

Six independent sets of determination of the empirical constant C reported by Lumley and Panofsky (1964) suggest that $C = 2.4 \pm 0.2$, while several independent determinations of vertical variances yield $A = 1.3 \pm 0.1$. The authors of the reference book remark that Russian observers have estimated A-values smaller than unity, possibly smaller than 0.8, but tend to discard the reality of these claims. Here, additional arguments in favor of $A \approx 1.3$ can be brought forward. Namely, it follows from the definition of the point value of the correlation coefficient (r) between fluctuations in u and w that $-r(u', w') = (A.C)^{-1} = 0.32$, if $C = 2.4$ and $A = 1.3$. But, this coefficient should be at least equal to 0.52 if $C = 2.4$ and if A would be smaller than, or equal to, 0.8; such high correlation coefficients appear relatively unrealistic in view of direct measurements. With $C/A \approx 2.4/1.3 \approx 1.8$ it follows that the ratio $\sigma(u)/\sigma(w)$ near the wall is about 1.5 times as great as the same ratio near the center of the channel.

Comparison with (22a) and (22c) shows that theoretically $C = Z/\ell$ and $A = X/\ell$. It may be recalled that for small distance from the ground, $\ell = k(z + z_0)$, where z_0 = aerodynamic roughness length of the interface. In view of the definition of the longitudinal length-scale Z in (17a) it will be argued that Z should be directly equal to $(z + z_0)$ which would make $1/C$ equal to the Karman constant k. Intuitively, it may be suggested that likewise the quantity A is not a new constant but follows from a relationship such as $A = C - 1$. Consequently, with the value of the Karman constant $k = 0.428$, it is suggested that

(23a) $$C = 1/k = 2.336; \qquad A = (1-k)/k = 1.336,$$

which agrees perfectly well within the range of probable errors of determination with Panofsky's estimate.

Finally, Panofsky can be quoted as stating that in contrast to A and C, $\sigma(v)/u_0^*$ is not the same at various micrometeorological sites, and, at the same place, tends to increase with height within the surface layer. Theoretically, it would follow from (20b) that

(23b) $$\sigma(v)/u_0^* = (\kappa\sqrt{2}/k) \log_e (1 + z/z_0) \approx 0.05 \log_e (z/z_0),$$

if the conventional logarithmic wind profile for the adiabatic surface layer is assumed, $\bar{u} = (u_0^*/k) \log_e (1 + z/z_0)$, with $k = 0.428$, and as

before, $\kappa = 0.0156$. According to Panofsky, $\sigma(v)/u_0^*$ was found to vary between 1.3 and 2.6, possibly depending on surface roughness (z_0) as well as distance from the interface (z). Let us assume that for the micrometeorological conditions encountered, $\log_e(z/z_0)$ may vary between approximately 4 and 12. Then, the theoretical expression (23b) would produce $\sigma(v)/u_0^*$ values between 0.2 and 0.6, which are decisively too small, while variations from place to place, and with height at the same place, may be qualitatively correct. Nevertheless, with respect to normalized fluctuations of the lateral cross shear component, the above developed model needs improvement. A similar shortcoming of the corresponding fluctuation component $\sigma(v)$ had been found for the two-dimensional jet while the profiles of normalized $\overline{u'w'}$, $\sigma(u)$, as well as $\sigma(w)$ were in quite satisfactory agreement with predicted values; reference is made to Lettau (1967). Intuitively, the mathematical structure of the set of relations (20) appears to suggest that the length-scale Y, as defined in (17a), should be a factor in the equation for $\overline{v'v'}$, so that a finite bounding value at $z = 0$ would prevail, instead of the possibly unrealistic form (22b).

8. Prediction of Variance Profiles Across a Channel

The results of the preliminary testings in Section 7 may be considered sufficiently encouraging so that it appears in order to attempt a combination of the two findings, for the purpose of predicting, with the aid of equations (20), complete variance profiles across a rectangular channel in fully developed flow. A prerequisite will be a mathematical formula for the profile of mean velocity. It is well known that this problem is related to the question of universal velocity distribution law; this, in turn, can be reduced to the problem of a universal mathematical expression for the lateral length-scale if (19a) is valid. It is convenient to transform length-scales, as well as the independent variable z, into dimensionless forms with the aid of the half-width R of the channel,

$$(24a) \qquad \ell/R \equiv \phi(\zeta); \quad z/R \equiv \zeta; \quad z_0/R \equiv \zeta_0 << 1,$$

where z_0 = aerodynamic wall roughness. Instead of mean velocity $\bar{u}$ (which goes from zero to $\bar{u}_{max} \equiv U$ if ζ goes from ζ_0 to 1) it is more practical to consider the velocity defect $(U - \bar{u})$, and to make it dimensionless by dividing through the wall-friction-velocity

$$(24b) \qquad \eta \equiv (U - \bar{u})/u_0^* ; \quad \text{with} \quad \eta_0 = U/u_0^*.$$

It should be remembered that the value of u_0^* follows directly from channel dimensions and the pressure head. One of the physical reasons for preferring η is the fact that in fully developed turbulence the cross-

sectional average $(\eta)_{av.}$ is not only independent of the Reynolds Number but equal to a constant which is "universal" for channels of the same geometry but different wall roughness. This constant $(\eta)_{av.}$ can be determined empirically by the direct measurement of three elementary flow parameters which do not involve details of structure, neither of mean flow profile nor of fluctuating velocities; they are (i) the fluid discharge or the cross-sectional average of mean flow $(\bar{u})_{av.}$, (ii) the total pressure head, under consideration of the mathematical conversion to $u_0{}^{*2}$, and (iii) the mean center speed $\bar{u}_{max} \equiv U$. According to the thorough measurements by Nikuradse, as summarized in Schlichting (1960, p. 525), fully developed flow in pipes artificially roughened with sand of different grain size to produce a considerable variation of wall roughness, yielded in "rough pipes" for the important empirical turbulence constant the universal value of $(\eta)_{av.} = 3.75$.

Theoretically, for steady mean states and constant pressure gradient, the governing equation for the mean velocity profile follows from the combination of (14b) and (19a) and reduces, with the aid of the defining identities (24), to

$$-\eta_\zeta = \sqrt{1-\zeta}/\phi, \tag{25}$$

where the subscript indicates differentiation with respect to the dimensionless independent variable ζ. To solve (25) various authors have employed (explicitly or implicitly) different mathematical expressions for the dimensionless length-scale of wall turbulence ϕ as a function of ζ. In any case, after $\eta(\zeta)$ is obtained by either numerical integration of (25) or in closed form, another integration with respect to cross-sectional area is possible and will produce a theoretical value for $(\eta)_{av.}$, which must be compared with the empirical result that $(\eta)_{av.} = 3.75$; as will be seen, this procedure serves to establish the numerical value of the Karman constant k.

It can readily be verified that according to (25), the velocity profile is strictly logarithmic in ζ if ϕ is chosen, somewhat artificially, as follows,

$$\phi/k = \zeta\sqrt{1-\zeta}, \tag{26a}$$

whereupon

$$k\eta_\zeta = -1/\zeta; \quad k\eta = -\log_e\zeta; \quad k\eta_0 = -\log_e\zeta_0; \quad (k\eta)_{av.} = 3/2. \tag{26b}$$

Nikuradse's empirical value of $(\eta)_{av.} = 3.75$ has frequently been compared with that resulting from the strictly logarithmic, but hypothetical

distribution (26b), whereupon $k = 1.50/3.75 = 0.400$. Clearly, this most often employed value of the Karman constant must be considered arbitrary as long as (26a) is not justified by independent reasonings.

Of the various other suggested forms for $\phi(\zeta)$ let us quote only one which appears even more artificial than (26a), namely,

$$\phi/k = 2(1 - \sqrt{1-\zeta})\sqrt{1-\zeta}, \tag{27a}$$

whereupon,

$$-k\eta_\zeta = 0.5/(1 - \sqrt{1-\zeta}); \quad k\eta = -\log_e(1 - \sqrt{1-\zeta}) - \sqrt{1-\zeta}; \tag{27b}$$

$$k\eta_0 = -0.3068 - \log_e \zeta_0; \quad (k\eta)_{av.} = 77/60 = 1.283.$$

Differentiations with respect to ζ will show that the velocity profile (27b) satisfies precisely the so-called "Karman similarity rule" which demands that

$$\overline{u'w'} = -k^2(\bar{u}_\zeta)^4/(\bar{u}_{\zeta\zeta})^2, \tag{27c}$$

if the form as quoted, for example, in Schlichting (1960, p. 487) is slightly rephrased. The numerical value of Karman's constant according to (27b) will be $1.283/3.75 = 0.34$. This appears to match statements such as can be found in Schlichting (1960, p. 512) that "Karman's universal velocity distribution law for very large Reynolds numbers" also agrees well with the experimental $\bar{u}$-profile values, if a smaller value, for example, $k = 0.36$, is chosen.

However, at $\zeta = 1$, both expressions (26a) and (27a) result in $\phi = 0$ accompanied by infinity of the cross-stream gradient ϕ_ζ. Such behavior is unlikely for the center region of flow if the concept of the length-scale should have physical reality. In the form of more or less loose physical reasonings, let us conjecture a set of rules which should govern the mathematical structure of Eulerian eddy displacement statistics and length-scales derived therefrom.

(I) Any length-scale of turbulence should remain positive and finite at any region of fully developed turbulent flow.

(II) If the nature of the fluid as well as the type of ducted mean flow suggests symmetry, any length-scale of turbulence should have its maximum value in the center of the channel; it should approach this maximum with a finite curvature when the cross-stream gradient goes gradually to zero.

(III) Independent of the type of mean flow, the lateral length-scale of wall-turbulence in the immediate vicinity of the boundary will be determined by the aerodynamic roughness of the interface; and the initial rate of increase will be given by the universal Karman constant; for example, when z is the lateral coordinate, in fully developed turbulence,

$$(28) \qquad \lim_{z \to z_0} \ell_z \equiv \lim_{\zeta \to \zeta_0} \phi_\zeta = k.$$

(IV) There are several distinct versions of elementary wall turbulence which include the following four elementary types: (i) frictionally driven plane Couette flow, (ii) pressure-gradient-driven flow in channels of uniform cross-section, (iii) inertia-force-driven flat plate boundary layer flow, and (iv) pressure-gradient-driven atmospheric boundary layer flow with significant Coriolis force effects. For at least these four elementary types of wall turbulence, it should be possible to express the lateral length-scale, in its functional dependence on distance from the boundary, by a unified mathematical form which must satisfy the above rules (I) to (III), especially (28).

Rule (IV) implies that there should exist a principle which governs the lateral length-scale in general. Interesting in this connection are ideas originally put forward by Rossby (1932) in his attempts to modify Karman's similarity rule (27c) for application to atmospheric and oceanic turbulence. What Rossby suggested amounts to saying that one should expect the length-scale of turbulence to increase if one descends from the region of free flow towards the boundary, an approach typical of the sounding techniques of the oceanographer. The meteorologist is sounding in the opposite direction, from the interface upwards into the region of free flow, and he will typically expect an increase of the length-scale with increasing distance from the interface. Rossby suggested that the oceanographer thus will tend to emphasize the role of the lower boundary as the source region of mechanical turbulence, while the meteorologist will tend to see in the surface layer a region of bias, and expect the free development of eddies to be ever more likely the greater the distance from the suppressing and damping boundary. In reality, starting at ground level and proceeding upwards the lateral length-scale may first increase but at a gradually decreasing rate, then pass through a maximum to decrease further upwards towards the region of free flow, in a physically reasonable combination of the two viewpoints outlined above.

In a first attempt to patch together two respective mathematical forms for the lowest versus the upper and larger portion of the atmospheric boundary layer, Rossby and Montgomery (1935) succeeded partially in explaining certain overall features of actual wind profiles; but, their solution (as well as other combined solutions offered later on by

various authors) proved unsatisfactory in profile detail, due to the lack of continuity of wind profile curvature, and due to the fact that Karman's rule appears to have realistic value only as a limiting condition in the approach to the boundary.

In 1958 the present author—in unpublished seminar lectures and discussions at the University of Wisconsin and at Purdue University—proposed a different verification of the original Rossby concept, by the introduction of the following mathematically continuous form for the dimensionless length-scale as defined by the identities (17b) and (24a),

$$\phi/k = \zeta/(1 + m\zeta^{1 + 1/m}), \tag{29a}$$

which conforms with all four rules listed above. Specifically, ϕ in (29a) reaches a maximum at $\zeta = 1$ for any positive value of the numerical parameter m, and goes asymptotically to zero for ever increasing ζ, because of

$$(\phi/k)_\zeta = (1 - \zeta^{1 + 1/m})/(1 + m\zeta^{1 + 1/m})^2. \tag{29b}$$

Lettau (1962) has shown that (29) applies fairly realistically to the atmospheric boundary layer if $m = 4$, for an unlimited range of positive ζ-values, while $m = 2$ for channel flow (of rectangular or circular cross section) with a restriction to the range $\zeta_0 \leq \zeta \leq 1$. As shall be demonstrated in a forthcoming publication, $m = 2$ applies also for flat plate boundary layer flow, while for the most elementary type of wall turbulence, namely, linear Couette flow, (29a) takes on its simplest form with $m = 1$, again restricted to $\zeta_0 \leq \zeta \leq 1$. If the flow is bounded only on one side, an equivalent "channel width" must and can be determined; for atmospheric boundary layers this problem was discussed and solved in Lettau (1962). In summary, it may be said that the systematic variation of m, from 1, to 2, to 4, appears to coincide with an increase of complexity of mean flow structure of the four elementary flow types. This seems to support the reality of Rule IV.

Specifically, for the rectangular channel under discussion here,

$$\phi/k = 3/(1 + 2\zeta^{3/2}), \tag{30a}$$

whereupon in (25), with the restriction that $\zeta_0 \leq \zeta \leq 1$,

$$k\eta = \log_e(1 + \sqrt{1-\zeta}) - \log_e(1 - \sqrt{1-\zeta}) - 2\sqrt{1-\zeta} + (\tfrac{1}{2} - \zeta)\sqrt{\zeta - \zeta^2} + \tfrac{1}{2}\sin^{-1}\sqrt{1 - \zeta}; \tag{30b}$$

(30c) $$k\eta_0 = 0.2210 - \log_e \zeta_0;$$

(30d) $$(k\eta)_{av.} = 1.607.$$

Hence, the combination of (30d) with Nikuradse's empirical value yields $k = 1.607/3.75 = 0.428$. This for Karman's universal constant must be preferred over the conventional but crudely approximative value of 0.40 which would require validity of the decisively less satisfactory ϕ-function (26a). In comparison with an empirical relationship discussed—and characterized as producing remarkable results—in Schlichting (1960, p. 510) it can readily be seen that (30a) resembles it closely enough to reproduce all its useful properties at $\zeta_0 \leq \zeta \leq 1$, but has the additional advantage that the new form is derived as a special case of a unifying expression, like (29), for the lateral length-scale of wall turbulence.

The last step in the chain of developments leading to the numerical prediction of variance profiles across a channel concerns the longitudinal length-scales. In Section 7 only the limiting values of X and Z according to (20), were established for the approach towards both center and wall. To satisfy Rule II, let us hypothesize for the larger of the two length-scales (which is Z as defined in (17a)) that across the entire channel, for $\zeta_0 \leq \zeta \leq 1$,

(31a) $$Z/\ell = k^{-1}(1 - \zeta + \frac{2}{3}\zeta^{3/2}); \text{ with } (Z/\ell)_\zeta = k^{-1}(\zeta^{1/2} - 1).$$

The exponent of 3/2 was chosen to match that in (30a), while other requirements to be satisfied concern the limiting value at small ζ (according to the discussion in Section 7, $Z \approx (z + z_0)$, at small values of z), as well as $Z_\zeta = 0$ for $\zeta = 1$, just as $\ell_\zeta = 0$ at $\zeta = 1$, according to Rule II.

Concerning the other longitudinal length-scale X, it will be hypothesized that X should vary in direct proportion to Z; thus, in consideration of the bounding values (23) established in accordance with the empirical findings of Panofsky in Section 7

(31b) $$X/Z = 1 - k; \text{ or } X/\ell = (1-k)Z/\ell.$$

Like ℓ_ζ and Z_ζ, X_ζ, too, goes to zero at $\zeta = 1$, and, thus, satisfies Rule II.

Upon recalling the original defining identities (17a) and (17b), an immediate consequence of the formulations (31a, b) and (30a), is a mathematical expression for the point value of the correlation coefficient, $r(x', z')$, between longitudinal and lateral eddy displacement components. Namely,

(31c) $$r(x', z') \equiv \ell^2/XZ = k^2/(k-1)\left(1 - \zeta + \frac{2}{3}\zeta^{3/2}\right)^2 .$$

The interesting result emerges that this correlation coefficient is uniquely determined by the Karman constant and the dimensionless distance from the wall, so that $r_0 \approx k^2/(k-1)$ at $\zeta = \zeta_0$, and $r_1 = 9r_0/4$ at $\zeta = 1$. Hence, the correlation increases from the wall towards the center. This behavior contrasts, of course, with that of the correlation coefficient between the eddy velocity components u' and w', which goes to zero at the duct center, but not in direct proportion to the Reynolds stress because the covariance $\overline{u'w'}$ is weighted by the variances or, $\sigma(u)$ and $\sigma(v)$, which results in a nonmonotonical behavior of $r(u', w')$.

Finally, in conclusion of the foregoing developments, let us summarize the practically useful formulas. They are obtained with the aid of (20), and employing the center speed U as reference for making standard deviations of velocity components dimensionless, but using, for convenience, velocity defect instead of $\bar{u}$, especially the form $\eta_0 \equiv U/u_0^*$ as defined in (24b), with κ = Laufer constant,

(32a) $$\sigma(u)/U = (\eta_0)^{-1}\sqrt{(1 - \zeta)(Z/\ell) + 3\kappa^2(\eta_0 - \eta)^2} ;$$

(32b) $$\sigma(v)/U = 2\kappa(\eta_0 - \eta) ;$$

(32c) $$\sigma(w)/U = (\eta_0)^{-1}\sqrt{(1 - \zeta)(X/\ell)^2 + 2\kappa^2(\eta_0 - \eta)^2} ;$$

(32d) $$r(u', w') = u_0^{*2}(1 - \zeta)/\sigma(u)\sigma(w) = \eta_0^{-2}(1 - \zeta)U^2/\sigma(u)\sigma(w).$$

The square roots in (32a) and (32c) are equal to $\sigma(u)/u_0^*$ and $\sigma(w)/u_0^*$, as follows directly from the definition of η_0.

Theoretical profiles of the diverse quantities (31a) through (32d), including $\bar{u}/U = 1 - \eta/\eta_0$ according to (30b), were computed (with slide rule accuracy) employing for the Laufer constant (as defined in Section 7) the value of $\kappa = 0.0156$. The results listed in Table 1 can be directly compared with empirical data illustrated by Laufer (1950), because the value assumed for $\bar{u}_{max}/u_0^* = \eta_0$ in the computations was 28.9 which corresponds to average conditions for the two higher Reynolds numbers used by Laufer. It should be mentioned that Laufer (1950) observed some irregularities in the pressure distribution along the channel for the largest Reynolds number (61,600), while an existing $(\overline{u'u'})_X$ of the order of 0.01 $\overline{\alpha p_X}$ evidenced that turbulence was not fully developed along the measurement section. Moreover, very smooth walls were used so that viscous sublayer effects were quite noticeable.

TABLE 1. Rectangular Channel of Halfwidth R. Theoretical dependency on the dimensionless independent variable $\zeta = z/R$ between center ($\zeta = 1$) and wall ($\zeta = \zeta_0 = z_0/R$ where z_0 = aerodynamic wall roughness), of the following functions: fully developed mean velocity $\bar{u}$, and standard deviations of indicated velocity fluctuation components (relative to mean center speed U); lateral length-scale ℓ and longitudinal length-scales X and Z (relative to half width R); correlation coefficients between Eulerian eddy displacement components x' and z', also between velocity fluctuations u' and w'. Numerical computations were based on $\tau_0/\rho U^2 = 0.00119$, or, $U/u_0* = 28.9$, with strictly linear stress distribution in ζ, or, $u*/u_0* = \sqrt{1 - \zeta}$, permitting direct comparison with empirical data by Laufer (1950).

ζ	$\bar{u}/U$	$\sigma(u)/U$	$\sigma(v)/U$	$\sigma(w)/U$	ℓ/R	X/R	Z/R	$r(x', z')$	$r(u', w')$
1.0	1.000	0.027	0.022	0.022	0.143	0.126	0.222	0.72	0.00
0.9	.995	.030	.022	.024	.142	.127	.222	.72	.17
0.8	.986	.036	.022	.026	.141	.128	.223	.71	.26
0.7	.973	.040	.021	.028	.138	.127	.224	.68	.32
0.6	.958	.044	.021	.030	.133	.125	.221	.64	.36
0.5	.940	.049	.021	.032	.125	.122	.215	.59	.38
0.4	.919	.054	.020	.034	.114	.117	.204	.54	.39
0.3	.892	.060	.020	.037	.097	.104	.183	.49	.38
0.2	.857	.066	.019	.040	.073	.083	.146	.44	.36
0.1	.799	.073	.018	.044	.040	.049	.087	.38	.33
0.05	.733	.078	.016	.046	.021	.027	.047	.35	.32
0.01	.615	.082	.014	.048	.004	.006	.010	.32	.30
ζ_0	.000	.081	.000	.046	$k\zeta_0$	$(1-k)\zeta_0$	ζ_0	.32	.32

With all necessary precautions it can be stated that of the four quantities predicted in Table 1 which can be directly compared by entering the theoretical values into corresponding graphs in Laufer (1950), $\bar{u}/U$, $\sigma(u)/U$, and $\sigma(w)/U$ agree satisfactorily with the empirical profile data. The predicted $\sigma(v)/U$ profile does not agree with the observations, except for the gradually approached center value. In comparison with the fluctuations u' and w', which are integral parts of the Reynolds stress, the component v' has significance only for fluctuation intensity. For this lateral cross shear fluctuation component, however, a similar discrepancy between predicted and observed distribution was found by Lettau (1967), in the free jet. Further developments will be necessary, and shall be reported on, in due time. For instance, the possibility must be explored whether or not $\sigma(v)$ depends on the longitudinal length-scale component Y as defined in (17a). Figure 1 is a comparison of data according to Laufer's observations, and theoretical equations (30b) and (32a, c) as also verified in Table 1.

9. Concluding Remarks

The foregoing discussions deal with preliminary results of a continuing investigation. Future work will be devoted to extensions of theoretical developments to other types of mean flow, as well as refinements of the previously investigated elementary mean motion (such as unidirectional shear flow, and the two-dimensional jet). Supplementary work is necessary with respect to the fluctuation component normal to both mean velocity and mean shear. Also, modification of mechanical turbulence by buoyancy forces, or the extension of the theory to stratified fluids will be considered. In addition to theoretical work, efforts will be made to improve the quality of available empirical data on fluctuating velocities in channel flow under laboratory conditions, and in the lower atmosphere. As far as experimental programs at the University of Wisconsin are concerned, it can be mentioned that after the development of electronic equipment, the voltages induced electrodynamically by flow of water through a strong magnetic field have been successfully employed to obtain turbulence spectra, as well as various profiles across circular ducts. Day and Villemonte (1965) have reported the results of such work, which is presently being conducted by R. Gratz at the Department of Civil Engineering.

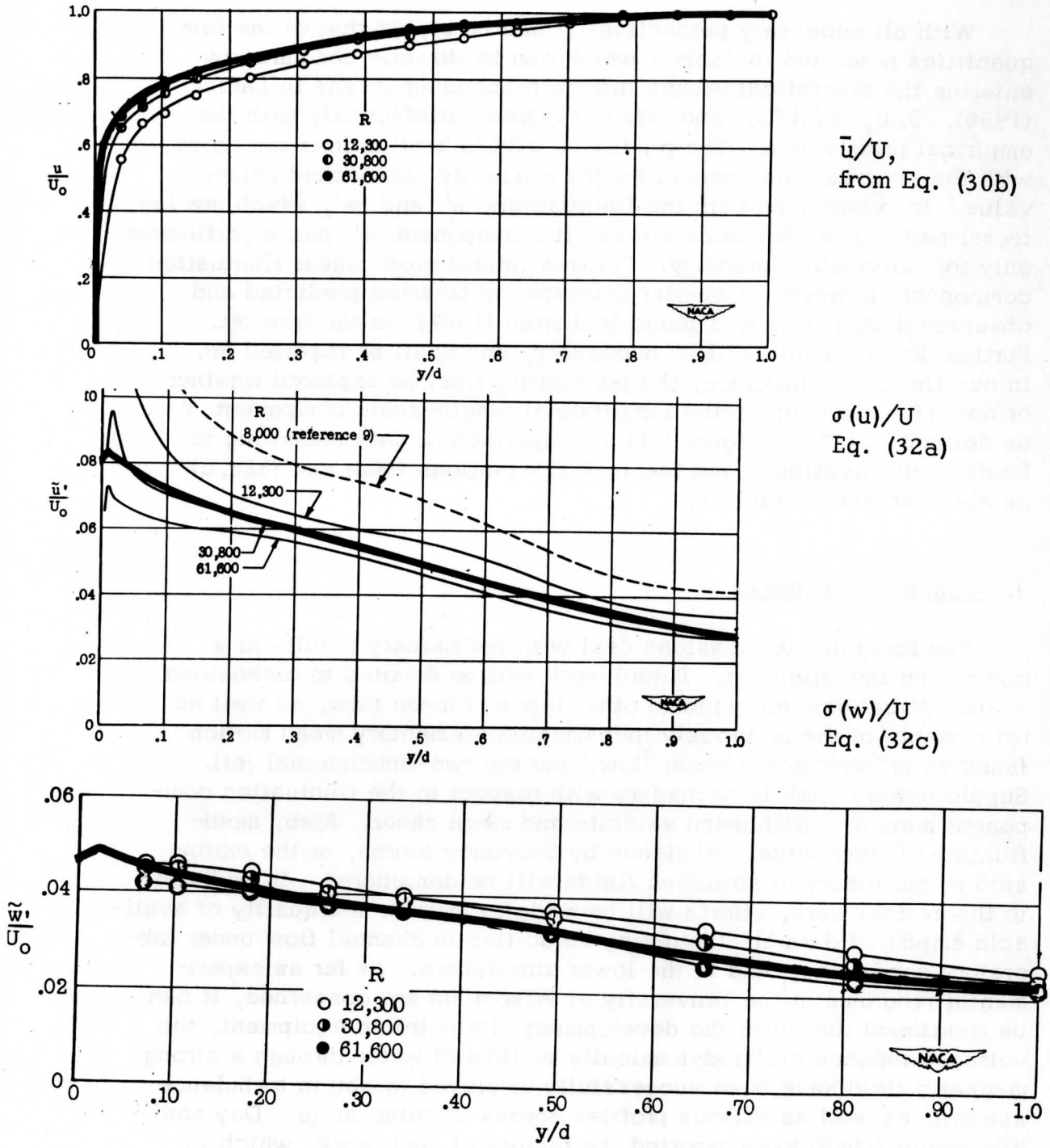

$\bar{u}/U$, from Eq. (30b)

$\sigma(u)/U$ Eq. (32a)

$\sigma(w)/U$ Eq. (32c)

Figure 1. Rectangular Duct — Laufer's (1950) measurements of mean velocity, and root-mean-square fluctuations of downstream and cross-stream components (all nondimensionalized with the aid of mean speed at the center), in comparison with computed profiles (heavy curves), as verified in Table 1.

Acknowledgments

The research reported is in part sponsored by the Department of Meteorology, U.S. Army Electronics Research and Development Activity, Fort Huachuca, Arizona, under Grant DA-AMC-28-043-66-G24, and under a matching grant WRC-67-015M by the Water Resources Research Center of the Department of the Interior.

References

Batchelor, G. K.: 1952. The Theory of Homogeneous Turbulence, 195 pp. Cambridge Univ. Press.

Batchelor, G. K. (editor): 1960. The Scientific Papers of Sir Geoffrey Ingram Taylor, Vol. II (Meteor., Oceanogr., and Turbulent Flow), 515 pages, Cambridge Univ. Press.

Day, H. J., and J. R. Villemonte: 1965. "Liquid Turbulent Investigations with an Electromagnetic Probe," Proceedings, 9th Midwestern Conference.

Friedlander, S. K., and L. Topper (editors): 1961. Turbulence—Classical Papers on Statistical Theory, 187 pages, Interscience Publishers, New York and London.

Heskestad, G.: 1962. "Measurements in a Two-Dimensional Jet," Report by the Department of Mechanics, The Johns Hopkins Univ., Baltimore.

Hinze, J.O.: 1959. Turbulence, 585 pp., McGraw-Hill Company, New York.

Laufer, J.: 1950. "Investigation of Turbulent Flow in a Two-Dimensional Channel," Nat. Adv. Council Aeronaut., Techn. Note 2133, Washington, D.C.

Lettau, H.: 1962. "Theoretical Wind Spirals in the Boundary Layer of a Barotropic Atmosphere," Beitr. Phys. Atmosph., 35, pp. 195-212.

Lettau, H.: 1964. "A New Vorticity-Transfer Hypothesis of Turbulence Theory," Journal Atmosph. Sciences, 21, pp. 453-456.

Lettau, H.: 1966. "Longitudinal versus Lateral Eddy Length-Scale," Journal Atmosph. Sciences, 23, pp. 151-158.

Lettau, H.: 1967. "A New Hypothesis for the Relationship between Eddy and Mean States," Physics of Fluids - to be published in supplemental volume.

Lumley, J.L., and H. A. Panofsky: 1964. The Structure of Atmospheric Turbulence, 239 pp., Interscience Monogr. Vol. 12, John Wiley & Sons, New York, 1964.

Phillips, O.M.: 1967. "The Maintenance of Reynolds Stress in Turbulent Shear Flow," Journal Fluid. Mech., 17, pp. 131-144.

Prandtl, L.: 1925. "Ueber die Ausgebildete Turbulenz," Zeitschr. Angew. Math. und Mech., 5, p. 136.

Reichardt, H.: 1938. "Messungen Turbulenter Schwankungen," Naturwissenschaften, 26, p. 404, 1938.

Reichardt, H.: 1941. "Ueber eine Neue Theorie der Turbulenz," Zeitschr. Angew. Math. und Mech. 21, p. 257.

Rossby, C.G.: 1932. "A Generalization of the Theory of the Mixing Length with Applications to Atmospheric and Oceanic Turbulence," Mass. Inst. Technol., Meteorol. Papers, Vol. 1, No. 4.

Rossby, C. G., and R. B. Montgomery: 1935. "The Layer of Frictional Influence in Wind and Ocean Currents," Mass. Inst. Technol. Meteorol. Papers, Vol. 3, No. 3.

Schlichting, H.: 1960. Boundary Layer Theory, Fourth Ed., 647 pp. McGraw-Hill Series in Mech. Eng., New York.

Taylor, G. I.: 1921. "Diffusion by Continuous Movement," Proc. London Math. Soc., 20, pp. 196-212.

Taylor, G.I.: 1935. "Statistical Theory of Turbulence," Proc. Royal Soc., A151, pp. 421-444.

Appendix

For comparison, it will be interesting to summarize corresponding results for fully developed free turbulence in a two-dimensional submerged jet. The "inductive theory" of Reichardt (1941), as well as empirical facts dealing with the rate of continuous downstream growth of jet width, or the normalized mean velocity profile as reported in Schlichting (1960), and recent fluctuation measurements by Heskestad (1962), have been brought into harmony with the new model presented by Lettau (1967). Noteworthy is that eddy displacement components show perfect isotropy in free turbulence while eddy velocities still exhibit a similar lack of isotropy as in channel flow. Namely, (15a) and (15b) apply to the free jet, but the covariance $\overline{x'z'}$, or the lateral length-scale, as in (17b), vanishes. Hence, the variances in (17a) are exactly equal to each other, which suggests the definition of a total longitudinal length-scale, $L^2 \equiv X^2 + Y^2 + Z^2 = 3X^2$, whereupon $L_x L = 3X_x X$.

Restraints due to the physical nature of the mean motion differ, obviously, in two-dimensional free jets from one-dimensional duct flow. The longitudinal length scale of free flow increases with x, so that in the jet $\overline{x'_x x'} > 0$, or $L_x = \text{const} > 0$. Lettau (1966) suggested that this L_x is a universal constant which plays for free turbulence a similar role as the Karman constant for wall turbulence, and proposed the name "Reichardt constant." Reanalysis of the data presented in Schlichting (1960) suggested $L_x = 0.065$, while Lettau (1967) found from the more recent and more detailed measurements by Heskestad (1962) $L_x = 0.0685 \pm 0.0015$. Due to isotropy conditions similar to (15a), the Reynolds average of squares of derivatives yields another constant in free turbulence,

$$m^2 \equiv \overline{x'_x x'_x} = \ldots = \overline{z'_z z'_z} .$$

The analysis of Heskestad's data showed that this constant m of free turbulence is significantly larger than 2κ, in (15c), for the center of duct flow. It was also concluded that m is really not a new constant since it appears to be numerically related to the "Reichardt constant" as follows

$$m^2 = 3L_x^2 = 9X_x^2 \quad \text{or,}$$

$$m = 0.0685 \cdot \sqrt{3} = 0.118 = 3X_x .$$

This can be statistically interpreted by assuming $X^2 \equiv \overline{x'x'}$ and $X_{xx} = 0$ (due to $X_x = \text{const}$), whereupon $(X_x)^2 = \overline{x'_x x'_x} + \overline{x'_{xx} x'}$. Thus, the above result holds true when $\overline{x'_{xx} x'} = -(2/3) \cdot \overline{x'_x x'_x}$.

Consequently, on the basis of similar developments for free turbulence which lead to (19) and (20) for duct flow, the Reichardt constant can be used to predict variances. At the center of the two-dimensional free jet, according to the theoretical model of Lettau (1967),

$$\sigma(u)/\bar{u} = m\sqrt{3} = 0.21; \quad \sigma(v)/\bar{u} = \sigma(w)/\bar{u} = m\sqrt{2} = 0.17.$$

Thus, for considerable differences in turbulence intensity, the same anisotropy as for the center of duct flow was obtained,

$$[\sigma(u)/\sigma(w)]_{\text{center}} = \sqrt{3/2} = 1.225.$$

Reading from graphs with which Heskestad (1962) illustrated his measurements, we find for the center of the jet:

(Heskestad) $\sigma(u)/\bar{u} = 0.23$ to 0.24; $\sigma(v)/\bar{u} = \sigma(w)/\bar{u} = 0.17$ to 0.18.

At the jet axis, $\sigma(u)/\bar{u}$ should be theoretically somewhat lower than a short distance from the center. It appears possible that the method of measurements tended to average out this secondary and relatively modest minimum value. With this in mind it may be concluded that predicted variances agree tolerably well with the observed data. There remain, though, some open questions, as pointed out by Lettau (1967), concerning the possible change of the m-value across the jet profile, in relation to lateral fluctuations of the velocity component perpendicular to both mean shear and main flow.

DISTRIBUTION LIST

Department of Defense

(50) Defense Documentation Center
ATTN: DDC-IRS
Cameron Station (Bldg 5)
Alexandria, Virginia 22314

Officeof Asst Sec of Defense
(Research & Engineering)
ATTN: Tech Library, RM 3E1065
Washington, D.C. 20301

Department of Navy

Chief of Naval Research
ATTN: Code 427
Department of the Navy
Washington, D.C. 20325

Naval Ships Systems Command
ATTN: Code 6312 (Tech Library)
Main Navy Building Room 1528
Washington, D.C. 20325

(2) Director
U.S. Naval Research Laboratory
ATTN: Code 2027
Washington, D.C. 20390

Commanding Officer & Director
U.S. Navy Electronics Laboratory
ATTN: Library
San Diego, California 92101

Commander
U.S. Naval Ordnance Laboratory
ATTN: Technical Library
White Oak, Silver Spring
Maryland 20910

AFSC STLO (RTSND)
Naval Air Development Center
Johnsville, Warmister
Pennsylvania 18974

Office of Naval Weather Service
Code 80
Washington Navy Yard (Bldg 200)
Washington, D.C. 20390

Officer in Charge
U.S. Navy Weather Research
Facility
Bldg R-48, US Naval Air Station
Norfolk, Virginia 23511

Department of Air Force

Headquarters
Strategic Air Command
ATTN: DOCE
Offutt Air Force Base
Nebraska 68113

Electronic Systems Div (ESTI) (2)
L. G. Hanscom Field
Bedford, Massachusetts 01730

AFCRL (CREW)
L. G. Hanscom Field
Bedford, Massachusetts 01730

Headquarters, Air Weather Svc
ATTN: AWSAE/SIPD
Scott Air Force Base
Illinois 62225

US Air Force Security Service
ATTN: ESD
San Antonio, Texas 78241

Air Proving Ground CTR (PGBPS-12)
ATTN: PGAPI
Eglin Air Force Base
Florida 32542

NOTE: One copy to each addressee unless otherwise indicated. Number of copies indicated in parentheses.

Headquarters
Research & Technology Div
ATTN: RTTC
Bolling AFB, D.C. 20332

Department of the Army

(2) Chief of Research & Development
Department of the Army
Washington, D.C. 20315

Commanding General
US Army Materiel Command
ATTN: AMCRD-RV-A
Washington, D.C. 20315

Commanding General
U.S. Army Missile Command
ATTN: AMSML-RRA
Redstone Arsenal, Alabama 35809

(3) Redstone Scientific Information Center
ATTN: CHIEF, Document Section
U.S. Army Missile Command
Redstone Arsenal, Alabama 35809

(2) Commanding Officer
Aberdeen Proving Ground
ATTN: Tech Library Bldg 313
Aberdeen Proving Ground,
Maryland 21005

(2) Headquarters
US Army Supply & Maintenance Command
ATTN: AMSEL-MR-M and AMSSM-MM
Washington, D.C. 20315

(3) Commanding General
US Army Combat Developments Command
ATTN: CDCMR-E
Fort Belvoir, Virginia 22060

Chief of Research & Development
ATTN: CRD/M
Department of the Army
Washington, D.C. 20310

Commanding Officer
US Army Combat Developments Cmd
Communications - Electronics Agcy
Fort Monmouth, New Jersey 07703

Commander
US Army Research Office (Durham)
Box CM-Duke Station
Durham, North Carolina 27706

Commanding Officer
US Army Sec Agcy Combat Dev Actv
Arlington Hall Station
Arlington, Virginia 22212

US Army Security Agency
ATTN: OACofS, DEV (CDA)
Arlington Hall Station
Arlington, Virginia 22212

US Army Security Agcy Processing Ctr
ATTN: LAVAPC-R&D
Vint Hill Farms Station
Warrenton, Virginia 22186

Technical Support Directorate
ATTN: Technical Library
Bldg 3330, Edgewood Arsenal
Maryland 21010

Commanding Officer (2)
US Army Nuclear Defense Lab
ATTN: Library
Edgewood Arsenal, Maryland 21010

Harry Diamond Laboratories
ATTN: Library
Connecticut Ave & Van Ness Street
Washington, D.C. 20438

Commanding General
USCONARC
ATTN: Recon & Survl Br
ODCS for Intel
Fort Monroe, Virginia 22351

Commandant
US Army Air Defense School
ATTN: C&S DEPT, MSL SCI DIV
Fort Bliss, Texas 79916

Commander, US Army Garrison
ATTN: Technical Reference Office
Fort Huachuca, Arizona 85613

Commanding General
US Army Munitions Cmd
ATTN: AMSMU-RE-R
Dover, New Jersey 07801

(3)Commanding General
US Army Test & Eval Command
ATTN: AMSTE-EL, -FA, -NBC
Aberdeen Proving Ground
Maryland 21005

Commanding Officer
US Army Cold Regions R&E Lab
ATTN: Library
Hanover, New Hampshire 03755

Commanding General
US Army Natick Labs
ATTN: AMXRE-EG
Natick, Massachusetts 01760

(2) Commanding Officer
US Army Ballistic Research Lab
ATTN: AMXBR-B & AMXBR-IA
Aberdeen Proving Ground
Maryland 21005

(2) Director
USA Engr Waterways Exper Station
ATTN: Research Center Library
Vicksburg, Mississippi 39180

Director
US Army Munitions Cmd
Operations Research Group
Edgewood Arsenal
Maryland 21010

Commanding Officer
US Army Frankford Arsenal
ATTN: SMUFA N-3400
Philadelphia, Penna 19137

Commanding Officer
US Army Picatinny Arsenal
ATTN: SMUPA-TV-3
Dover, New Jersey 07801

Commanding Officer
US Army Dugway Proving Ground
ATTN: Meteorology Division
Dugway, Utah 84022

President
US Army Artillery Board
Fort Sill, Oklahoma 73503

Commanding Officer
US Army Artillery Combat Dev Agcy
Fort Sill, Oklahoma 73504

Commandant
US Army Artillery & Missile School
ATTN: Target Acquisition Dept
Fort Sill, Oklahoma 73504

Commanding Officer
US Army CDC, CBR Agency
ATTN: Mr. N. W. Bush
Fort McClellan, Ala 36205

Commander
US Army Electronic Proving Ground
ATTN: Director, Test Directorate
Fort Huachuca, Arizona 85613

Commanding General
Deseret Test Center
ATTN: Tech Library
Fort Douglas, Utah 84113

Commandant
US Army Chemical Center & School
Micrometeorological Section
Fort McClellan, Ala 36201

Commandant
US Army Signal School
ATTN: Meteorological Dept
Fort Monmouth, New Jersey 07703

Asst Chief of Staff for Intel
ATTN: ACSI-DSRSI
Department of the Army
Washington, D.C. 20310

Asst Ch of Staff for Force Dev
CBR Nuclear Opns Directorate
Department of the Army
Washington, D.C. 20310

Asst Secretary of the Army (R&D)
Department of the Army
ATTN: Deputy Asst for Army (R&D)
Washington, D.C. 20315

CO, US Army Limited War Laboratory
ATTN: CRDLWL-7C
Aberdeen, Maryland 21005

CG, US Army Electronics Command
ATTN: AMSEL-MR
225 South 18th St
Philadelphia, Pa 19103

Chief, Willow Run Office
CSTA Lab, USAECOM
P.O. Box 618
Ann Arbor, Michigan 48107

Headquarters
US Army Combat Dev Command
ATTN: CDCLN-EL
Fort Belvoir, Va 22060

USAECOM Liaison Officer
MIT, Bldg 26, Rm 131
77 Massachusetts Ave
Cambridge, Mass 02139

USAECOM Liaison Officer
Aeronautical Systems Division
ATTN: ASDL=9
Wright-Patterson AF Base
Ohio 45433

Chief
Atmospheric Sciences Office
US Army Electronics Command
White Sands, N. Mex 88002

Chief (20)
Atmospheric Sciences Research
Division
ASL, USAECOM
ATTN: AMSEL-BL-RD
Fort Huachuca, Arizona 85613

Commanding General (total 14)
US Army Electronics Command
Fort Monmouth, N.J. 07703

AMSEL-EW
AMSEL-PP
AMSEL-IO-T
AMSEL-RD-MAT
AMSEL-RD-MAP (Record Copy)
AMSEL-RD-LNR
AMSEL-RD-LNA
AMSEL-XL-D
AMSEL-WL-D
AMSEL-NL-D
AMSEL-KL-D
AMSEL-VL-O
AMSEL-HL-CT-D
AMSEL-BL-D

Other Recipients

(2) NASA Sci & Tech Info Fac
ATTN: S-AK/DL
P.O. Box 33
College Park, Maryland 20740

(2) DASA Info and Analysis Center
General Electric-Tempo
816 State Street
Santa Barbara, Calif 93102

Institute of Science & Technology
The University of Michigan
P.O. Box 618 (IRIA Library)
Ann Arbor, Mich 48107

Vela Seismic Info Center
University of Michigan
P.O. Box 618
Ann Arbor, Michigan 48107

Battelle-Defender Info Center
Battelle Memorial Institute
505 King Avenue
Columbus, Ohio 43201

Director, Atmospheric Turbulence & Diffusion Laboratory, ESSA
P.O. Box E
Oak Ridge, Tennessee 37830

Chief, Atmospheric Sciences Section
National Science Foundation
1800 G Street, NW
Washington, D.C. 20550

Director
Bureau of Research & Development
Federal Aviation Agency
Washington, D.C. 20545

Chief
Fallout Studies Branch
Division of Biology & Medicine
Atomic Energy Commission
Washington, D.C 20546

Atmospheric Sciences Library
Environmental Sciences Svcs Admin
Silver Spring, Maryland 20910

NASA, Office of the Space Sci & Applications
ATTN: Space Appl Prog & Dir of Met (SAD)
Washington, D.C. 20546

Air Resources Field Research Office
c/o Robert A Taft Sanitary Engr Center
4676 Columbia Parkway
Cincinnati, Ohio 45226

Director
Atmospheric Physics & Chemistry Lab
Environmental Sci Svcs Admin
Boulder, Colorado 80302

National Center for Atmospheric Research
NCAR Library, Acquisitions
Boulder, Colo 80302

OCE, Bureau of Reclamation
ATTN: Code 755 Bldg 53
Denver, Colo 80225

US Department of Agriculture
Forest Service
ATTN: E.P. Van Arsdel
Lake States Forest Exp Sta
St. Paul Campus, Univ. of Minn.
St. Paul, Minnesota 55101

Commanding Officer
U.S. Army Biological Lab
ATTN: K. L. Calder
Ft. Detrick
Frederick, Md. 21701

Director
Environmental Biology Program
National Science Foundation
Washington, D.C. 20550

Commanding General
CDC Experimentation Center
Fort Ord, Calif. 93941

Director, Meteorology Dept
University of Arizona
Tucson, Arizona 85717

Director, U.S. Water Cons Lab
4331 E. Broadway
Phoenix, Arizona 85040

Director
Pac SW Forest & Range Exp Sta
Box 245
Berkeley, Calif 94704

Director, Meteorology Department
University of California
Los Angeles, Calif 90052

Director
US Salinity Laboratory
ATTN: Dr. S. L. Rawlins
Box 672
Riverside, Calif 95616

Dept of Water Science & Engr
ATTN: Mr. W. O. Pruitt
University of California
Davis, Calif 95616

Dept of Agr Eng
ATTN: Mr. W. B. Goddard
University of California
Davis, Calif 95616

Meteorology Department
San Jose State College
San Jose, Calif 95113

Chief, Radio Prop Lab
US National Bur of Standards
Boulder, Colo 80301

Dept of Civil Engr
ATTN: Dr. J. E. Cermak
Colorado State University
Fort Collins, Colo 80521

Forest Service Exp Sta
ATTN: Mr. M. Martinelli
Rm 221 Forestry Bldg, CSU
Fort Collins, Colorado 80521

Director, Meteorology Dept
Florida State University
Tallahassee, Florida 32301

Director, S Piedmont Cons Res Cen
PO Box 555
Watkinsville, Georgia 30677

Rosenwald Library
Meteorology Collection
University of Chicago
1101 E. 58th St
Chicago, Illinois 60637

Dept of Agronomy
ATTN: Dr. R. H. Shaw
Iowa State University
Ames, Iowa 50010

Director, Soil & Water Cons Res Div
ARS-USDA
Beltsville, Md 20705

Director, Dept of Civil Engr
Johns Hopkins University
Baltimore, Md 21233

Executive Secretary
American Meteorological Society
45 Beacon Street
Boston, Mass 02109

Director, Meteorology Dept
University of Michigan
Ann Arbor, Michigan 48105

Director, Meteorology Dept
Mass Institute of Technology
Cambridge, Mass 02138

Director, Meteorology Dept
St. Louis University
St. Louis, Missouri 63120

Dept of Soils
University of Missouri
Columbia, Missouri 62501

Department of Geophysics
Washington University
St. Louis, Missouri 63120

Director, Meteorology Dept
New York University
University Heights
New York, N. Y. 10001

Dr. E. R Lemon, ARS-USDA
Microclimate Investigations
Plant, Soil & Nutrition Lab
Ithaca, New York 14850

Scientific Research Inst
Oregon State University
Attn: Atmos Sci Br
Corvallis, Oregon 97330

Director
Meteorology Department
Pennsylvania State University
University Park, Pa 16802

Department of Oceanography
and Meteorology
Texas A&M University
College Station, Texas 77840

Electrical Engr Research Lab
University of Texas
Route 4, Box 189
Austin, Texas 78761

Department of Meteorology
University of Utah
Salt Lake City, Utah 84116

Director
National Research Council
National Academy of Sciences
2101 Constitution Avenue
Washington, D.C. 20315

Director
Meteorology Department
University of Washington
Seattle, Washington 99703

Director
Meteorology Department
University of Wisconsin
Madison, Wisconsin 53706

Officer-in-Charge
Meteorological Curriculum
US Naval Postgraduate School
Monterey, Calif 92801

Department of Soils
University of Wisconsin
ATTN: Dr. C B. Tanner
Madison, Wis 53705

Director
Geophysical Research
USAF Cambridge Research Center
ATTN: CRZHB (Hanscom Field)
Bedford, Mass 01730

Asst Sec for Defense
Office of Sec Defense
ATTN: Geophysical Sciences
Washington, D.C. 20315

USAF Climatic Center
ATTN: CCCAD
Air Weather Service (MAC)
Annex 2, 225 D St., SE
Washington, D.C. 20315

Forestry Library
260 Walter Mulford Hall
University of California
Berkeley, Calif 97404

Commander
AF Cambridge Research Lab
ATTN: Chief, Boundary Layer Br
Bedford, Mass 01730

Argonne National Lab
ATTN: Mr. Harry Moses, Met Bldg
9700 South Cass Ave
Argonne, Ill 60440

Prof. J. E. Pearson
Gen Engr Dept
Atmos Sciences Lab
University of Illinois
Urbana, Ill 61801

Brookhaven National Lab
ATTN: Meteorology Group
Upton, Long Island, N. Y. 11101

Director
National Security Agency
ATTN: C3/TDL
Ft. George G. Meade, Md 20755

US Naval Ordnance Test Station
CODE 40306
ATTN: Dr. Richard Jackson
China Lake, Calif 93555

Weather Bureau Forecast Center
Rm 911, Federal Office Bldg
Kansas City, Missouri 64106

Dr. Kenneth R. Knoerr
School of Forestry
Duke University
Durham, North Carolina 27706

Commander
US Naval Ordnance Test Sta
ATTN: CODE 164, Lt Col Clark
China Lake, Calif 93555

Mr. H. J. Spiegel
Southern Connecticut St College
Dept of Sciences
501 Crescent St
New Hven, Conn 06515

Prof. W. E. Reifsnyder
School of Forestry
Marsh Hall, 360 Prospect St
Yale University
New Haven, Conn 06511

Dr. Leo J. Fritschen
College of Forestry
University of Washington
Seattle, Washington 98105

ARS, Snake River Cons Res Cen
ATTN: Dr. J. L. Wright
Route 1, Box 186
Kimberly, Idaho 83341

Dr. C. H M. van Bavel
Institute of Life Sciences
Texas A&M University
College Station, Texas 77843

Dr. Winton Covey
117 Plant Science
Department of Agronomy
Cornell University
Ithaca, N.Y 14850

Dr. Raymond E. Leonard
Northeastern Forest Exp. Station
SUNY College of Forestry
Syracuse, New York 13210

Institute for Storm Research
The University of St. Thomas
3812 Montrose
Houston, Texas 77006

UNCLASSIFIED

Security Classification

DOCUMENT CONTROL DATA - R & D

(Security classification of title, body of abstract and indexing annotation must be entered when the overall report is classified)

1. ORIGINATING ACTIVITY *(Corporate author)*

University of Wisconsin
Madison, Wisconsin 53705

2a. REPORT SECURITY CLASSIFICATION

Unclassified

2b. GROUP

3. REPORT TITLE

STUDIES OF EFFECTS OF BOUNDARY MODIFICATION IN PROBLEMS OF SMALL AREA METEOROLOGY

4. DESCRIPTIVE NOTES *(Type of report and inclusive dates)*

Annual reports 1966-1967

5. AUTHOR(S) *(First name, middle initial, last name)*

Heinz H. Lettau, Charles R. Stearns, Walter F. Dabberdt, and Joseph Zabransky

6. REPORT DATE	7a. TOTAL NO. OF PAGES	7b. NO. OF REFS
February 1968	164 + vii	78

8a. CONTRACT OR GRANT NO.	9a. ORIGINATOR'S REPORT NUMBER(S)
DA-AMC-28-043-66-G24	
b. PROJECT NO. 1TO-14501-B53A	
c. Task -08	9b. OTHER REPORT NO(S) *(Any other numbers that may be assigned this report)*
d.	ECOM 66-G24-A

10. DISTRIBUTION STATEMENT

Distribution of this document is unlimited.

11. SUPPLEMENTARY NOTES	12. SPONSORING MILITARY ACTIVITY
	US Army Electronics Command Atmospheric Sciences Laboratory Fort Huachuca, Arizona 85613

13. ABSTRACT

Of the six sections of this first report, two deal specifically with the physics of the air and soil layer close to dry desert ground, because the general problem of energy conversion from insolation to heat can best be studied when the moisture factor is eliminated. The observations on which the discussion in Sections 1 and 5 are based were obtained at a site in the Peruvian desert, where the mean annual rainfall is measured as "traces." The region includes climatic stations which hold the world record of dryness.

Section 2 is concerned with small area meteorology under most humid conditions, in airflow over an inland lake. The investigation of details of wind structure around obstacles (Sections 3 and 4) establishes connections to a broad range of related problems, from the tower "bias" of conventional anemometer exposure, to the structure of airflow between complicated roughness elements like the trees of a forest.

For the last problem, that of airflow under plant canopies, the theoretical discussion in Section 6 (which includes a rationalization of the previously introduced concepts of longitudinal and lateral length-scales of turbulence) offers new prospects of application, which will be followed up in the forthcoming final report.

Each of the six individual sections of this report is accompanied by an abstract which summarizes the specific problems discussed and details of the results.

DD FORM 1 NOV 65 1473 REPLACES DD FORM 1473, 1 JAN 64, WHICH IS OBSOLETE FOR ARMY USE.

UNCLASSIFIED

Security Classification

14. KEY WORDS	LINK A		LINK B		LINK C	
	ROLE	WT	ROLE	WT	ROLE	WT